

futurities

The Simulation Based Engineering & Sciences Magazine

Year 21
02
Summer
2024



SPOTLIGHT

When art meets technique

MBD Productivity & Quality Software



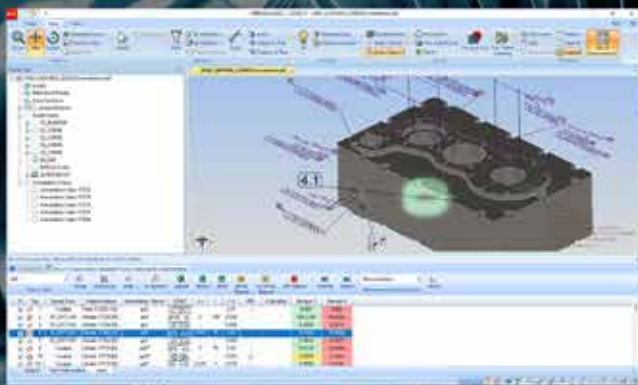
Auto balloon 2D drawings & create automated inspection reports

MIV Balloon 2D

- Convert 2D annotations into machine-readable Bill of Characteristics for easy-to-create FAI, PPAP, APQP, and other inspection reports.
- Publish inspection reports to Excel, PDF, HTML, Net-Inspect, etc.
- Future proof to MBD workflows.



Deploy MBD workflows across the enterprise



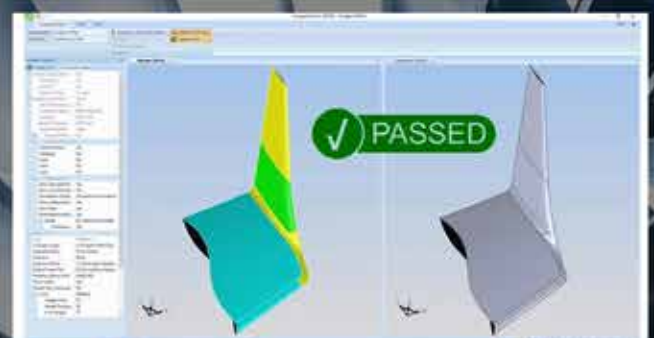
MIV MBDVidia

- Publish native CAD into ISO standard 3D MBD neutral CAD (QIF or STEP242) w/ PMI for downstream consumption.
- Publish inspection reports to Excel, PDF, HTML, Net-Inspect, etc.
- Harvest data for business-driven insights.

Manage CAD revisions & validate derivative models

clv CompareVidia

- Validate customer product definition requirements like Boeing DPD.
- Compare derivatives (NX to QIF), revisions (Rev 1 to Rev 2), or versions (Creo 9 to Creo 10).



- Editor's Note

With the longer summer days and seasonal holidays of the Northern Hemisphere in mind, the Spotlight of this issue of *Futurities* contains a meaty read that lends itself to a more leisurely consumption under an umbrella. Penned by veteran civil structural engineer Livio Furlan, the Spotlight this month delves into the vast subject of structural engineering beginning with a philosophical bent and arguing for the necessity of a skillful and artful intertwining of Engineering, Numerical Simulation, Art and Technology to achieve structures that are both eminently functional yet attractive and appealing. Seasoned with multiple examples, the piece also incorporates the many technical aspects of the topic and reviews the regulatory conditions to be met, so our regular readers are sure to find this a satisfying summer read.

The **Spotlight** in this issue also contains a technical contribution from Cimolai, a leading Italian steel construction company together with the European Southern Observatory about a CFD analysis they conducted to ensure that the Extremely Large Telescope (ELT) currently under construction in the Chilean Andes could withstand the action of the wind sufficiently to meet its performance requirements across the entire observation field. The ELT is a 40m-class optical, near and mid-infrared telescope that will be the largest optical and infrared telescope in the world. The **Spotlight** is rounded out by an overview of SDC Verifier, software created to streamline steel connection design.

This issue's **Technology Transfer** section shares a contribution from Endurica, a widely validated fatigue life simulation system for elastomers which compares fatigue analysis for metals to fatigue analysis for rubber, and the important implications that these differences have for various applications.

The **Know-how** section in this edition features an article from Indian EV-battery design specialists, oorja, which examines EV battery behaviour analysis and how to identify the Goldilocks Zone for electrochemical parameters in order to ensure that EV batteries achieve optimal performance for different operating conditions. In another article, Wolf Star Technologies together with Menet Aerospace which sells a unique type of tethered unmanned aircraft system, or drone, that provides secure, on-demand

wireless communications to support high-bandwidth digital battlefield communications, signal intelligence, electronic warfare, or force protection and targeting, discuss the initial implementation of Wolf Star's True Load software undertaken as the initial phase of a larger project to help Menet Aero better understand the loading on its drone blades so that they can design and optimize better aircraft. A contribution from SPM Engineering which discusses a dynamic CFD analysis of a top-loading washing machine with a hydraulic balancer concludes this section.

In the **Product Peeks**, we present SmartUQ which offers unique tools to address the specific challenges of simulation including long run times and accuracy issues using artificial intelligence and machine learning for both simulation and digital twins. The other Product Peek from TSNE looks at how to use Ansys Fluent's solar load model to analyse shadows in solar power plants in order to minimize their impact on power generation.

The **Research and Innovation** section has an interview by the EuroHPC Joint Undertaking with the OPTIMA project leader, Iakovos Mavroidis, researcher at the Technical University of Crete (TUC), which explores the key features of the OPTIMA project and how it is reshaping HPC in Europe. The project, led by a consortium of ten partners including six European SMEs from six different countries in Europe, completed its work in November 2023. OPTIMA uses field-programmable gate array (FPGA) technologies, which are programmable computer chips that boost performance and minimize energy consumption. The ultimate objective is to foster new, more economic and environmentally friendly approaches to HPC supercomputing for industrial applications, such as simulation in the fields of robotics, geosciences and computational fluid dynamics (CFD).

We wish you happy reading and to those of you in the north of the globe, a restorative summer break!

Stefano Odorizzi

Editor in chief



“

...a skillful and artful intertwining of Engineering, Numerical Simulation, Art and Technology to achieve structures that are both eminently functional yet attractive and appealing.



Futurities

Year 21 n°2 - Summer 2024

To receive a free copy of the next magazine, please contact our Marketing office at: marketing@enginsoft.com

All pictures are protected by copyright. Any reproduction of these pictures in any media and by any means is forbidden unless written authorization by EnginSoft has been obtained beforehand. ©Copyright EnginSoft.

EnginSoft S.p.A.

24126 BERGAMO c/o Parco Scientifico Tecnologico
Kilometro Rosso - Edificio A1, Via Stezzano 87 • Tel. +39 035 368711
50127 FIRENZE Via Panciattichi, 40 • Tel. +39 055 4376113
35129 PADOVA Via Giambellino, 7 • Tel. +39 049 7705311
72023 MESAGNE (BRINDISI) Via A. Murri, 2 - Z.I. • Tel. +39 0831 730194
38123 TRENTO fraz. Mattarello - Via della Stazione, 27 • Tel. +39 0461 915391
10133 TORINO Corso Marconi, 20 • Tel. +39 011 6525211

www.enginsoft.com

e-mail: info@enginsoft.com

Futurities is a quarterly magazine published by EnginSoft SpA

COMPANY INTERESTS

EnginSoft GmbH - Germany
EnginSoft UK - United Kingdom
EnginSoft Turkey - Turkey
EnginSoft USA
E-SOFT France
Particleworks Europe
www.enginsoft.com

CONSORZIO TCN www.consorziotcn.it • www.improve.it
M3E Mathematical Methods and Models for Engineering www.m3eweb.it
AnteMotion antemotion.com

ASSOCIATION INTERESTS

NAFEMS International www.nafems.it • www.nafems.org
TechNet Alliance www.technet-alliance.com

ADVERTISING

For advertising opportunities, please contact our Marketing office at: marketing@enginsoft.com

RESPONSIBLE DIRECTOR

Stefano Odorizzi

PRINTING

Grafiche Dalpiaz - Trento

Autorizzazione del Tribunale di Trento
n° 1353 RS di data 2/4/2008

The *Futurities* editions contain references to the following products which are trademarks or registered trademarks of their respective owners:

Ansys, Ansys Workbench, AUTODYN, CFX, Fluent, Forte, SpaceClaim and any and all Ansys, Inc. brand, product, service and feature names, logos and slogans are registered trademarks or trademarks of Ansys, Inc. or its subsidiaries in the United States or other countries. [ICEM CFD is a trademark used by Ansys, Inc. under license] (www.ansys.com) - **modeFRONTIER** is a trademark of ESTECO Spa (www.esteco.com) - **Flownex** is a registered trademark of M-Tech Industrial - South Africa (www.flownex.com) - **MAGMASOFT** is a trademark of MAGMA GmbH (www.magmasoft.de) - **LS-DYNA** is a trademark of LSTC (www.lstc.com) - **Cetol 6σ** is a trademark of Sigmetrix L.L.C. (www.sigmetrix.com) - **RecurDyn™** and **MBD for Ansys** is a registered trademark of FunctionBay, Inc. (www.functionbay.org) - **Maplesoft** is a trademark of Maplesoft™, a subsidiary of Cybernet Systems Co. Ltd. in Japan (www.maplesoft.com) - **Particleworks** is a trademark of Prometech Software, Inc. (www.prometechsoftware.com) - **Multiscale.Sim** is an add-in tool developed by CYBERNET SYSTEMS CO.,LTD., Japan for the Ansys Workbench environment - **Rocky** is a trademark of ESSS (www.esss.co) - **industrialPhysics** is a trademark of Machineering GmbH (www.machineering.com) - **SIMUL8** is a trademark of SIMUL8 Corporation (www.simul8.com) - **ViveLab Ergo** is a trademark of ViveLab Ergo Ltd. (www.vivelab.cloud) - **True-Load** is a trademark of Wolf Star Technologies (www.wolfstartech.com) - **FEMFAT** is a trademark of ENGINEERING CENTER STEYR GMBH & CO. KG (www.femfat.magna.com) - **SDC Verifier** is a registered trademark of SDC Verifier Holding BV (sdcverifier.com) - **oorja.energy** is a trademark of Weedy Software Private Limited (oorja.energy) - **Endurica** is a trademark of Endurica LLC (endurica.com).

Contents

TECHNOLOGY TRANSFER

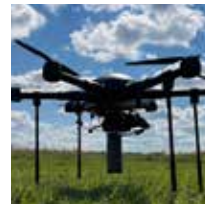


36 Rubber fatigue ≠ metal fatigue: mean strain effects
by *Endurica LLC*

KNOW-HOW



39 Battery modelling and the Goldilocks zone
by *oorja*



42 Tethered drones: understanding rotor loads
by *Menet Aero and Wolf Star Technologies*



46 Dynamic CFD analysis of a vertical-axis washing machine with a hydraulic balancer
by *SPM Engineering*

RESEARCH & INNOVATION



50 OPTIMA project revolutionizes HPC for industrial applications: interview

PRODUCT PEEKS



53 Introduction to shading analysis for solar complexes
by TAE SUNG S&E



56 Leverage SmartUQ to achieve modern artificial intelligence and machine learning for simulation and digital twins
by SmartUQ

SPOTLIGHT



- 6** **Of the marvels and mathematics of structural engineering**
- 7** Structural Engineering | Beyond the Otherness between Art and Technique- Part 1
by EnginSoft
- 16** Structural Engineering | Beyond the Otherness between Art and Technique- Part 2
by EnginSoft
- 24** CFD analysis for ESO's extremely large telescope (ELT) in Chile: Wind screening performance of the dome and main structure
by Cimolai, ESO
- 31** Accuracy in steel connection design: A practical look at SDC Verifier
by SDC Verifier



SPOTLIGHT

Of the marvels and mathematics of structural engineering

It could be argued that since Ancient Egyptian and Roman times, Structural Engineering has always shaped, and will continue to shape, our environment and therefore the ways in which our societies evolve, develop socialize, and prosper.

Embracing everything from roads, railways and bridges, to sport stadiums, skyscrapers, dams and artificial islands, such as the Palm Jumeirah in Dubai in the United Arab Emirates, or the Kansai International Airport in the Greater Osaka area of Japan, structural engineers are responsible for planning these structures and ensuring their safety, security, and longevity in time against their own physical characteristics as well as their interactions with the environmental elements they contain, harness or withstand, such as wind, water, waves, snow, sand, fire and earthquake.

Since many of them are megastructures with an imposing presence and formidable effect on their surroundings, our Spotlight in this issue, written by veteran civil structural engineer, Livio Furlan, examines specifically how Art, Technology and Engineering all contribute — and should be harnessed together — to create safe, functional structures that are both aesthetically aspirational and awe-inspiring while also satisfying all necessary regulatory requirements. This is neatly summarized in the words of Professor Sir Edmund Happold, a highly influential English structural engineer who contributed to landmark buildings such as the Sydney Opera House: “A world which sees art and engineering as divided is not seeing the world as a whole.”



Structural Engineering | Part 1

Beyond the Otherness between Art and Technique

by Livio Furlan
EnginSoft

I would like to begin with a question: what is engineering? Paraphrasing Wikipedia's definition, "Engineering is an applied science that uses scientific principles to design and construct machines or vehicles, devices or circuits, buildings or infrastructures, plants or systems, programs or algorithms and other elements necessary to achieve one or more objectives, such as exploiting the natural resources available to man or solving a problem. It is an activity of using knowledge for something practical, and its objectives include the design, development, maintenance, repair, and/or improvement of equipment, materials, and processes".

It is clear therefore that, taken as a whole, engineering is a science (or discipline) that covers decidedly broad and articulated areas. Over time, this multi-disciplinarity has created several distinct branches, each of which further differs in terms of themes and methods. The following is an (incomplete) list of the main engineering practices that have developed their own distinctive identities:

- Environmental Engineering (Agricultural, Climate, Geoengineering, Mining);
- Civil Engineering (Structural, Construction, Hydraulics, Transport, Seismic, Geotechnics);
- Management Engineering (Economic, Financial);

- Industrial Engineering (Aeronautical, Aerospace, Chemical, Mechanical, Naval);
- Information Engineering (Automation, Computer Science, Electronics, Communications).

In the context of Structural Engineering (the writer is a veteran civil structural engineer) the following definition strikes a strong chord: "Structural Engineering is the Art of moulding materials we do not wholly understand into shapes we cannot precisely analyse, so as to withstand forces we cannot really assess, in such a way that the community at large has no reason to suspect the extent of our ignorance."

This quote is often attributed to Dr A.R. Dykes and is apparently from the President's Address he delivered in 1976 to the British Institution of Structural Engineers. Irrespective of the details, I believe it accurately captures the essence of the challenge that all engineers (including structural engineers) face every day: even if part of the job is preventing the public from suspecting the extent of the engineers' ignorance, the engineers themselves must acknowledge their own ignorance and bear it in mind during the daily practice that drives their choices and decisions.

In fact, to live a life full of wonder (both as a human being and as a structural engineer) also means having doubts, asking questions, and accepting that you do not know everything. Having only certainties robs you of the ability to savour the taste of discovery and to develop and improve your skills.

As William Shakespeare wrote (Hamlet, Act 4, scene 5) "We know what we are but know not what we may be", and we can certainly become much more than we are: all we have to do is listen with the intellectual humility that creates empathy and understanding.

Engineering (structural, specifically, but also the other branches) is about solving problems or at least limiting their effects for the benefit and advantage of the community at large — for example, the search for safe responses by structures to seismic actions so that quality of life hopefully improves.

Achieving this obviously requires commitment and responsibility starting with the available information, data, events and experiences (that sometimes require interpreting in the light of specific stories); considers the objectives; and then uses judgement to find solutions. That judgement should seek and include knowledge, intuition, integrity, foresight, trust, and the ability to discerningly assess the available information and the needs to be met, and then create solutions through inspiration, artistic and logical thinking, and decision-making, combined with the essential ability to work with (and for) others to reach shared solutions in a clear and synergetic manner.

It is for this reason that Dykes' definition and the fact that it begins with "...Art..." resonates so strongly with me: in my opinion Structural Engineering cannot do without Art — both in the strict sense as the ability to generate emotions by giving shape to unique "structural" works, and in a general sense as a "way of acting".

Now to turn to the other parts of that definition: "...moulding materials we do not wholly understand into shapes we cannot precisely analyse, so as to withstand forces we cannot really assess...". To understand materials requires application and experimentation because each responds according to its own characteristics and these have been deciphered over the past decades precisely because of the need to use the materials in specific, responsible and sustainable ways.

The analysis of form and shape today allows the most complex geometries to be investigated with high reliability and an adequate level of confidence thanks to modern virtual prototyping tools.

And finally, with regard to the forces "we cannot really assess", today we have numerical methods as well as calculation and verification methods that consider the randomness of the forces' actions, and apply appropriate factors to their characteristic values, which are also a function of the probability that the forces combine favourably or unfavourably, again with their characteristic values.

Among numerical methods, an example is computational fluid dynamics which makes it possible to assess the actions induced, for

instance, by wind on structures, as well as fluid-structure interaction. Over time, the calculation and verification methods have migrated from the deterministic sphere (for instance the method of admissible stresses) to the semi-probabilistic or probabilistic spheres (such as the limit-state method) and have also moved into the regulatory context.

Virtual prototyping

In industrial production, each new product undergoes the same basic cycle: first, it is designed, then a (physical) prototype is built and tested, leading, if necessary, to modifications and updates of the prototype itself. At each step, indications for a new iteration are obtained. This standard process is generally slow and, since physical prototypes must be constructed, expensive.

When it comes to designing a completely new product, the modus operandi can become even more onerous: after extensive practical tests, the physical prototype is virtualized — a phase that until some time ago involved bringing the prototype right back to the drawing board for subsequent production.

A current solution to these problems is to use virtual prototyping right from the design stage. Virtual work environments offer innovative tools for simulation and interactive visualization of the product from the earliest, preliminary stages of development, thereby offering the attractive prospect of optimizing time and costs while increasing quality and reliability.

Where virtual prototyping shortens the design-validation-fabrication path in industrial production, in Structural Engineering it cannot be disregarded unless one limits oneself to designing and creating simple systems where pre-packaged handbooks and tables are sufficient.

A "special" structure is in fact already a prototype, but one that cannot be tested only in reality. On the contrary, if not properly studied using appropriate methods, specific functional characteristics could be lost or the structure or its important parts could be lost or collapse.

Virtual prototyping therefore constitutes an essential resource in seeking the structural forms to be moulded, particularly for Conceptual Structural Design, which does not apply Structural Engineering's rational methods at the end of the design process merely to verify the feasibility and static/seismic safety of the morphological choices previously defined by other means, but rather applies them at the beginning of the design process of structural morphogenesis.

The finite element method

The overall path that governs virtual prototyping within the sphere of Structural (and Civil) Engineering uses specific calculation methods to assess the correctness and robustness of the design solutions adopted. One of these that plays a fundamental role is the Finite Element Method (FEM) and it has become one of the most versatile approaches for solving structural problems using automatic calculation.

FEM is well known as a numerical technique for finding approximate solutions to problems described by partial differential equations by reducing them to a system of algebraic equations. The discretization phase of the method corresponds to the transition from a problem posed in the continuous, endowed with infinite degrees of freedom to a problem defined in the discrete and characterized by a finite number of degrees of freedom. This requires one to generally renounce the determination of the exact (analytical or closed-form) solution of the initial problem in favour of an approximate solution, which must include appropriate discretization and suitably chosen shape functions of the elements used to represent the structural continuum. Subdivision is, therefore, a delicate phase and should be conducted with the competence and experience progressively gained in using FEM.

Thus, a model that could pass for “trivial” (due to the use of beam elements with an “exact” formulation) still has to be implemented by duly considering the assumptions made (and justified in relation to the actual behaviour of the simulated system) when critically evaluating the results following the calculation.

Design and FEM analysis

"Mechanics is the paradise of mathematics because it is here that the fruits of mathematics are reaped. There is no certainty in science if mathematics cannot be applied to it, or if it is not related to it." — Leonardo da Vinci.

Unquestionably, Structural Mechanics is also rooted in this Mechanics, since it underlies the development and study of numerical methods and theoretical models that can describe, with relevance to reality and based on relationships drawn from both mathematics and physics, the state of stress and deformation of the structures that form the resistant part of a manufactured article (civil, industrial, or aeronautical construction).

Obviously, FEM as summarized briefly above must be classified as part of the methods for determining the mechanical-structural response of the planned structure, which must not disregard aesthetics if it is to be harmonious. Aesthetics is not something separate, independent, successive; it is not a time that comes afterwards to adorn the technical realization, but is symbiotic with the structure, defining its lines and being defined by the balance between the built and surrounding environments.

This is how Mathematics and Form, while remaining distinct, intertwine in the ingenious ability to innovate and combine Architecture, Engineering and Art. And it is why some structures are bold, aesthetically beautiful, and iconic, while others, untroubled by a spirit of research, remain anonymous and devoid of their own identity. Contextualizing works with respect to the environments in which they arise stems from the wisdom with which projects capable of maintaining a healthy, balanced link with these environments (natural or previously defined by human intervention) are conceived.



This is the case, for instance, with bridges and viaducts that become landscape enhancements and works of art when they are designed using criteria that consider their environmental impact as well as the relative load conditions experienced in service and during the temporary installation/launching phases.

The way in which bridges, viaducts and overhead crossing works generally are conceived to pass over a continuous uninterrupted impediment (defined as a natural constraint e.g. a sea, lake, river, or valley) or an objective one, such as a transport or service network e.g. railway, motorway, or power line can play a decisive role as early as the preliminary drafting stage of projects.

The final elevated structure (bridge or viaduct) is realized by raising segments prefabricated on site or in the workshop, or by launching the structure, assembled in the area behind one of the two abutments, forward from the rear. Obviously, both approaches require specific structural analyses to be conducted with dedicated FEM models developed specifically to study the behaviour of the structure during the temporary assembly phases.

A special technique was conceived by Studio Ing. Romaro¹ and the Italian company Cimolai for launching the deck of the Chavanon Viaduct in Messeix in France (built and installed by Cimolai and inaugurated in 2000, see Fig. 1): they used main cables and pendants to advance the deck itself Tarzan-style, with the deck head passing from one pendant to the next.

[1] Studio Ing. Romaro no longer exists having been absorbed into Cimolai, first as Romaro Engineering, and then being merged completely into the acquiring company.



Fig. 1. Chavanon Viaduct, opened in 2000.

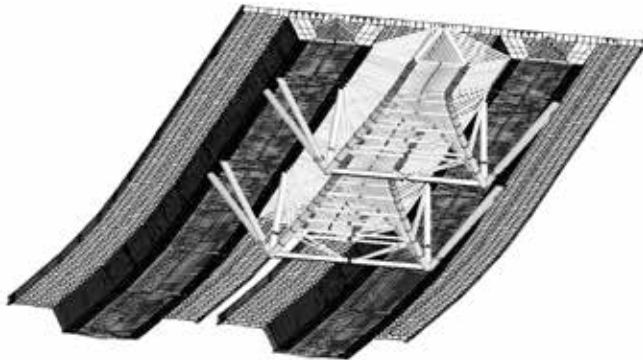


Fig. 2. Portion of the FEM model of a viaduct deck with a central reticular structure.

FEM models were used extensively to study the technique because the behaviour of the main cables had to be analysed for conditions that differed to their intended purpose/behaviour for regular operating conditions.

Needless to say, FEM models are used to study temporary conditions such as launching and also more broadly for designing works in relation to their operating conditions, particularly if the works are structurally innovative and require the support of advanced design, calculation and verification methods. Fig. 2 shows a portion of a FEM model relating to the deck of a viaduct.

In this context, it is worth remembering EnginSoft's heritage as an asset to draw upon for developing innovative and sustainable projects due to the significant role it has always played and continues to play in the field of numerical simulation. Moreover, in the field of Structural Engineering, EnginSoft's dedicated team, active since 1989, has always taken advantage of the evolution of calculation methods and

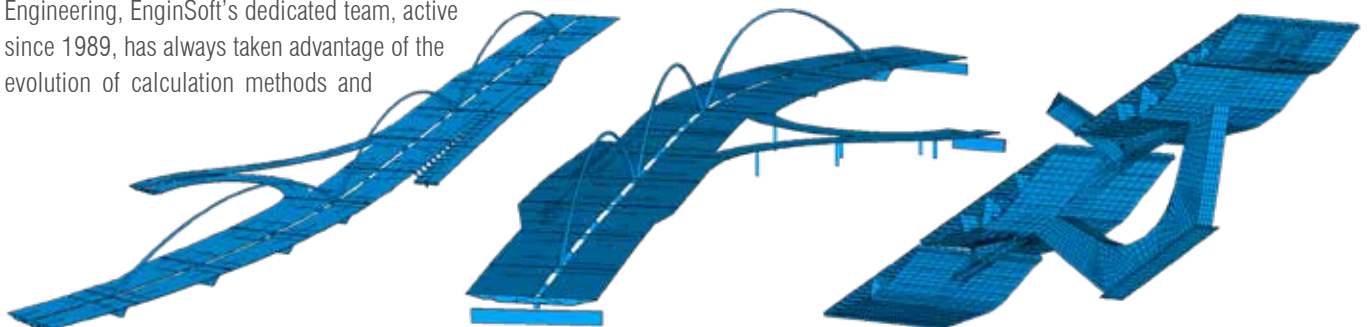


Fig. 3. FEM model of the Darwin Viaduct in East Padua in Italy.

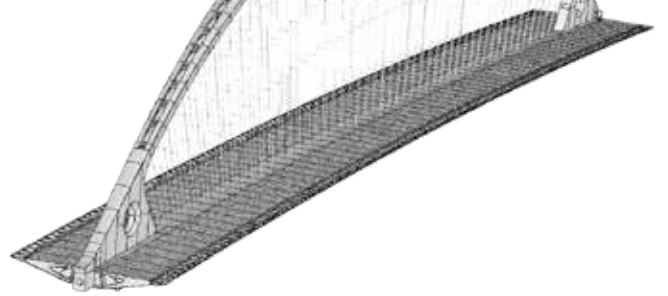


Fig. 4. FEM model and view of the Flyover Bridge over the A1 Motorway and the High-Speed Railway in Reggio Emilia in Italy.

virtual prototyping to help professionals and companies adopt them as an everyday system rather than tools for episodic use. This has led to collaborations with prestigious companies such as Studio Ing. Romaro and Cimolai, which have also made use of EnginSoft's skills and knowledge to design, calculate, and realize works of outstanding importance all over the world, demonstrating yet again that Italian engineering needs fear no comparison.

With this in mind, here is a brief review of some of the works in which these teams were involved.

The Padua East Viaduct (Darwin Bridge) in Italy, built by Cimolai, is approximately 540m in length and uses monolithic piers with decking. In the summer of 2005, EnginSoft developed a FEM model (with beam and shell elements) representing the viaduct as a whole (see Fig. 3) to study its behaviour: firstly, to evaluate the sensitivity of its response to variations in the stiffness of the foundations (modelling the interaction with the soil by means of user-defined beam elements), and secondly, to identify better solutions (including those relating to vibration and fatigue behaviour) compared to the basic design.

The A1 motorway and high-speed railway flyover bridge in Reggio Emilia in Italy, completed in 2006 and discussed in the EnginSoft Newsletter No. 3, 2006. This arch bridge has a deck span of 220m suspended by stays, and an arch height of 50m from the deck level. An overall FEM model of it was developed (with beam, shell and cable elements) to determine the generalized tension and deformation levels under operating conditions using geometric non-linearity analysis, as an in-depth study of the arch stability which is crucial for the safety of the designed structure. Obviously, detailed FEM models were also performed to structurally optimize the connections of the stays (pendants) to the arch.

The Bridge of Strings in Jerusalem in Israel, built to carry the city's surface metro system, designed by the Spanish architect Santiago Calatrava and built/installed by Cimolai. The bridge was inaugurated in June 2008, about two years after the completion of the modelling, analysis, calculation, and verification activities undertaken by EnginSoft in collaboration with Studio Ing. Romaro and Cimolai. This cable-stayed bridge has a 140m-wide curvilinear deck, supported asymmetrically by stays that converge on a 120m-high steel pylon.

Given its structural complexity, an overall FEM model was developed for this bridge

using beam, shell and chord elements (see Fig. 5) for the purpose of revisiting certain design aspects. Using geometric non-linear analysis, the levels of generalized tension and deformation under operating conditions were determined, and an in-depth study of the pylon's stability and the assembly and tensioning sequences of the stays supporting the deck was conducted.

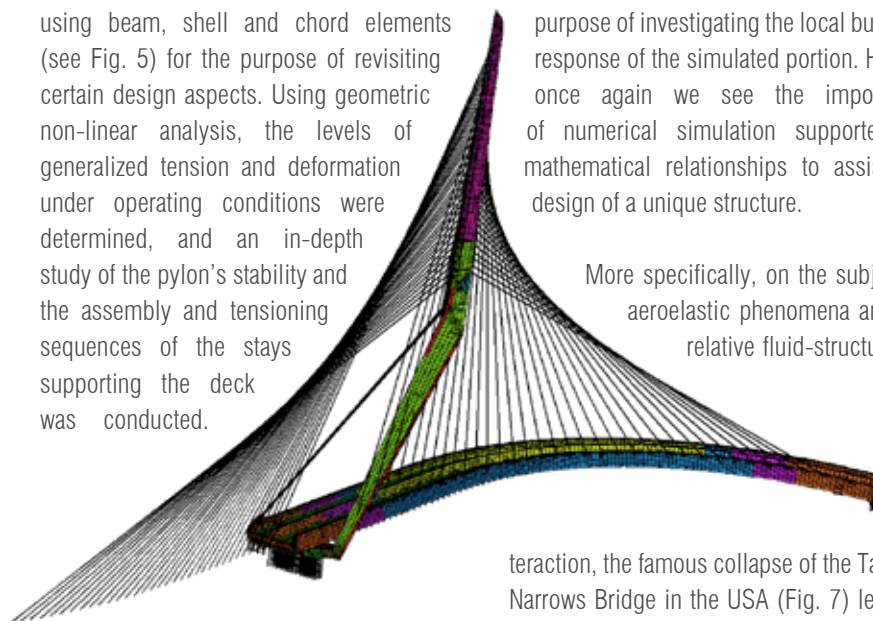


Fig. 5. FEM model of the Bridge of Strings in Jerusalem in Israel.

Detailed FEM models were also performed to adequately investigate the stress levels at the foot of the pylon and to optimize the connections of the stays to the pylon.

In terms of bridge design, the proposed bridge over the Strait of Messina off the southern tip of Italy is a gigantic challenge and certainly a distinctive one in terms of technical expertise and knowledge of the structure-environment interactions (not least of which the aeroelastic phenomenon) that affect the feasibility of this unprecedented work.

During one of the design phases of the bridge (specifically the one in 2005), a FE model of a portion of the pylons was developed as a preparatory phase (see Fig. 6) for the

purpose of investigating the local buckling response of the simulated portion. Hence, once again we see the importance of numerical simulation supported by mathematical relationships to assist the design of a unique structure.

More specifically, on the subject of aeroelastic phenomena and the relative fluid-structure in-

teraction, the famous collapse of the Tacoma Narrows Bridge in the USA (Fig. 7) led to a period of intense research that applied aeroelasticity to Civil Engineering to study the behaviour of a deformable body immersed in a moving fluid and the relationship between the forces exerted by the fluid and the deformations and displacements of the body.

One of the most dangerous aeroelastic phenomena is flutter, given its catastrophic effect. It consists of oscillations of progressively increasing amplitude of the bridge deck that occur at a certain critical speed of the incident wind. These oscillations can lead to structural collapse, as was the case with the Tacoma Narrows Bridge.

For this reason, "autofinanced" benchmarks were conducted to validate the 2D-3D approach adopted to predict the critical flutter velocity of suspended bridge decks, resulting in a satisfactory approximation

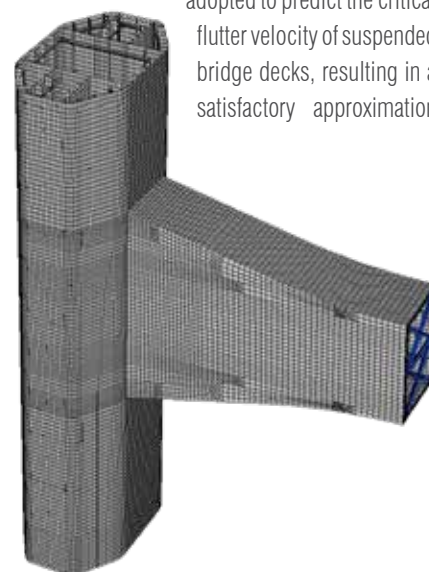
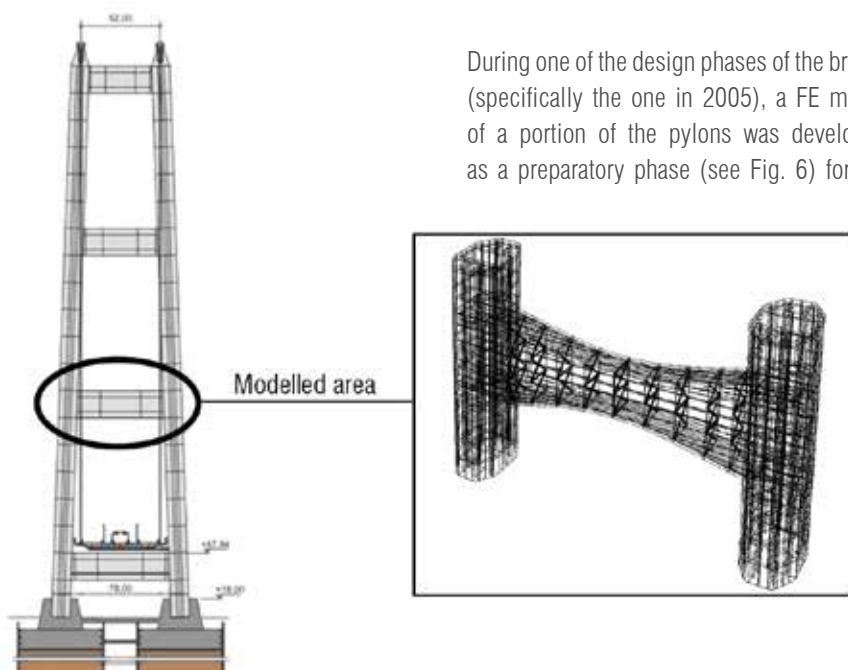


Fig. 6. Bridge over the Strait of Messina: FEM model of Pylone-Traverso region.



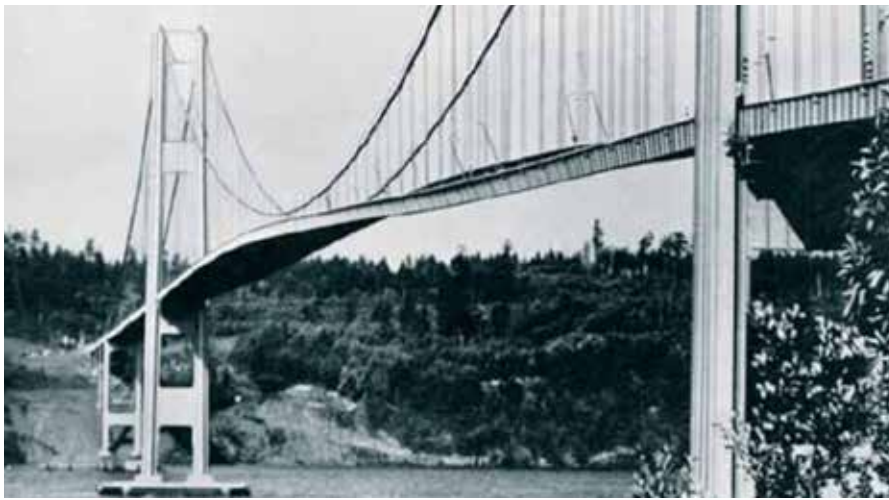


Fig. 7. The Tacoma Narrows Bridge in torsional oscillation on the morning of 7 November 1940. (from https://www.unirc.it/documentazione/materiale_didattico/599_2010_264_7525.pdf)

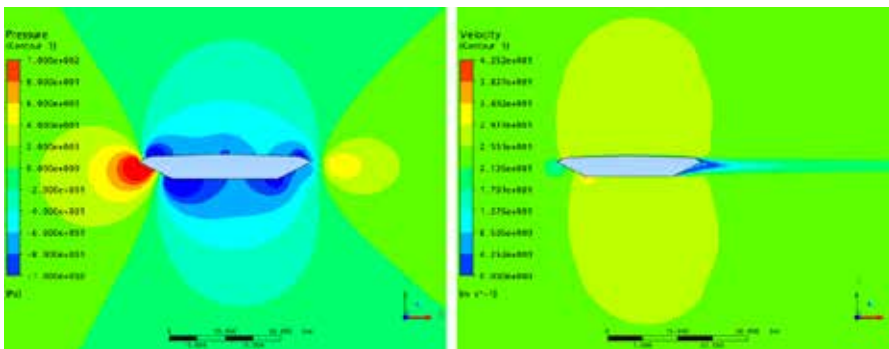


Fig. 8. 2D CFD model of a section of the Storebælt Bridge: pressure and velocity field.

between the declared and calculated critical velocity values. In the benchmarks developed between 2010 and 2011, two bridges were referenced: the Storebælt or Great Belt Bridge in Denmark and the Strait of Messina Crossing Bridge between Sicily and Calabria.

Using CFD (computational fluid dynamics), 2D models were implemented and solved (see Fig. 8) of the deck (of the Storebælt, specifically) immersed in fluid. A variable angle of attack of the fluid section's relative velocity was associated with the fluid, and for each value of the angle and using a $k-\omega$ SST turbulence model, the lift (CL), drag (CD) and moment (CM) coefficients were calculated. These were subsequently used to solve the dynamic equilibrium equation:

$$M\ddot{x} + C\dot{x} + Kx = F$$

and determine, in the time domain, as the relative fluid-deck velocity and the value of the damping increase (this last of 2%, 3%, 5% with respect to the critical damping), the dynamic response, in terms of displacement

$x(t)$, of a 3D model representative of the bridge under investigation (see Fig. 9).

The wind speed for which the solution diverges (i.e. increasing vertical displacement and/or increasing rotation of the bridge's midsection — see, for example, the graphs in Figs. 10 and 11) constitutes the critical speed at which the flutter phenomenon occurs.

Obviously, a good design matches a critical velocity value greater than the wind speeds that were historically recorded and/or can be predicted at the site.

In Structural Engineering, FEM models are also developed during design definition for special structures whose functionality, strength and robustness must be considered in conjunction with the search for aesthetically “fascinating” solutions.

In addition to the installed conditions, which are characterized by loads resulting from the self-weights accidental actions, wind,

earthquake, and impacts, the assembly/installation phase is important for these structures. If designed competently, time can be saved on execution while also achieving the necessary safety for the workers involved in realizing the works.

The term “special structures” is used here to refer to those structures that are truly special in terms of morphology or size (large structures), using steel as the main material. Thus, we refer to structures that have little to do with the context of traditional civil construction. Such is the case of the roofing structures of stadiums dedicated to pedestrian sports or, in the Olympics, to athletics. It is also the case of structures to support and protect telescopes (such as the Extremely Large Telescope (ELT), which operates in the visible and infrared spectrum, or the Čerenkov Large Sized Telescope, which operates in the gamma-ray spectrum); or of protective structures such as the encapsulation of Reactor 4 of the Chernobyl Nuclear Power Plant.

Similar to the collaboration on several bridge projects briefly mentioned above, EnginSoft's structural engineering team supported Cimolai in the engineering development of several significant special structures, contributing technical knowledge and numerical simulation experience derived from its efforts in the field since the almost pioneering days of virtual prototyping applications. At the same time, the team's

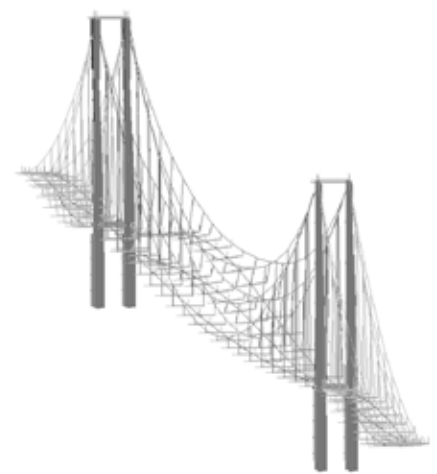


Fig. 9. Deformations of the Storebælt Bridge as the wind speed changes.

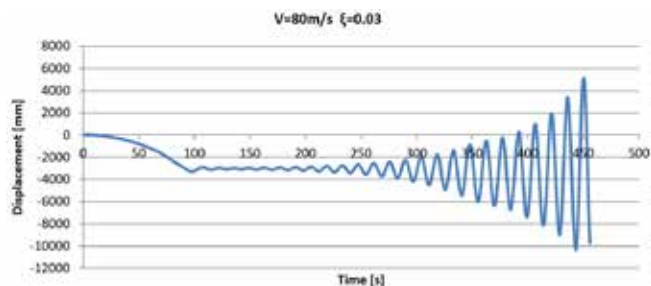


Fig. 10. Deformations of the central section of the Messina Strait Bridge at wind speeds of 80m/s (about 290km/h) and structural damping equal to 3% of critical damping.

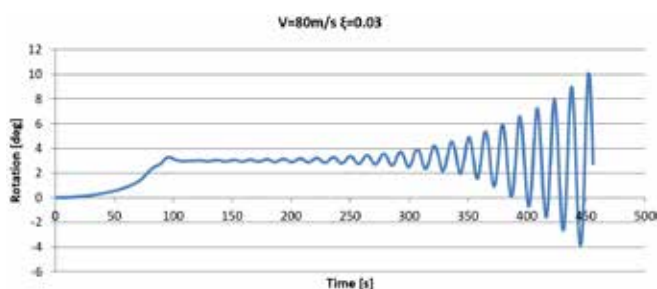


Fig. 11. Rotation of the central section of the Messina Strait Bridge at wind speeds of 80m/s (about 290km/h) and structural damping equal to 3% of the critical damping.

synergies with the expertise, skills and design knowledge of Cimolai’s managers/technicians helped to achieve the objectives with assured quality and within satisfactory timeframes.

Below we briefly describe some of the works to whose realization EnginSoft and its dedicated team made a significant contribution.

First and foremost is the roofing of what became the **Olympic Stadium in Athens** for the 2004 Olympic Games, designed by Spanish architect Santiago Calatrava and constructed by Cimolai using an innovative assembly sequence. EnginSoft contributed analytical supervision to the development of the overall FEM model of the roof (see Fig. 12) and directly developed detailed FEM models and specific numerical analyses of key areas of the roof structure such as its four ground supports (the so-called “shoes”, one pair of which is fixed to the ground and the other is movable to allow structural “breathing” and to avoid unwanted internal stresses — Fig. 13 shows the FEM model of a fixed “shoe”); and the four connection regions between the torsion tube and the arch (in which the arch push is absorbed by the arch);

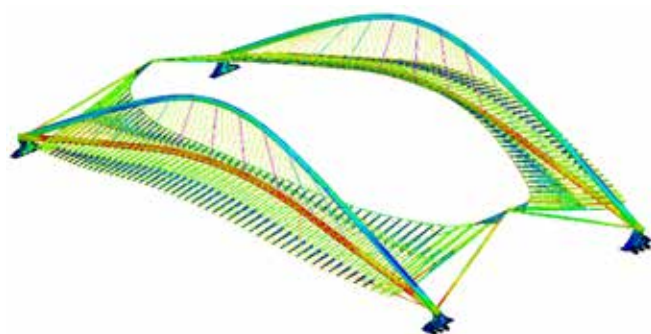


Fig. 12. FEM model of the roof of the Athens Olympic Stadium (2004 Olympic Games).

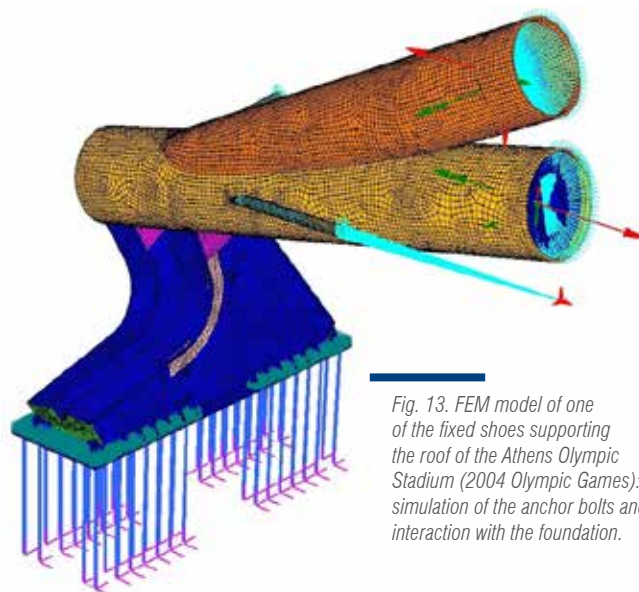


Fig. 13. FEM model of one of the fixed shoes supporting the roof of the Athens Olympic Stadium (2004 Olympic Games): simulation of the anchor bolts and interaction with the foundation.

and the two main connection nodes of the east and west halves of the roof or by the bolted joints connecting the ashlar used to construct the arch.

The **AVIVA Stadium in Dublin**, inaugurated in 2010, apart from hosting football matches, is a temple of rugby. This is only to be expected in Ireland where the game of the oval ball, imported from England in the second half of the 19th century, is played by more than 255 clubs. The state-of-the-art facility replaced Europe’s oldest sports ground, Lansdowne Road (dating back to 1872). In 2007, EnginSoft produced an overall FEM model (Fig. 14) of the roof structure of the stadium (built by Cimolai) primarily for the purpose of independently verifying the sections of the members drawn from earlier preliminary calculations. Naturally, normative verifications were conducted for the design load conditions to be considered, including those arising from wind actions, which were obtained from tunnel model tests due to the roof’s shape.

After assessing the general level of use of the members, some optimization of the structural efficiency, defined as the relationship between performance and weight, was performed in compliance with the regulatory requirements (EN 1993-1-1 and EN 1993-1-8).

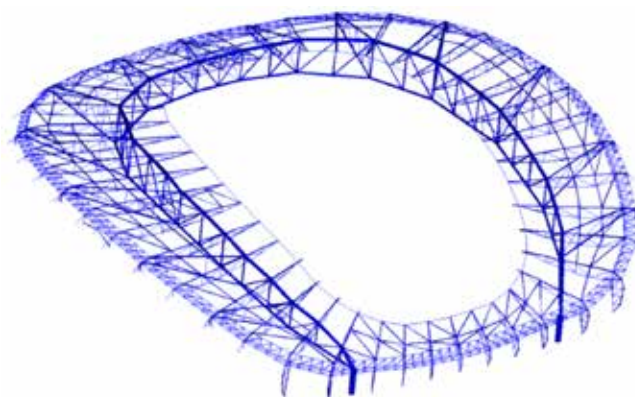


Fig. 14. FEM model of the roof of the AVIVA Stadium in Dublin in Ireland used for rugby and football.

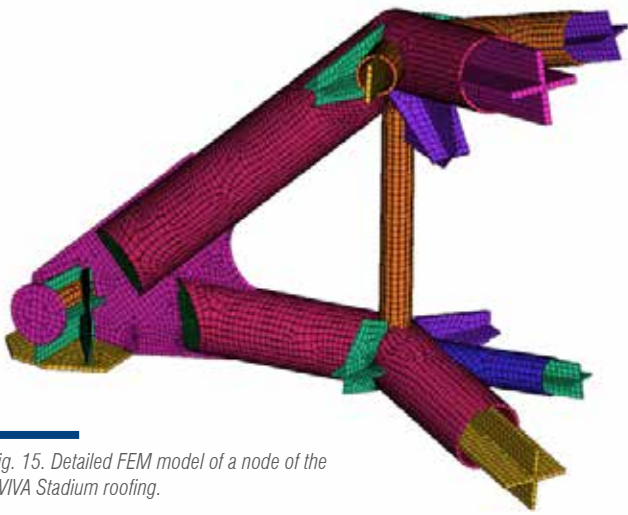


Fig. 15. Detailed FEM model of a node of the AVIVA Stadium roofing.

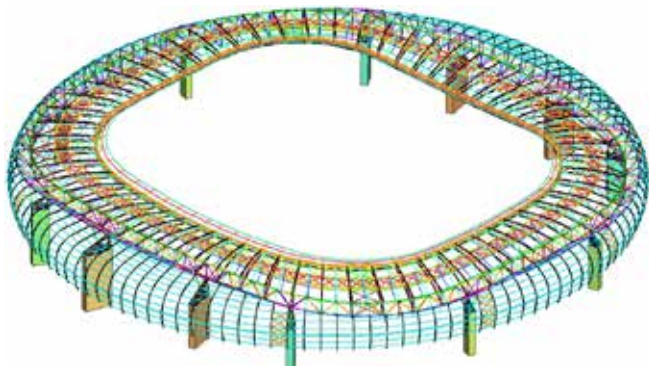


Fig. 16. FEM model of the roof of the Soccer City Stadium in Johannesburg in South Africa (2010 FIFA World Cup Final).

This was achieved by the iterative use of an automatic verification routine that updated the profile sections based on the structural responses, adjusted the properties of the members within the FEM model, provided instructions for re-running the analyses, and then used the new stresses to perform the necessary stress and stability checks. Investigations of localized stress situations at the nodes were conducted by means of detailed FEM models (see example in Fig. 15).

With regard to developing routines and/or verticalizations, and particularly for subjects that may require normative verification, FEM models implemented with commercial software must frequently be supplemented with procedures that allow the search/processing/synthesis of all useful/sensitive data for identifying the levels of functionality, safety and reliability of structures that are far from trivial. These virtualizations, implemented almost daily by EnginSoft not only in Structural Engineering, undoubtedly constitute additional value to complete products (commercial software) that sometimes lack post-processing tools.

In 2007, EnginSoft also created the full FEM model of the roof structure of **Johannesburg's Soccer City Stadium** built by Cimolai for the 2010 World Cup in South Africa (see Fig. 16). After completing the model with all the design load conditions necessary to qualify the structure's behaviour during its operational life, structural analyses were performed to determine the stresses used for code checks

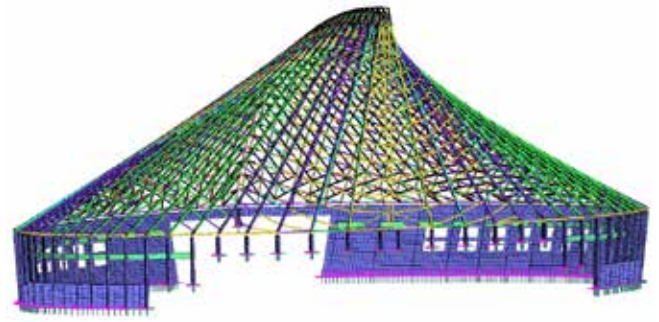


Fig. 17. Multipurpose sports complex in Tor Vergata in Rome in Italy: FEM model of one of the two roofs.

and conducted using automatic verification routines, implemented in accordance with both DIN 18800 and EN 1993-1-1. Once these routines had been tested, all of the constituent members of the structure were checked for all design load conditions. Calculations and verifications were supplemented with numerical analyses on detailed FEM models of some critical areas characterized by intersections of members and the presence of bolted connections.

Another significant contribution from EnginSoft in 2008 concerned the engineering of the two roofs of the **Tor Vergata Multipurpose Sports Complex in Rome in Italy**, designed by Santiago Calatrava and built (actually only one of the two) by Cimolai. These roofs were generated on ruled surfaces and characterized by families of nodes with topologically equal but dimensionally different geometries. Once the overall FEM model was finalized complete with the reinforced concrete support walls of one of the two roofs (see Fig. 17), structural analyses were performed for all the design conditions foreseen for ULS (Ultimate Limit State) and SLS (Serviceability Limit State) to determine the stresses to be used for the normative verification according to EN 1993-1-1 for members and EN 1993-1-8 for welded

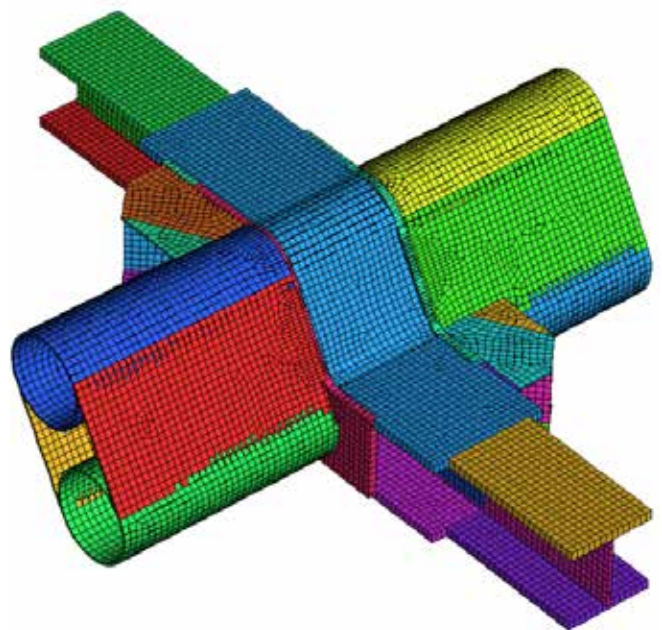


Fig. 18. Multipurpose sports complex in Tor Vergata in Rome in Italy: Parametric FEM model of a node.

and bolted connections. The bolted joints were dimensioned according to two different stress transfer mechanisms, namely the friction mechanism for SLS conditions and the shear mechanism for ULS conditions.

To finalize the structural control of the entire roof, detailed parametric FEM models of the strut-brace joints were implemented (see Fig. 18) in addition to the overall FEM model, in order to obtain topologically “equal” but dimensionally different geometries.

In essence, the notable parameters were obtained by operating on the actual dimensions of each node within the same family/type, resulting in virtual prototypes on which the stress parameters relevant to that specific family were obtained. This was done after having performed an envelope of the stress parameters relevant to that specific family (identified, for example, by a specific interval of the angle between the plane containing the axes of the two struts and the planes containing the axes of the braces or even by a specific interval of the distance between the working points on the axes of the two struts).

The virtual prototypes were then used for numerical analyses, also in material non-linearity (according to Annex C of EN 1993-1-5) to evaluate and validate both the stress fields and, for nodal regions characterized by gross structural discontinuities and therefore by stress peaks with values above the proportionality limit, the associated plastic deformations were also evaluated and validated.

Conclusions

The ability to develop advanced designs is undoubtedly proportional to the skills acquired in using software (programs/calculation codes) dedicated to implementing FE models and to executing the numerical analyses necessary to evaluate the relative structural responses.

In this sense, software can improve productivity, accuracy, and efficiency, as well as enable complex and innovative projects to be tackled. However, being familiar with the software may not be sufficient. In



fact, a common mistake in interpreting the predictions of a FE model is to not consider the limitations of the model — no matter how complex and complete it may be.

This may sound trivial, but every model is based on assumptions that impose limitations on its scope of applicability. If the assumptions and formulations underlying the prototyping/simulation process are not robust and relevant, the results will only support inaccurate or even unsupported solution scenarios. In other words, apart from aspects related to so-called artificial intelligence (which in any case only responds on what it has “learnt” and does not understand creativity and empathy), the model will return as a function of the hypotheses and theories on which it is based. If these are inaccurate or imperfect, or if the model lacks representativity, the computer can only react accordingly. From this point of view, a university professor of Automatic Calculation of Structures (namely Stefano Odorizzi, President of EnginSoft) told me in 1979 that computers are a school that trains humility.

This is why Structural Engineering requires the constant acquisition and deepening of technical-theoretical skills to which knowledge of calculation software becomes an effective complement. It goes without saying that continuous learning accompanied by a healthy curiosity and a determined desire to move beyond one's personal comfort zone are essential to maintaining a high level of skill, to overcoming challenges, to identifying solutions, and to providing answers to ever newer and progressively stimulating questions.

For more information:
Livio Furlan – EnginSoft
l.furlan@enginsoft.com



Structural Engineering | Part 2

Beyond the Otherness between Art and Technique

by **Livio Furlan**
EnginSoft

This continues and concludes the reflections on Structural Engineering as an Alterity between Art and Technique. It begins with the regulatory framework that Structural Engineering cannot ignore.

Speaking of standards...

Structures must be designed to ensure their safety. However, good practice may often be insufficient, especially if the structures are complex. Safety is defined through the use of specific standards that determine approaches, criteria, rules, and relationships that must be considered during the design phase so that the design is not over-dimensioned and does not have any deficiencies that may compromise its safety.

Historically, structural engineering has used the calculation and verification criteria associated with the Working Stress Design (WSD) method, also known as the Allowable Strength Design (ASD) method. It is based on purely deterministic criteria, i.e. it assumes that all loads considered cannot exceed their nominal value. This same assumption also applies to the value of material resistance, which

is obtained by dividing the characteristic strength (which may be the yield strength) by an appropriate safety coefficient.

In this sense, the WSD method uses a single safety factor irrespective of the type of load, although, for conditions defined by environmental loads, the “basic” admissible stress may be increased (e.g. by 12.5% according to the CNR-UNI 10011 standard, now out of use, or by 33% according to the AISC — Manual of Steel Construction 9th Edition standard), provided that the stresses caused by these environmental loads are lower than those caused by permanent loads.

But how should one proceed if one is dealing with a calculation action that has greater uncertainties (and is, therefore, ill-defined) compared to other design actions? To simplify, one may decide to proceed by adopting the Load and Resistance Factor Design (LRFD) method (or Limit-State method), which is supported by many years of research and which has actually been made almost compulsory by current standards such as EN (1990 to 1999), ISO (19900 to 19904), and NTC 2018 in Italy.

The method allows higher safety margins (in the form of higher partial safety factors) to be applied to design parameters that are considered less predictable or that could have a negative impact on the design. This provides a more explicit way of accounting for the uncertainties introduced by design parameters, compared to the WSD method.

Therefore, behind the seemingly trivial relationship:

$$E_d \leq R_d$$

whereby E_d and R_d are defined respectively as the design values of the generic effect (E_d) taken into consideration, and of the corresponding resistance (R_d) within the limit state examined (Ultimate — ULS, Serviceability — SLS), one must verify, by means of the method of partial coefficients, that no limit state is violated in any design situation. There are also statistical studies of structural reliability that have resulted in the definition of values for the various partial safety factors and combination factors that consider the probability of different events occurring simultaneously (and unfavourably) to that specific structure.

Evaluation of the structural response to seismic action

For structures in general, and therefore also for special structures and/or for large structures as well as bridges, determining the response to seismic events is fundamental and must be placed within specific regulatory requirements/standards.

Italy has created an operational framework aimed at enhancing the precise specification of the basic seismic hazard. In the governing Italian regulations, NTC 2018, a basic seismic hazard is defined in terms of the maximum expected horizontal acceleration, a_g , in free field conditions on a rigid reference site with a Category A horizontal topographic surface, as well as the ordinates of the corresponding elastic response spectrum in acceleration, $S_e(T)$, with reference to pre-established PVR exceedance probabilities, in the reference period V_R . NTC 2018 foresees four Limit States for seismic action, two of which are Operational (SLO and SLD) and two Ultimate (SLV and SLC). They are briefly summarized below:

- Immediate Operational Limit State (or *Stato Limite Operativo*, SLO) is particularly useful as a planning and design reference for works that must remain operational during and immediately after an earthquake (e.g. hospitals, military barracks, civil protection centres);
- Damage Limit State (or *Stato Limite di Danno*, SLD) is instead defined as the limit state that guarantees only temporary uninhabitability in post-earthquake conditions; in other words, the damage occurring for this limit state must not put users at risk and must not significantly compromise the structure's resistance and stiffness to vertical and horizontal actions, thereby guaranteeing continued use even if the use of (part of) the equipment is interrupted;
- Lifesaving Limit State (or *Stato Limite di Salvaguardia della Vita*, SLV) in which there is substantial damage to structural components and a (significant) loss of stiffness in relation

to horizontal actions, but the structure maintains part of its resistance and stiffness against vertical actions and offers a margin of safety against collapse from horizontal seismic actions;

- Collapse Limit State (or *Stato Limite di Colasso*, SLC), in which the structure has experienced serious breakage and collapse of the non-structural and plant engineering components and very serious damage to the structural components, but still retains a margin of safety for vertical actions and a small margin of safety against collapse from horizontal actions. This last limit state is particularly suitable as a design reference for certain structural types (structures with seismic isolation and energy dissipation).

Consequently, the four limit states allow four different situations to be identified. As the seismic action progressively increases, the four limit states, ordered by increasing seismic action (SLO, SLD, SLV, SLC), are progressively exceeded, corresponding to a steady increase in the damage to the structure, its non-structural elements, and its systems overall. This unambiguously and almost continuously identifies the performance characteristics that are required of a generic construction.

In terms of the contribution of computational methods to determining the structural response to seismic action, four types of analysis are allowed, each of which depends on the geometric simplicity (or complexity) of the structure being analysed and on the design performance target, by which engineers verify that the structure can withstand the design event, and even, often importantly, establish how the structure withstands the event, i.e. to what level of damage.

These four computational methods are:

- Linear Static Analysis (LSA),
- Linear Dynamic Analysis (LDA),
- Non-Linear Static Analysis or Pushover (NLSA),
- Non-Linear Dynamic Analysis (NLDA).

The linear analyses (LSA and LDA) involve elastic analyses for determining the deformations and stresses of each structural component. Any non-linearities are conventionally considered through appropriate parameters. Therefore (as stated in Section 7.3.1 of NTC 2018) linear analyses can be used to calculate seismic demand for both non-dissipative and dissipative structural behaviour. In both cases, whatever modelling is used for the seismic action, seismic demand is calculated by referring to the design spectrum obtained for each limit state and by assuming the limits/values specified in the standard for the behaviour factor q , which are a function of the structural type and ductility class.

In all cases, linear procedures must be used with awareness and rationality since they are likely to provide unrealistic results if the structure's behaviour under earthquake action deviates significantly from the elastic one, or if there are localized ductility requirements, or for tall buildings that are generally characterized by pronounced elastic-plastic behaviour.

Non-linear types of analyses involve static (pushover) analyses by applying monotonically increasing horizontal forces to the structure up to a predetermined limit (NLSA), or dynamic step analyses with direct integration of the equation of motion (NLDA).

Non-linear approaches allow elastic-plastic modelling of the structure with the possibility of considering during analysis all dissipative capacities that the structure is able to exhibit and that cannot be considered directly in a linear procedure.

The following combinations should be considered for LSA, LDA and NLSA methods:

$$\begin{aligned} &1.0 E_x + 0.3 E_y + 0.3 E_z \\ &0.3 E_x + 1.0 E_y + 0.3 E_z \\ &0.3 E_x + 0.3 E_y + 1.0 E_z \end{aligned}$$

where:

- E_x represents the set of effects (stresses and displacements) caused by applying the seismic action along the chosen horizontal x-axis of the structure;
- E_y represents the set of effects (stresses and displacements) caused by applying the same seismic action along the orthogonal horizontal y-axis of the structure;
- E_z represents the effects (stresses and displacements) arising from applying the vertical component of the seismic action.

Linear static analysis

Linear static analysis consists of representing the structure (via beam and/or shell elements) as a linear elastic system, and the seismic action as a system of static forces applied near the individual nodes/slabs where the masses of the structure/construction are assumed to be concentrated. After implementing the FEM model, we proceed to solve the equation:

$$Kx=F$$

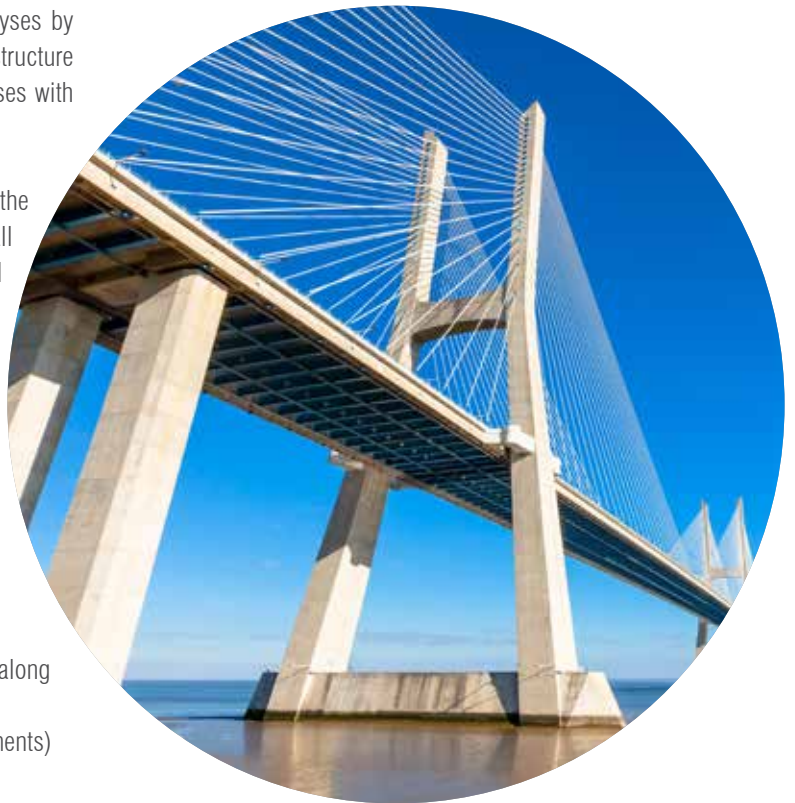
where K is the structure's elastic stiffness matrix, x is the vector of generalized nodal displacements (i.e. displacements and rotations, the result of the solution), and F the vector of equivalent seismic actions.

The calculation of displacements results in determining the stresses acting on the various structural components; their investigation is completed by normative verifications.

This method allows a system of forces approximating the structure's first mode of vibration to be applied to the structural model. Consequently, linear static analysis returns reliable results only if the structure's seismic response in each principal direction is not significantly affected by vibration modes greater than the first (NTC 2018, Section 7.3.2).

Linear dynamic analysis

Linear dynamic analysis is actually the so-called modal analysis with response spectrum (again, see NTC 2018). Proposed by R. W.



Clough and E. L. Wilson in the early 1960s, this procedure determines the effects of seismic action after first determining the eigenvalues (eigenfrequencies) and eigenvectors (modes of vibration) of the structure considered in the elastic field.

In essence, the equation:

$$Mx''(t)+Cx'(t)+Kx(t)=-Mx''_g(t)$$

which summarizes the dynamics of the structure subjected to an earthquake, where M is the mass matrix (of the structure), C its damping matrix, K its stiffness matrix, and $x''_g(t)$ the ground acceleration defined by the seismic event, is solved in the space of eigenvectors identified through modal analysis, with the seismic forcing represented by the elastic spectrum relative to the specific limit state under consideration. The analysis must account for all modes of vibration that contribute significantly to the dynamic response of the structure.

The current standard (see Section 7.3.3.1) requires all modes with significant participating masses to be considered. This criterion is considered satisfied if the sum of the effective modal masses, for all the modes considered, totals a significant percentage of the structure (85%), or if all modes with participating masses above a minimum percentage (5%) are considered.

Each of the vibration modes identified is associated with a participation coefficient, and this in turn makes it possible to evaluate the maximum vectors of the equivalent static forces relative to the various modes in relation to the design spectrum. Once the maximum effect in terms of stresses and displacements at each point of the structure being analysed has been found for each vibration mode,

the overall effect is evaluated by considering the contribution of each mode of vibration to the maximum response.

The maximum probable value, E , of any effect (displacement, stress, etc.) is given by statistically derived formulae. The most commonly used combinations of seismic responses to obtain maximum effect values are: SRSS (square root of the sum of the squares of the modal responses), E_i and CQC (complete quadratic combination).

The current standard requires the proper use of the CQC combination, defined by the following relationship:

$$E = \sqrt{\sum_i \sum_j \rho_{ij} E_i E_j}$$

where:

- E_i and E_j are the effects relative to modes i and j
- ρ_{ij} is the correlation coefficient between mode i and mode j , calculated by proven methods such as the one below:

$$\rho_{ij} = \frac{8 \sqrt{\xi_i \xi_j} (\beta_{ij} \xi_i + \xi_j) \beta_{ij}^{3/2}}{(1 - \beta_{ij}^2)^2 + 4 \xi_i \xi_j \beta_{ij} (1 + \beta_{ij}^2) + 4 (\xi_i^2 + \xi_j^2) \beta_{ij}^2}$$

where

- ξ_i and ξ_j are the viscous dampings of modes i and j
- β_{ij} is the ratio of the inverse of the periods of each i - j mode pair ($\beta_{ij} = T_j/T_i$)

Non-linear static analysis (pushover analysis)

A structure's ability to resist seismic action depends primarily on its ability to deform in a ductile manner. In static and dynamic methods of elastic analysis, possible excursions in the plastic field are conventionally evaluated through the use of the behaviour factor q , which reduces the elastic spectrum but does not provide any information on the actual distribution of inelasticity demand when the elastic limit is exceeded.

This is where pushover analysis (non-linear static analysis on a multi degrees of freedom (MDOF) model) can be performed. It consists of subjecting the structural model with associated non-linearities of material and geometry to gravitational loads and to a system of lateral forces that represent the inertial forces activated by the earthquake, which are increased monotonically so as to increase the horizontal displacement of a control point in the structure (e.g. the centre of gravity of the top floor) until the ultimate conditions are reached.

Numerically speaking, this means that the material response, due to inelasticity, can no longer be predicted by a single parameter (the slope of a straight line in the stress-strain plane), but can only be simulated by following the relationship between these two quantities step by step. This in turn implies a transition to an incremental analysis in which, at each load increment, appropriate solving methods (e.g. the Newton-Raphson iterative method) have to be applied to trace the curve representing the intrinsic elastic-plastic behaviour of the material as closely as possible.

The end result of pushover analysis is the building capacity curve, also known as the pushover curve, which is a diagram in which the abscissa shows the displacement value of the control point and the ordinate the base shear.

After introducing the SDOF (single degree of freedom) system, equivalent to the "real" MDOF structural system (see Section C7.3.4.2 of Circular No. 7 of 21 January 2019 C.S.LL.PP.), we assess the displacements of the structure at predefined seismic load levels and check that the displacement requirements exceed the displacements for achieving the reference performance levels, evaluated according to the pushover analysis on the "real" model.

Pushover analysis also enables the behaviour factor q to be determined and thus permits more reliable linear dynamic analyses in terms of structural behaviour that implicitly accounts for the elastic-plastic response.

Non-linear dynamic analysis (time history)

This type of analysis, also called path following analysis (pushover analysis is a path following analysis) allows the seismic response of the modelled structure to be assessed by directly integrating the equations of motion, thus considering the non-linear behaviour of both material and geometry. Gravity loads and accelerograms compatible with the elastic response spectrum(s) are applied to the three-dimensional model of the structure, which is represented with beam and/or shell elements as appropriate.

This is the most complete procedure for evaluating a structure's stresses and deformations in the time domain, however, it is also the most complex form of analysis requiring close attention to defining a model capable of describing the structure's post-elastic behaviour to load-unload cycles, as well as careful selection of the accelerograms to be used.

For this latter reason, the Italian standard requires the use of at least three triads of accelerograms (each characterized by three



accelerograms acting simultaneously in the three main directions) to calculate the heaviest response. Here it is important to remember that the main qualitative difference between linear and non-linear analysis is the fact that the principle of superposition of effects is lost.

In linear analysis, the structure's response to a combination of different actions can be obtained by totalling the single responses for each of the actions that "belong" to that specific combination; in non-linear analysis, on the other hand, each of the possible load combinations (and not each action) must be analysed.

As already mentioned, incremental path-following analyses require suitable solution methods such as the iterative Newton-Raphson method. One disadvantage of this method is that it does not allow post-peak strength loss (corresponding to softening behaviour) to be captured without the addition of specific numerical techniques.

In fact, due to its formulation, the Newton-Raphson method is a poor choice in cases where the structure's stiffness matrix is not purely positive, impeding analysis in problems that present instabilities in the form of loss of stiffness (of a geometric and/or material nature).

To overcome this difficulty, various numerical strategies are often used with the Newton-Raphson method, including the Arc Length or Modified Riks Method. Used as an extension to the Newton-Raphson method, this is a powerful numerical technique to solve systems of highly non-linear equations efficiently and accurately even where Newton-Raphson fails.

Case study of the seismic improvement of a nuclear power plant

The challenges that arise can have considerable formal and conceptual complexities. Therefore, it is worthwhile analysing the case of the redevelopment of a nuclear power plant because of the breadth and articulation of the activities developed.

For this nuclear power plant, specific studies performed in the last decade of the last century and in the first decade of the 2000s identified a new and higher seismic hazard value, on a probabilistic basis and for a return period of 10,000 years, compared to the one used during the plant's design phase. This resulted in the definition of a precise RLE (Review Level Earthquake), which required a seismic adjustment of the buildings constituting the facility.

The associated RLE spectrum (see Fig. 1) relative to an SL-2-level earthquake according to the International Atomic Energy Agency i.e. with a return period of 10,000 years, is characterized by an average PGA (peak ground acceleration) of 0.143g, conservatively assumed to be 0.17g of horizontal acceleration, with a damping equal to 5% of the critical. The vertical spectrum is assumed to be two-thirds of the horizontal spectrum.

The seismic retrofitting of the power plant, developed by EnginSoft together with the contracting company, was conducted by specifically considering and modelling:

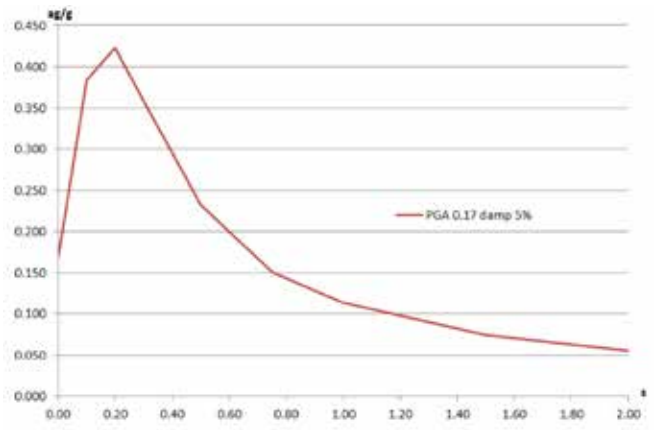


Fig. 1. RLE spectrum used in the multimodal dynamic analyses.

- the Reactor Building with:
 - the actual Reactor Building (housing the Reactor Primary Loop)
 - the Longitudinal Side Electrical Building
 - the Turbine Hall
- the Reactor Primary Loop
- the Auxiliary Building

The objective of the activities undertaken was to determine the seismic response of the above buildings and of the Reactor Primary Loop (RPL) to assess each structural element/component's safety level and to identify any structural improvements necessary to restore the safety margins to acceptable values.

The study, and the (correct) interpretation of over 2000 drawings, were used to generate the FE models of the structures (Reactor Building and Auxiliary Building) and of the RPL.

Shell elements were used to model the reinforced concrete structures (partitions, walls, full-thickness slabs, mixed-structure floors), while beam elements were mainly used to model the steel structures, given their type. Finally, shells, pipe elements and beam elements were used to model the RPL and its components.

The FEM models were statically analysed for the operating conditions defined by self-weight, permanent and temporary loads, snow loads and thermal loads (as well as pressure loads for the RPL). Subsequently, after extracting the eigenvalues (and eigenvectors) using the Block Lanczos algorithm combined with a sparse solver, multimodal seismic response spectrum analyses were conducted specifically for the Reactor Building, the RPL and the Auxiliary Building.

The two RLE spectra (horizontal and vertical) shown above were considered for the Reactor Building and for the Auxiliary Building. For the RPL (housed in the Reactor Building) and for other notable facilities/points identified by the customer the in-structure response spectra (ISRS), calculated from the results of dynamic analyses in the time domain conducted on the Reactor Building for seven different time histories of triplets of accelerations in x, y, z, were considered.

The following procedure was used to determine the ISRS of interest for the RPL. Transient analyses of the Reactor Building model were performed for the seven triplets of acceleration supplied by the customer. These were used to calculate the displacements in the time domain according to the directions defined by the three Cartesian axes, and the accelerations by double derivation. Next, using FFT, ISRSs (as a function of damping equal to 5% of critical damping) were assessed for each significant location of facilities and/or equipment. Then, the three ISRSs (in x, in y, and in z) were determined for each notable point as the average of the seven triads of spectra.

The differences in the structural responses of the Reactor Building were considered negligible when referring to the same equipment in the RPL. Consequent to this assumption, the acceleration spectra applied to the connection points of one equipment are the average of the acceleration spectra of all connection points related to that same equipment.

Regarding the response spectrum analysis of the Reactor Building (which consists of two nearly symmetrical parts separated by an expansion joint) specifically about 9,000+9,000 modes were used, so that a participating mass in the order of 90% of the relative total masses was “activated” for each part.

Therefore, some of the structure’s mass is lacking in the dynamic analysis. This was addressing by using the “missing mass method”. The high-frequency region of the spectrum ($> f_{ZPA}$ in Fig. 7) has no amplification of the peak acceleration of the input time history. In essence, an SDOF oscillator with a frequency $> f_{ZPA}$ is accelerated in phase and at the same amplitude (acceleration) as the applied acceleration.

A system with a fundamental frequency of $> f_{ZPA}$ is therefore correctly analysed as a static problem subject to a load equal to M times ZPA where M is the Missing Mass and ZPA is the Zero Period Acceleration. This concept can be extended to high-frequency modal responses ($> f_{ZPA}$) of multimodal systems.

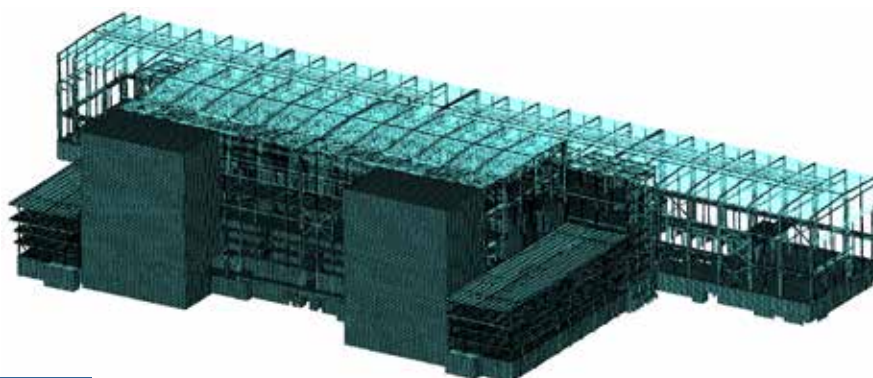


Fig. 2. FEM model (beam and shell) of the Reactor Building, Longitudinal Side Electrical Building, and Turbine Hall.

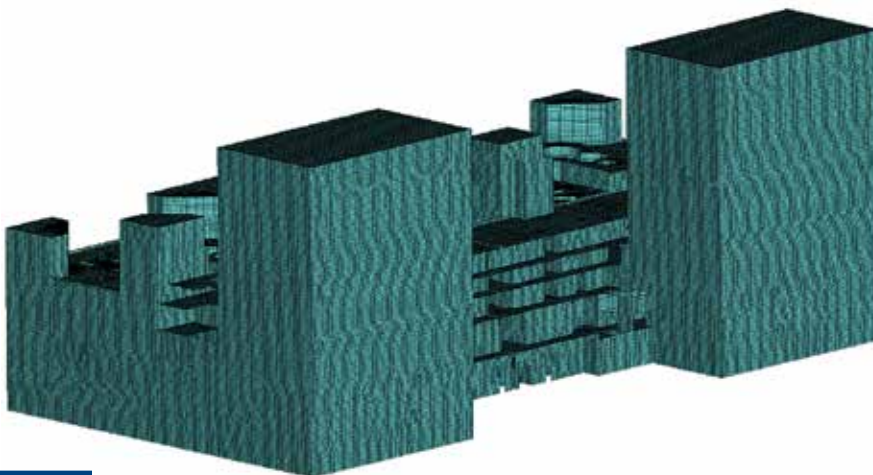


Fig. 3. Reactor Building: shell model of reinforced concrete parts.

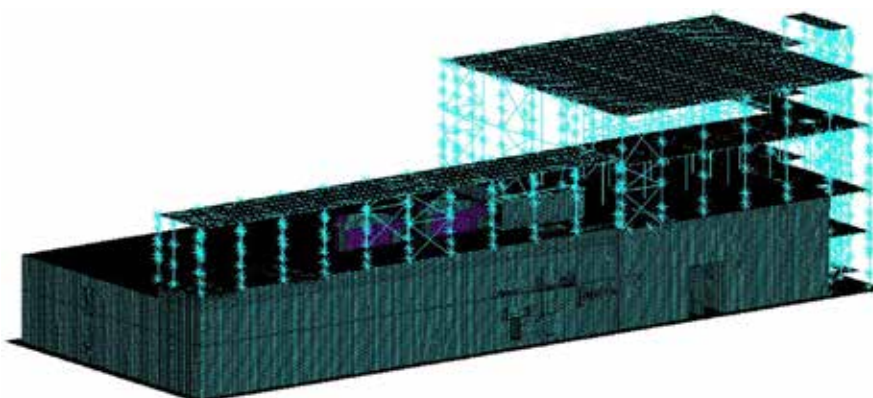


Fig. 4. FEM model (beam and shell) of the Auxiliary Building.

In computational terms, ZPA was assumed to be 0.23g. This corresponds to a frequency of about 30Hz ($T=0.0333s$) if we assume that the response spectrum varies linearly from $T=0s$ (0.17g) to $T=0.1s$ (0.348g). It should be noted here that the highest value of the extracted eigenvalue for the Reactor Building is about 30Hz.

It is common practice, as well as a requirement of some standards (including EN 1998-1 (EC8), which guided the seismic retrofitting of the nuclear power plant) to add some incidental mass eccentricity to

increase the distance between the centre of mass and the centre of stiffness.

This is easily resolved and clear for regular structures and/or in situations where the concepts of centre of mass and centre of stiffness are well-defined in general and in different planes. In these cases, eccentricity of mass is often described as an additional torsional moment defined by means of an “additional moment arm” (equal to 5% of the size of the plane perpendicular to the direction of seismic action) being applied to the seismic shear at different levels.

The Reactor Building is anything but a regular structure: it has a variety of partial interplanes, a very uneven distribution of stiffness, and parts of the structure that do not behave like a frame but are closer to a box structure since they somehow extend over more than one floor. As such, concepts such as centre of mass, centre of stiffness, and eccentricity of seismic shear at floor level do not apply to the Reactor Building in a manner that can be unambiguously defined.

This is also confirmed by the analysis of the modal forms: about 9,000 autosolutions (as mentioned above) were considered to capture over 90% of the mass participating in the seismic shear for each of two blocks forming the Reactor Building, and no decidedly dominant modes were found that could suggest how to apply eccentricities to improve torsional behaviour.

Therefore, the EN 1998-1 requirement (to consider accidental eccentricity) was addressed in two distinct phases:

- in the modelling phase, by considering that there is a random error in the quantification of masses, which satisfies or exceeds the effect of any arbitrary eccentricity of 5%;
- in the tension/resistance assessment following the analyses, by carefully examining the status of any critical structural elements (particularly walls and columns in peripheral regions) and suggesting, where appropriate, some feasible modifications to achieve additional safety margins.

To evaluate the seismic response (HCLPF calculation, see below), the loads related to the operating conditions were combined with actions resulting from the RLE earthquake:

- Static load combination: $1.0 D + 1.0 L + 1.0 E_{stat}$
- Seismic load combination: $1.0 RLE + 1.0 E_{dyn}$

where:

- D = Permanent loads (including self-weight)
- L = Accidental loads, in concurrent altitude with the presence of the earthquake
- E_{stat} = Static ground pressure
- RLE = Dynamic actions resulting from the earthquake RLE
- E_{dyn} = Dynamic ground pressure due to effects of the earthquake

The **HCLPF** (high confidence of low probability of failure) approach taken for seismic verification is based on the fact that almost all structures show at least some degree

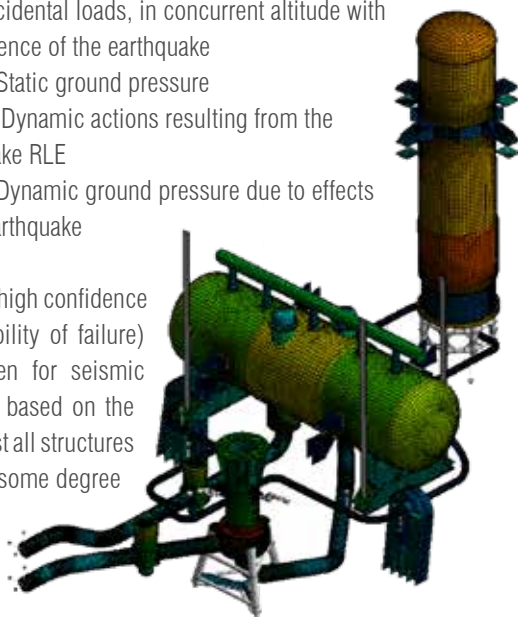


Fig.5. FEM model (beam, pipe, and shell) of the Reactor Primary Loop. All RPL interfaces with the Reactor Building are equipped with dampers, which were appropriately represented in the relevant FE model.

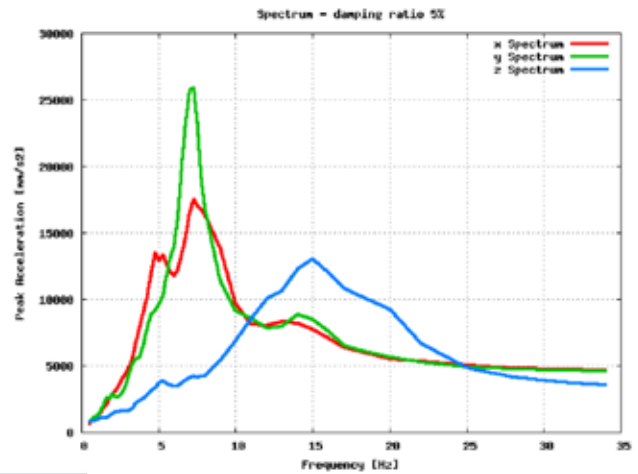


Fig. 6. RPL: in-structure response spectra for one of the notable points.

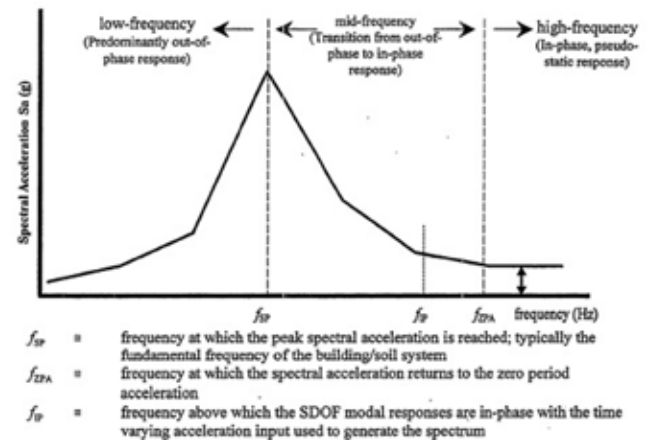


Fig. 7. Definition of ZPA and f_{ZPA} .

of ductility, i.e. the ability to deform beyond the purely elastic limit (ductility is defined by the behaviour factor, also referred to here as ductility factor).

Given the oscillatory nature of seismic motion, the degree of ductility can only increase the seismic margin against failure of structures or components.

HCLPF values for each structural element and for the whole set of structures pertaining to the upgrade, were calculated using the CDFM (Conservative Deterministic Failure Margin) approach as defined by EPRI NP6041-SL "A Methodology for Assessment of Nuclear Power Plant Seismic Margin" August 1991 Rev. 1.

The relationship used in the verifications, which is declined according to the type of structure (reinforced concrete, steel, steel-concrete), is as follows:

$$HCLPF = CDFM = \frac{C_{CDFM} - D_{NS}}{D_{CDFM} + \Delta C_{CDFM}} q RLE$$

and is derived from the equation "capacity = demand":

$$(FS)_E D_{CDFM} + D_{NS} = C_{CDFM} - (FS)_E \Delta D_{CDFM}$$

where:

- $(FS)_E = (1/q)(HCLPF/RLE)$ = Elastic scaling factor
- RLE = Review Level Earthquake (0.17g)

- q = Behaviour factor (or ductility factor)
- C_{CDFM} = Deterministic capacity of the section being checked
- D_{CDFM} = Deterministic elastic seismic demand calculated at RLE level
- D_{NS} = non-seismic demand for all non-seismic loads in the load combination
- ΔC_{CDFM} = Reduction in section capacity due to concurrent seismic loads

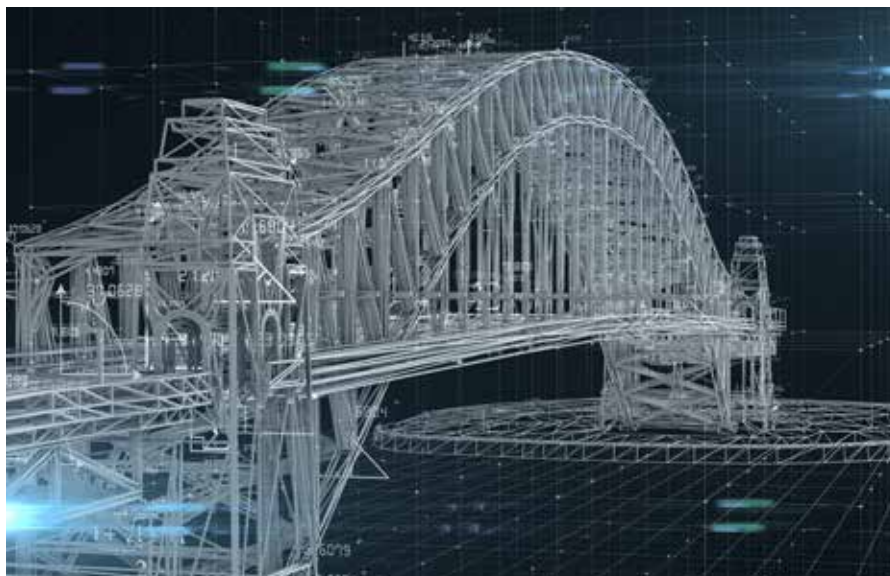
With reference to the behaviour factor q , the following conservative choice was made for all failure modes:

- $q = 1.25$ for systems/plants with dominant frequencies $< 8\text{Hz}$
- $q = 1.00$ for systems/plants with dominant frequencies $> 33\text{Hz}$
- q varying linearly between 1.25 and 1.00 for systems with dominant frequencies $> 8\text{Hz}$ but $< 33\text{Hz}$

Final conclusions

There can be no doubt that the introduction of Computational Analysis to Structural Engineering has greatly influenced the development of the design phase, not only in terms of calculation speed, but also in the procedural approach.

The focus of this important innovative and “evolutionary” phase is certainly structural modelling, to be understood as the process by which a structure and the actions acting



on it are reduced to a more or less simplified virtual prototype.

Use of the virtual representation of real behaviour is necessary because structures are generally remarkably complex physical systems whose behaviour is influenced by a large number of variables. But implementing a structural scheme that is both “lean” enough to be easily calculable and complex enough to consider the effect(s) of the most important variables is a crucial problem of structural design (or of the redevelopment and retrofitting of existing structures) since both the numerical accuracy of the analyses and the reliability of the results depend on its implementation. Therefore, what is needed is a “digital strategy” (modelling and simulation) that not only considers

what needs to be studied/designed, but also the tools, methods, models, data and IT infrastructure available.

This remains the major task of the Structural Engineer who must be able to operate at different levels of complexity and make choices to ensure that representativeness and reliability are not affected by approximations that relate more to decision-making than numbers.

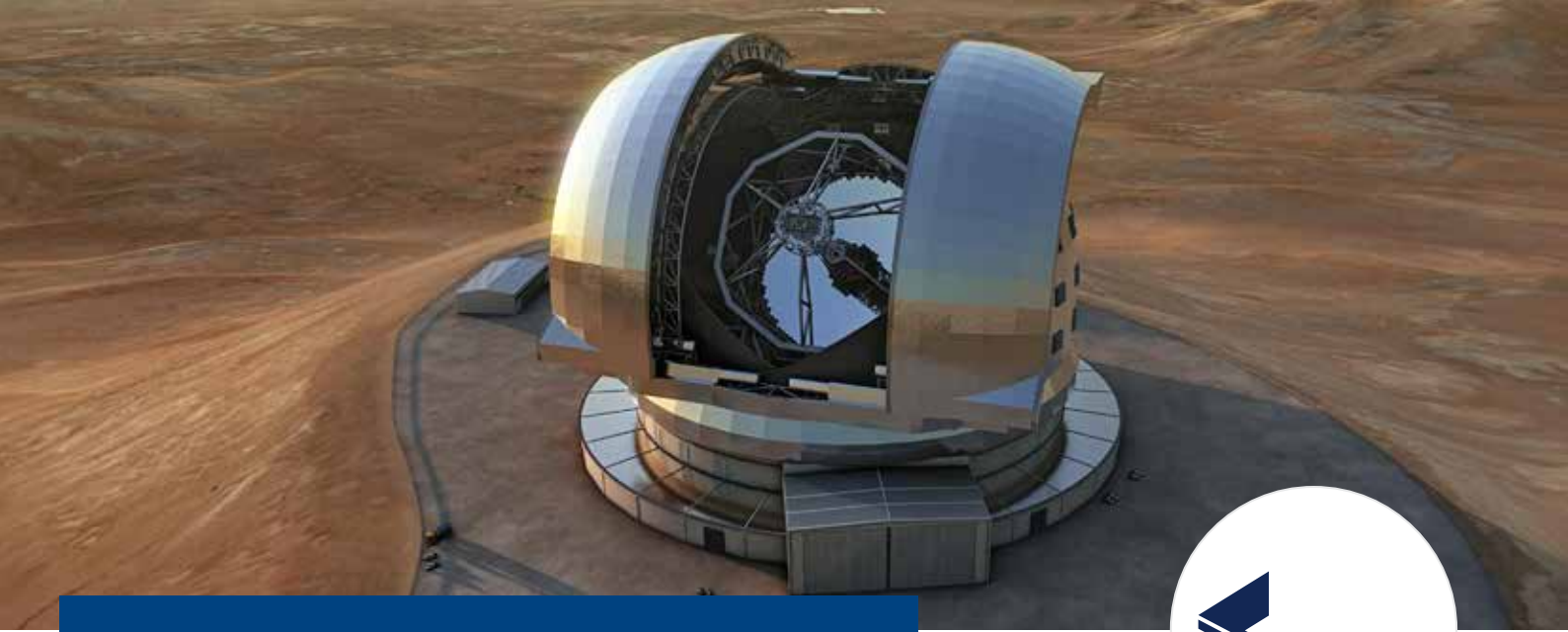
For more information:

Livio Furlan - EnginSoft
l.furlan@enginsoft.com

Without stones there is no arch... We are the stones... and we can build the arch!



Ponte della Maddalena at Borgo a Mozzano (LU).



CFD analysis for ESO's extremely large telescope (ELT) in Chile: Wind screening performance of the dome and main structure

by Cimolai, ESO

The Extremely Large Telescope (ELT) is a 40m-class optical, near and mid-infrared telescope located at Cerro Amazonas in the Chilean Andes about 150km south of the city of Antofagasta. Currently under construction, it will be the largest optical and infrared telescope in the world and will be operated and serviced by the ESO Paranal Observatory located approximately 20km away.

The design, manufacture, transport to site, assembly and testing of the ELT has been entrusted to the ACe consortium, led by the Italian company Cimolai. Success in this major engineering and technical challenge requires close cooperation between various technical and commercial departments, suppliers and workshops.

The telescope has an altitude-azimuth mount weighing approximately 4,700t housed in an enclosure called a dome and supported by a concrete base. The telescope itself comprises a rotating steel structure (the main structure, MS) that integrates numerous subsystems, including the optics, electronics, and controls.

In summary, the ELT consists of the following main components: concrete dome foundation and pier; auxiliary dome building; rotating part of the dome; concrete MS foundation and pier; rotating MS structure. The MS consists of a steel space-frame structure with a highly optimized rotating mass that simultaneously guarantees the dynamic requirements and system-level performance (including pointing stability and tracking capability).

To meet the performance requirements across the entire observation field, the telescope structure must be adequately protected from the action of the wind. Indeed, due to its large size, the mirrors and

hosted units (HU) are susceptible to wind effects that can affect the accuracy of observations.

A retractable windscreen (WS) was thus implemented to protect the mirrors and hosted units from gusts of wind by controlling the flow entering the dome chamber. The ELT windscreen has four porous aluminium panels, each with a span of 42m and a height of 10m, that can be fully deployed or retracted depending on the elevation of the main structure. Each is designed with a minimum permeability of 20% (ratio of perforated area to total area), necessary for thermal performance as it promotes air recirculation within the telescope to improve thermal homogeneity within the dome chamber during

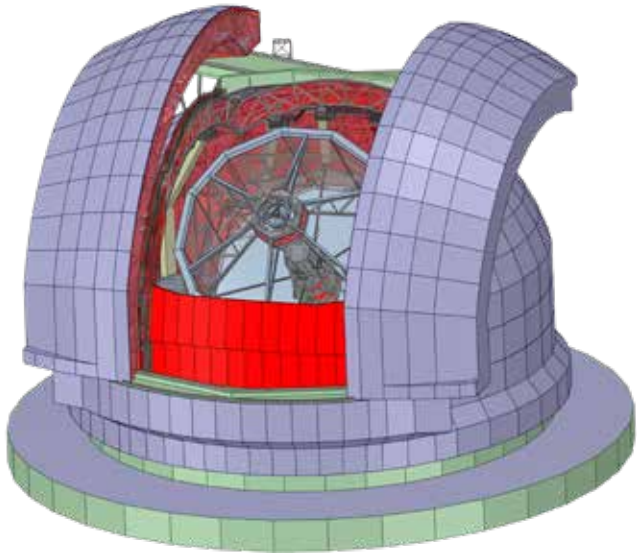


Fig. 1. Non-simplified DMS geometry.

observation. Thermal behaviour is, in fact, a crucial aspect of the main structure's performance.

A CFD (computational fluid dynamics) analysis was carried out to evaluate the windscreen's performance in controlling wind velocity in the vicinity of the mirrors and the hosted units under typical environmental conditions and to test different types of porous panels. Today, CFD has become common practice in the industrial process of civil structures as it provides an in-depth view of the flow field.

However, the geometric complexity of the dome and main structure (DMS) system (Fig. 1) does not support simplified modelling but requires an intense effort to condense the geometric and aerodynamic characteristics using a methodical, subsystem-based approach. This work was conducted by extensively using the concept of porous volumes, i.e. fluid volumes capable of representing specific aerodynamic properties of the real system.

Specifically, the characterization of the porous media representing the windscreen was performed in three steps: first, the CFD model of the panel, with explicitly modelled holes, was validated against experimental data obtained from wind tunnel tests (WTT) performed in previous design phases. Second, a porous numerical model of two different porous panel geometries one flat (OP) and one corrugated (CP), was characterized to provide the same pressure drop and deflection angles as the models with explicitly modelled holes, but with a reasonable computational effort.

Finally, a benchmark validation of the free flow was performed to demonstrate the effectiveness of the porous model in a real flow. A similar characterization was performed for the lattice structures inside the dome, which did not require explicit modelling. The porous models were then introduced into the overall CFD model, thereby enabling the calculation of the flow field inside the dome chamber for various angles of attack of the wind.

Modelling approach

Model objectives

A CFD model was constructed with the aim of determining the mean field of motion near the M1, M2 and M4 mirrors to verify the performance requirements of the windscreen, which were formulated in terms of the maximum permissible velocity in a series of specific probes, shown in Fig. 2:

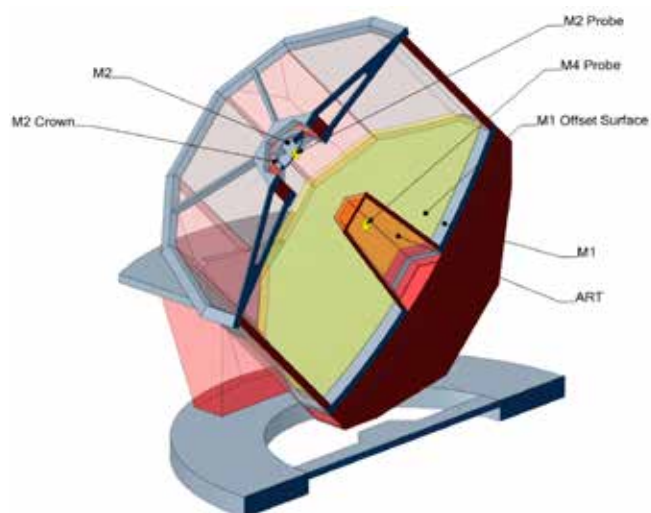


Fig. 2. Probe locations.

- Probes M2 and M4 positioned at the vertices of mirrors M2 and M4, respectively.
- M1 offset surface provides spatially continuous data interpolated from the values of the nearest cell node.
- M1 mean is calculated as a weighted average (facet area) over the entire offset surface.
- M1 max is the maximum (spatial) value on the offset surface.

The analysis was performed for different load cases (LC), different altitude positions and wind attack angles (Fig. 3):

- LC-AZ0-(20 | 60 | 90 | 180)-ALT45: altitude 45° and azimuth 0°, 20°, 60°, 90°, 180°, respectively, to evaluate performance in typical conditions.
- LC-WT-AZ0-ALT90: altitude 90° and azimuth 0°, considered to validate the model with the wind tunnel test.

In the two elevation configurations, the windscreen panels are correspondingly unfolded and modelled as independent bodies, allowing the airflow in the interstices to be simulated.

Sub-system decomposition

The ELT geometry is extraordinarily complex due to the large number of lattice truss structures and highly detailed components that may or may not affect the flow within the dome chamber. The introduction of porous media (Fig. 4) was necessary because such a highly detailed 3D CFD computational grid cannot be handled using reasonable

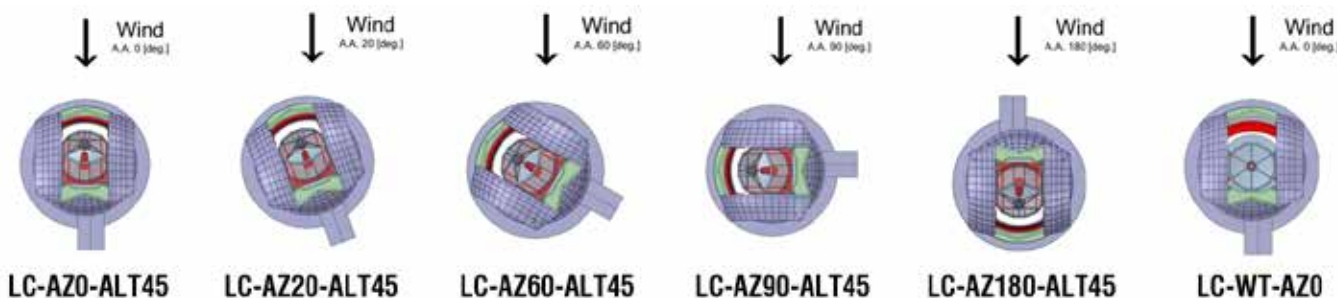


Fig. 3. Load cases.

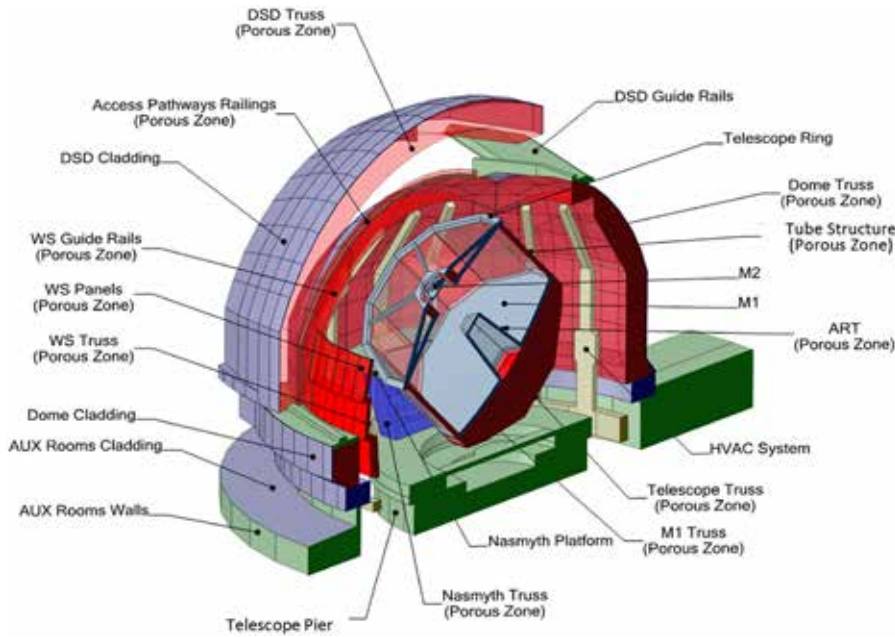


Fig. 4. ELT geometry and section.

computational resources. Porous zones are fluid volumes that enable the passage of air while offering the same resistance to flow as a real body but with a significantly reduced number of cells.

Numerically, this is accomplished by introducing a “sink” term in the Navier-Stokes equation that must be properly calculated. Given its primary importance in the aerodynamic behaviour of the structure, specific CFD tests were performed on the windscreen panel to correctly calibrate the porous media in terms of pressure loss and deflection angle.

Further CFD studies were conducted to estimate the pressure loss coefficients of other elements that are considered to affect the wind flow in the Hosted Units, such as the dome truss and dome sliding doors

(DSD) truss; the windscreen truss, the tube structure and the adaptive relay tower (ART) structure. Less detailed porous media were also used for other complex truss structures that have a marginal influence on the flow field. In these cases, an analytical fine-tuning of the porous parameters was conducted.

Porous media modelling Windscreen

Each windscreen panel consists of two porous zones: a thin high-resistance zone representing the perforated panels and a thicker lower-resistance zone representing the truss structure (Fig. 5).

Special care was required to develop accurate porous modelling of the thin perforated panel because it had to provide a realistic aerodynamic response for the actual panel both in terms of pressure loss and flow deflection. The porous model of the

perforated windscreen panel was developed in three stages:

- Validation of the CFD model of the perforated panel with explicitly modelled holes against wind tunnel data.
- Calculation of the porous model parameters providing the same pressure drop and deflection angles as the explicit CFD models of the perforated panel in two panel geometries, flat (OP) and corrugated (CP).
- Benchmarking the performance of the porous model for a finite-sized panel immersed in free flow.

Truss structures

Lattice structures are very numerous within the DMS. However, they play a minor role in influencing the flow field within the dome chamber, which is mainly driven by the outer cladding and the windscreen. Therefore, their effect was reproduced macroscopically through porous media (Fig. 6).

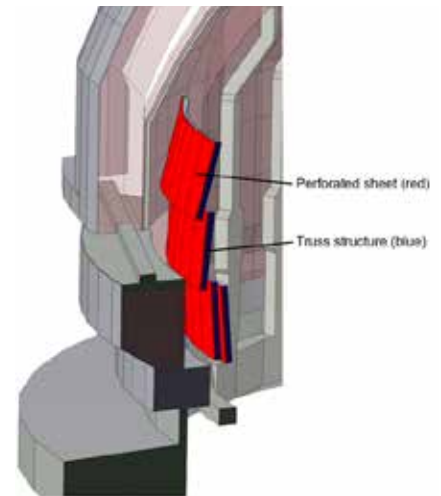


Fig. 5. Representation of porous windscreen.

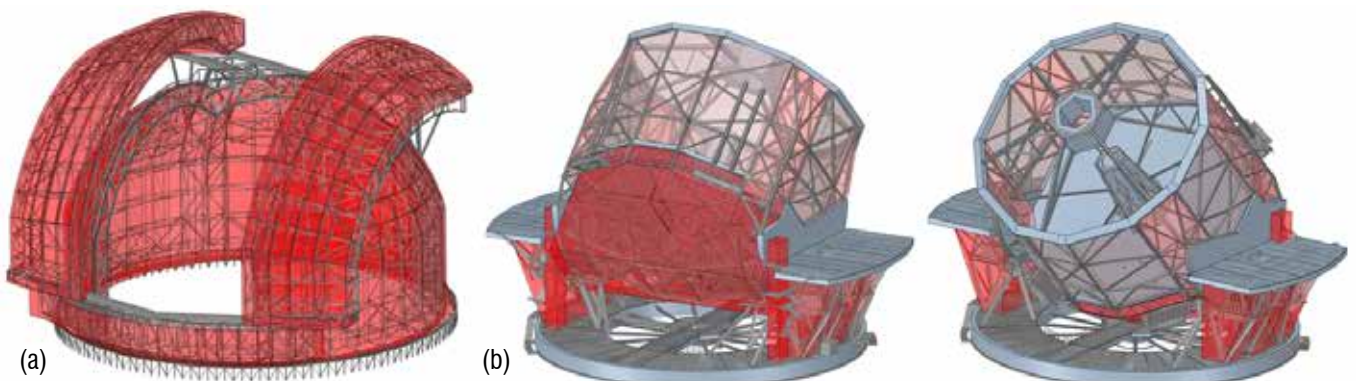


Fig. 6. Porous zones (red) of the dome and DSD and, b) of the main structures.

Pressure loss coefficients were defined using both an analytical and a CFD approach.

Overall CFD model

Model configuration

The purpose of this model is to determine time-averaged information for specific areas of the DMS structure, so a steady state RANS (Reynolds-Averaged Navier-Stokes) simulation was performed using Ansys Fluent software. The RANS equations are derived from the instantaneous Navier-Stokes equations using Reynolds decomposition, whereby an instantaneous quantity is decomposed into its time-averaged and fluctuating parts. Thus RANS equations include an apparent stress term (Reynolds stress), which originates from the fluctuating part of the non-linear acceleration terms and is solved using turbulence models.

In RANS methods, the entire turbulence spectrum is modelled and only the mean flow is resolved. RANS models have been remarkably successful in providing the industry with sufficient and reasonably accurate design information and are considered an industry standard. In this work, the Realizable $k-\epsilon$ Turbulence Model was used with the Ansys Fluent Scalable Wall Treatment.

Steady-state simulations were performed on a scaled model using the same geometric scale as the one used in the wind tunnel tests (1:70) to allow validation of the results. The boundary conditions applied to the overall model are summarized in Table 1.

Boundary	Velocity	Pressure	Turbulence Characteristics
Inlet	ABL	$\partial p/\partial x=0$	ABL
Outlet	$\partial U/\partial x=0$	ABL Outlet	Zero Gradient
Ground	$U=0$	$\partial p/\partial x=0$	Zero Gradient
Sky	Symmetry B.C	Symmetry B.C	Symmetry B.C
Left/Right	Symmetry B.C	Symmetry B.C	Symmetry B.C

Table 1. Overall model boundary conditions.

A correct ABL configuration at the inlet is essential to obtain meaningful results from a CFD study. Moreover, the inlet wind velocity profile and turbulence model variables (turbulent kinetic energy and viscous dissipation) were calculated so that the resulting wind profile at the telescope location are close to the requested environmental conditions. The roughness of the terrain was also set to allow the turbulence intensity to persist through the domain.

Mesh sensitivity

To check the numerical uncertainty, several simulations were performed with different grids showing that the simulation results were grid-independent. A grid independence study was performed to assess the best level of refinement of the grid (Fig. 7). Furthermore, an appropriate refinement was performed with approximately ten layers of inflation at the walls leading to y^+ between 30 and 300. The lower limit cannot be met for many surfaces within the dome due to the extremely low wind speeds. This has little impact on the

solution as it is reasonable to expect that the velocity and pressure fields inside the dome depend only marginally on the behaviour of the inner wall. Nevertheless, Fluent’s Scalable Wall Functions were used so that viscous regions could be modelled correctly in these situations. Since the windscreen is modelled as a porous volume it does not function as a wall and therefore y^+ cannot be defined for it.

Different model geometry assumptions were tested to assess the influence of the grid on the flow field at the probes, as shown in Table 2.

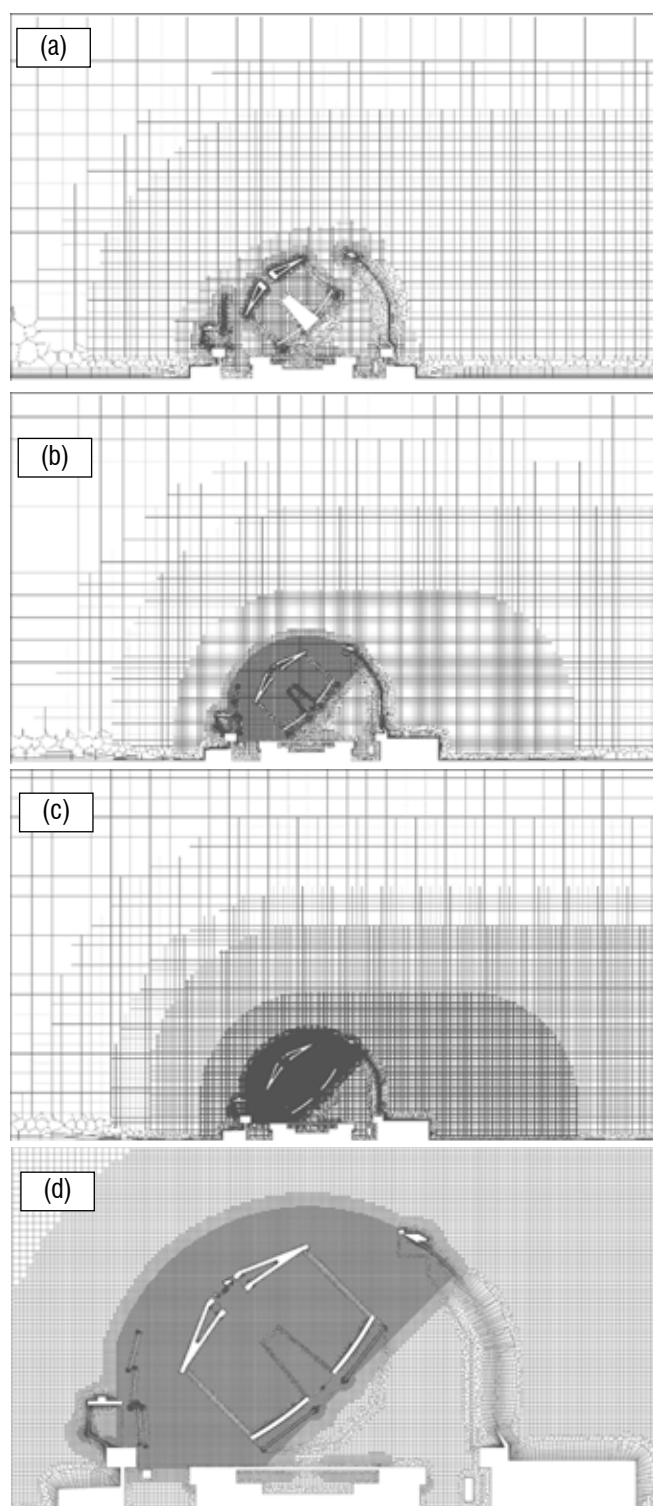


Fig. 7. Different levels of mesh: a) coarse, b) medium, c) fine, d) detail of fine mesh.

Mesh #	#of Cells	M1 mean	M1 max	M2 probe	M4 probe	Note
1	$8 \cdot 10^6$	$0.85V_{ref.1}$	$1.16V_{ref.2}$	$0.92V_{ref.3}$	-	Coarse Mesh
2	$24 \cdot 10^6$	$1.05V_{ref.1}$	$1.68V_{ref.2}$	$0.85V_{ref.3}$	-	Medium Mesh
3	$24 \cdot 10^6$	$1.01V_{ref.1}$	$0.99V_{ref.2}$	$1.00V_{ref.3}$	$1.01V_{ref.4}$	Same as 2. Porous ART and M2 are introduced
4	$24 \cdot 10^6$	$1.00V_{ref.1}$	$1.00V_{ref.2}$	$1.00V_{ref.3}$	$1.03V_{ref.4}$	Same as 3. Internal mesh inflation layer is introduced.
5	$40 \cdot 10^6$	$1.01V_{ref.1}$	$1.00V_{ref.2}$	$1.00V_{ref.3}$	$1.10V_{ref.4}$	Geometry same as 4. Model is in full scale (1:1)
6	$50 \cdot 10^6$	$V_{ref.1}$	$V_{ref.2}$	$V_{ref.3}$	$V_{ref.4}$	Fine mesh. Geometry and inflation layer settings the same as in 4.

Table 2. Mesh sensitivity results for LC-AZ0.

A full-scale simulation was also performed which demonstrated the independence of the result from the Reynolds number. Based on the results, mesh refinement grade 4 (Medium) was used for the complete calculations.

Results

This section shows a selection of representative results of the analyses in configurations LC-AZ0-ALT45, LC-AZ90-ALT45, and LC-WT-AZ0.

LC-AZ0-ALT45

In this load case the windscreen's performance is crucial as the incoming wind encounters no other obstacles. Fig. 8b shows the effect of the windscreen on the velocity field.

LC-AZ90-ALT45

In this load case, the opening is almost completely shielded by the DSD and dome cladding. The M2 mirror lies in the full slipstream of the cladding. The windscreen here has less effect on the flow field than in LC-AZ0-ALT45, however, some flow still enters through the observation slit in the slipstream of the dome cladding (Fig. 9).

LC-WT-AZ0

This simulation was performed specifically to validate the model's ability to accurately estimate speeds at the hosted units. It was quantified by comparing the results of case LC-AZ0-ALT90 against measurements in the wind tunnel test at the same probe locations. The wind tunnel model represents a comparable situation in terms of boundary conditions and elevation angle of the telescope.

Point	V WTT [m/s]	V CFD WS OP [m/s]	V CFD WS:CP [m/s]
P1	7.75	7.21	7.23
P2	2.81	2.92	3.08
M1-Top	0.31	0.34	0.38
M1-Centre	0.20	0.10	0.12
M1-Right	0.32	0.38	0.31
M1-Left	0.11	0.38	0.31
M1-Bottom	0.32	0.05	0.08
M2	4.26	4.84	4.88
M4	0.58	0.96	1.08

Table 3. Velocity comparison between the WTT and CFD.

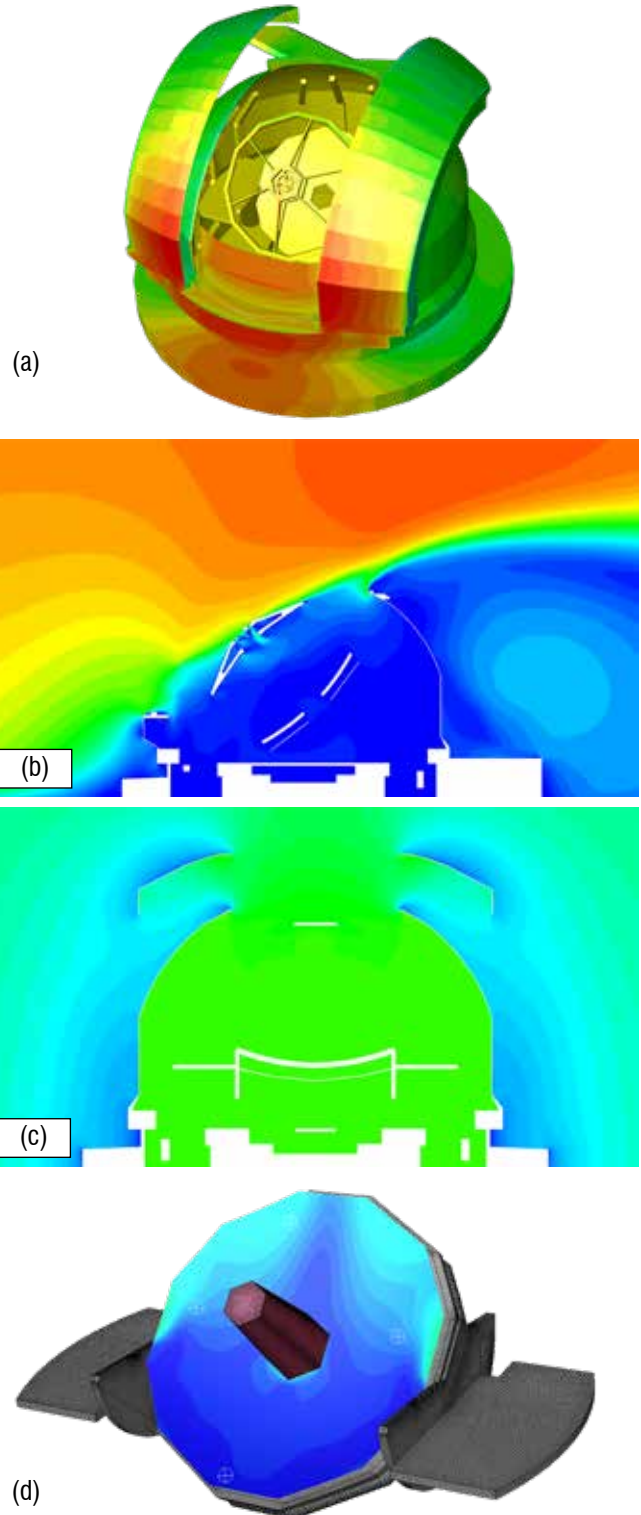


Fig. 8. Pressure contours: a) overall, b) orthogonal plane: velocity contours, c) longitudinal plane, d) M1.

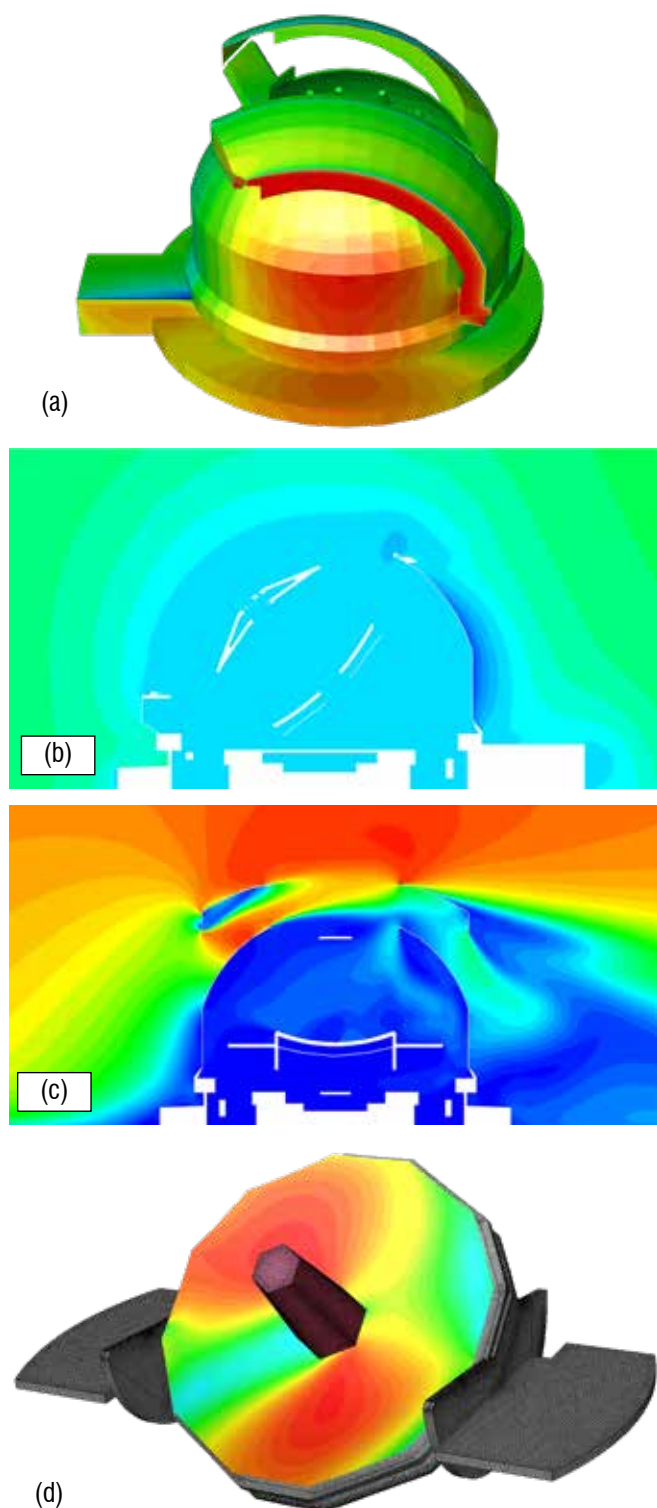


Fig. 9. Pressure contours: a) overall, b) orthogonal plane: velocity contours, c) longitudinal plane, d) M1.

The results obtained from the CFD calculation in terms of the velocity measured on the probes, shown in Fig. 10, are very close to those obtained in the wind tunnel test. The position of the probes on M1 is shown in Fig. 10c; the probe on M2 and on M4 is positioned according to Fig. 2.

The results of this analysis confirm the validity of the study presented here, particularly concerning speed measurements in the vicinity of the mirrors, which is the main focus of the study.

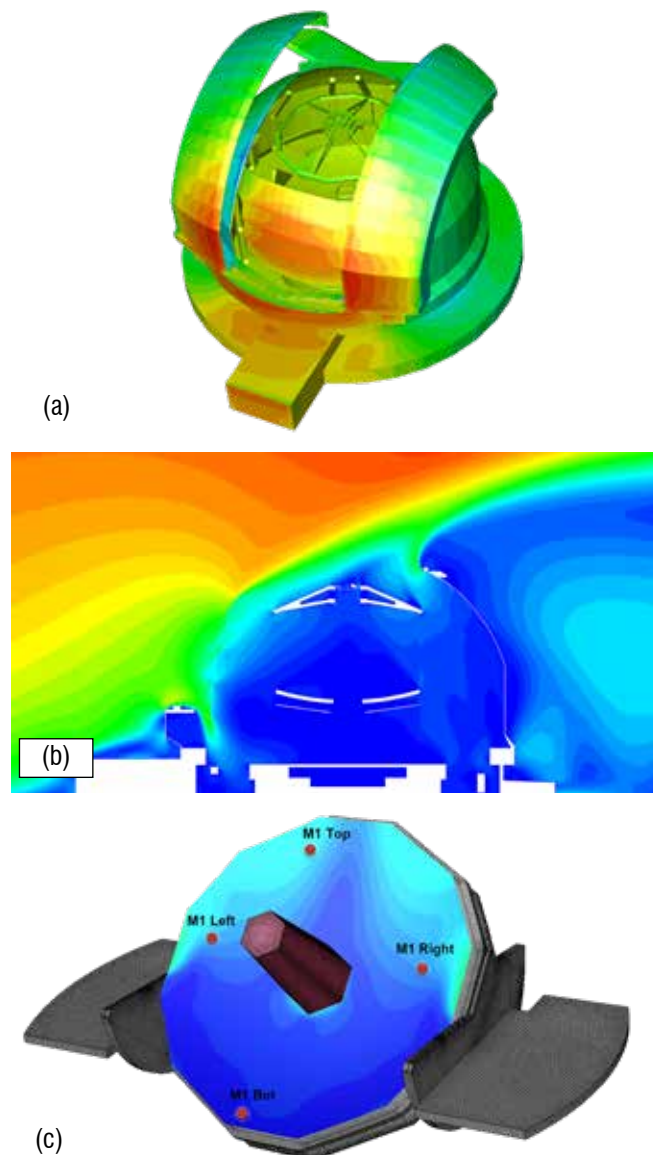


Fig. 10. Pressure contours: a) overall, b) orthogonal plane: velocity contours, c) M1.

The wind tunnel test results were also validated in terms of both local and integral pressures.

Effects on hosted units

The windscreen's performance was measured by the CFD model in terms of velocities near the M1, M2 and M4 mirrors.

The simulations resulted in the following values for both the flat perforated sheet (OP) and the corrugated perforated sheet (CP). Only the results for Azimuths 0° and 90° are shown here.

Velocity [m/s]	OP		CP	
	0°	90°	0°	90°
M1 mean	0.17	1.20	0.16	1.15
M1 max	0.45	1.60	0.45	1.60
M2	4.84	0.30	4.88	0.38
M4	0.38	0.40	0.44	0.40

Table 4. WS performance - OP and CP.

These results demonstrate the windscreen's effectiveness in shielding from external wind during observation. Both designs (OP and CP) result in remarkably similar velocity values at the mirrors and represent a viable solution for windscreen performance.

Currently, the CP design is preferred from a structural point of view. It is also thermodynamically preferred due to its lower permeability as it provides better flow recirculation.

Conclusions

The CFD analysis was performed following the ESO Technical Specifications and demonstrated the windscreen's effectiveness in shielding the Hosted Units from the wind. First, the geometric model for the CFD simulation was created at a scale of 1:70 based on wind tunnel assumptions and considering suitably simplified geometric characteristics; porous regions were inserted in place of truss structures.

The windscreen was also modelled as a porous region. Given the windscreen's importance in internal wind flow behaviour, the porous windscreen model was rigorously analysed and the porous model parameters were identified.

The performance of the porous windscreen model was also compared with both wind tunnel tests and high-fidelity CFD simulations, yielding satisfactory results in terms of pressure drop, deflection angle, resultant forces, nearby velocity field and nearby pressure field.

Auxiliary CFD studies were performed to obtain the properties of other porous regions that replaced various truss structures. The boundary conditions were set to meet the requirements of the specifications on velocity profiles and turbulence intensity level. These conditions were tested on an empty domain, demonstrating good persistence of the above-mentioned characteristics throughout the domain.

Several sensitivity studies were performed to determine the sensitivity of the model to both mesh size and other model assumptions such as geometry, scale, roughness, etc. In total five load cases were considered with varying angles of attack for the 45° altitude configuration. In addition, a 90° altitude configuration with the windscreen fully extended was considered as a benchmark test. The benchmark tests showed good agreement with the wind tunnel tests.

This CFD model also serves other purposes beyond calculating the windscreen performance. It is part of the numerical chain to calculate convective heat exchanges in the night-time thermal analysis of the Main Structure. This is crucial to assess the main structure's thermal deflections during the observational part of its thermal analysis. In that simulation, the model also considers the effect of the louvers.

This study allowed us to understand the characteristics of wind flow within the dome under typical observational conditions and to demonstrate the windscreen's adequacy in protecting the telescope from the effect of the wind in order to allow observation tasks.

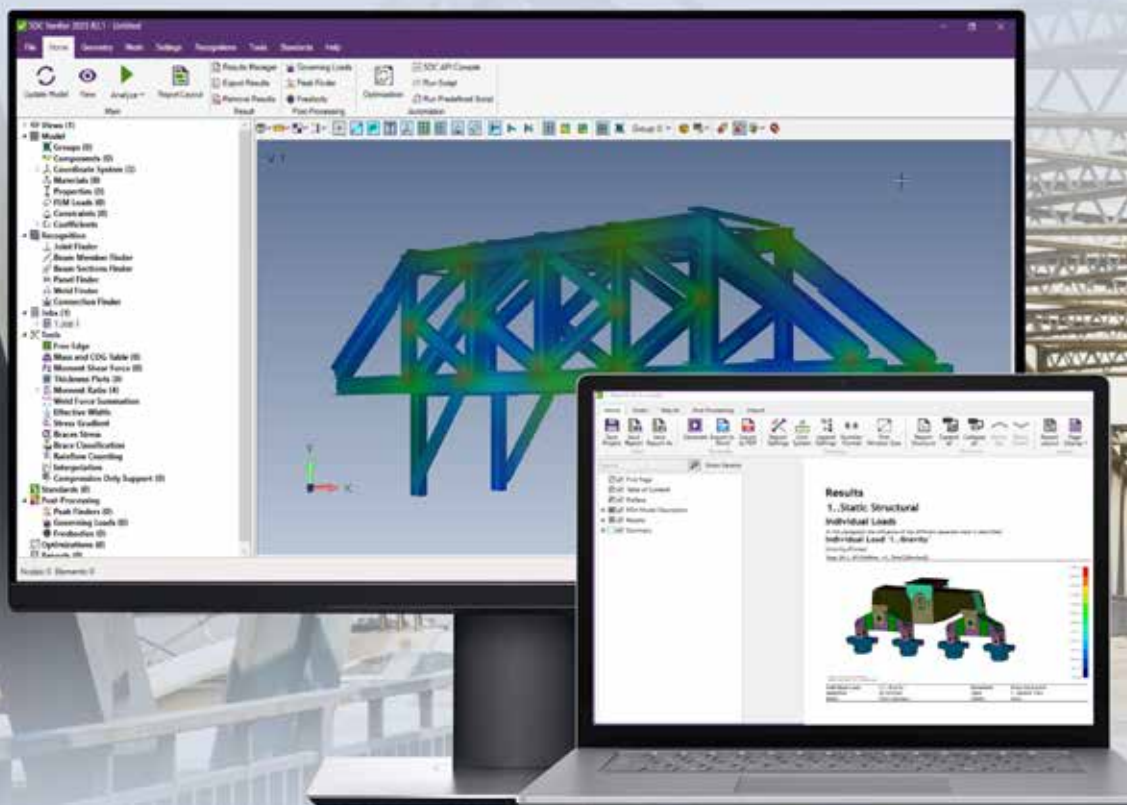
About Cimolai

Cimolai is a leading metal construction company based in Italy. It has been engaged in the design, manufacture, and erection of complex steel structures for over 70 years. Over time, Cimolai has diversified its activities in the field of industrial, civil, military, naval and oil and gas engineering. It also operates in the field of curtain walling, special cladding and oversized element handling systems. The company has been entrusted with iconic projects around the world, including the planet's largest telescope, the ELT (Extremely Large Telescope) in Chile; Calatrava's "Oculus" underground station at Ground Zero in New York; the Vessel honeycomb structure in the Hudson Yards complex in Manhattan in New York; the new Pilot Tower in Genoa in Italy; lot 2 of Line 17 of the Paris Metro; the new Fiumicino Airport Terminal in Italy; the new railway station in Sesto San Giovanni in Milan in Italy; and the Al Wasl Plaza Dome for the 2020 World Expo in Dubai. For more information, visit: cimolai.com

About ESO

The European Southern Observatory (ESO) enables scientists worldwide to discover the secrets of the Universe for the benefit of all. It designs, builds, and operates world-class observatories on the ground and promotes international collaboration for astronomy. Established as an intergovernmental organization in 1962, today ESO is supported by 16 member states (Austria, Belgium, Czechia, Denmark, France, Finland, Germany, Ireland, Italy, the Netherlands, Poland, Portugal, Spain, Sweden, Switzerland, and the United Kingdom), the host state of Chile, and Australia as a strategic partner. ESO's headquarters and its visitor centre and planetarium, the ESO Supernova, are located close to Munich in Germany, while the Chilean Atacama Desert hosts the telescopes. ESO operates three observing sites: La Silla, Paranal and Chajnantor. At Paranal, ESO operates the Very Large Telescope and its Very Large Telescope Interferometer, as well as survey telescopes such as VISTA. At Paranal ESO will also host and operate the Cherenkov Telescope Array South, the world's largest and most sensitive gamma-ray observatory. Together with international partners, ESO operates ALMA on Chajnantor, a facility that observes the skies in the millimetre and submillimetre ranges. At Cerro Armazones, near Paranal, it is building "the world's biggest eye on the sky" — ESO's Extremely Large Telescope. It supports its operations in the country and engages with Chilean partners and society from its offices in Santiago in Chile.

For more information:
media@cimolai.com



Accuracy in steel connection design: A practical look at SDC Verifier

by Oleg Ischchuk
SDC Verifier

Steel connections are the backbone of civil and structural engineering, ensuring the safe transfer of loads throughout a structure. However, designing and verifying these connections can be a time-consuming and error-prone process due to complex calculations and compliance with various codes and regulations.

This article explores SDC Verifier, a software solution that streamlines steel connection design.

Steel connections are critical components of civil and structural engineering, ensuring the transfer of loads throughout a structure. However, the design and testing of these connections can be time-consuming and error-prone due to:

1. The intricate calculations for factors such as bolt and weld strength to test the durability and behaviour of connections, especially complex connections.
2. The comprehensive set of codes and standards that govern failure modes in aspects such as material properties, weld configurations, and bolt capacities.

This article explores SDC Verifier, a software solution designed to address these challenges in steel connection design. We will discuss how the software automates tasks, simplifies code compliance, and ultimately enhances efficiency and accuracy for engineers working on steel connection projects.

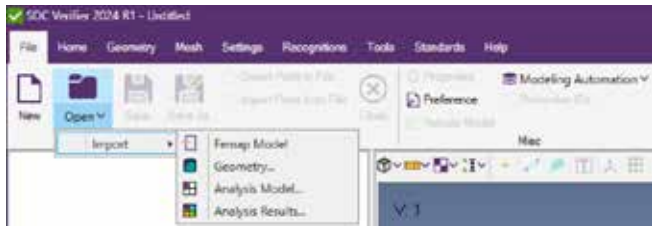
Steel connection design with SDC Verifier

Designing steel connections often involves manual calculations and juggling separate software for modelling, simulating, and checking codes. This disjointed approach can be slow and error prone, especially for complex projects.

SDC Verifier tackles these challenges by offering a comprehensive software solution specifically designed for steel connection design. It integrates key functionality within a single, user-friendly platform:

Simplified modelling

No more tedious data entry! Import existing CAD models of your steel connections directly into SDC Verifier. Alternatively, create new models within the software. This ensures consistency between your design and analysis.



Powerful simulation

SDC Verifier uses advanced finite element analysis (FEA) to simulate connection behaviour under various loads. This allows you to visualize stress distribution, strain, and potential failure points, to support informed design decisions.



Automated code checking

Keeping up with ever-changing engineering codes can be time-consuming. SDC Verifier integrates a vast library of pre-built codes relevant to steel connections, covering material properties, weld configurations, and bolt capacities. The software automatically checks your design against these standards, ensuring code compliance and minimizing errors.



By combining these features, SDC Verifier empowers engineers to design and verify steel connections with greater efficiency and accuracy.

Automating steel connection analysis

Traditionally, bolt checks involve tedious manual calculations and the referencing of separate design codes. SDC Verifier eliminates this burden by offering:

Pre-built code libraries encompassing popular standards for civil engineering like Eurocode 3 (EC3, EN 1993-1-8), AISC 360-10 and VDI 2230 ¼ the software seamlessly integrates the relevant provisions for bolt checks.

Definitions for bolt diameter, material properties, and other characteristics directly within the software ¼ no need to juggle separate spreadsheets or data tables.

- **Shear strength:** Includes standard requirements for the shear capacity of the bolt(s) considering factors like thread area and material properties.
- **Bearing strength:** Verifies that the connected materials can withstand the bearing force exerted by the bolt(s).

3. Bolt M20. Class 8.8

Property	Value	Property Shape
Type / Elements	Beam / 4	
Material	1. Steel F4510	
Mass	0.15	
Gravity Center	{-0.01; 0.00; 0.00}	
Area	3.142e-04	
I1	7.854e-09	
I2	7.854e-09	
I12	0	
Torsion Constant	1.569e-08	
Y Shear Area	2.784e-04	
Z Shear Area	2.784e-04	
Nonstructural Mass	0	
Perimeter	0.06	
Warping Constant	0	
Y Neutral Axis Offset A	0	
Z Neutral Axis Offset A	0	
r	0.01	

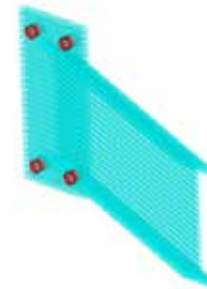
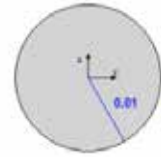


Fig. 1. Verification of Class 8.8 M20 bolts in SDC Verifier.

- **Minimum fastener tension:** Ensures sufficient tension in the bolt(s) to maintain a secure connection, preventing gaps and loosening under normal loads. This indirectly contributes to axial strength and slip resistance.
- **Axial strength:** Analyses the bolt's capacity to resist forces acting along its length (tension or compression), preventing bolt failure under excessive pulling or pushing forces.
- **Slip resistance:** Assesses the clamped joint's ability to resist shear forces that tend to make the connected parts slide past each other. By ensuring sufficient clamping force (achieved through minimum fastener tension), SDC Verifier helps mitigate slip resistance failures.

The integrity of steel connections relies heavily on the strength of the welds. SDC Verifier simplifies weld strength checks by: Selecting from pre-built code libraries like EC3 (EN 1993-1-8) for weld strength calculations, like bolt checks.

The software automatically assesses the weld strength based on the selected standard, considering factors like:

- **Weld size and geometry:** The weld dimensions and configuration, including its type, size, and quality, are factored into the analysis.
- **Material properties:** The properties of the base metal and weld material are considered.

SDC Verifier can visualize stress distribution around the weld, providing valuable insights into potential weak points for further design optimization.

By automating these tasks, the software helps ensure that your welds meet the necessary strength requirements, leading to more reliable and secure steel connections.

Code compliance for steel connections

Code compliance is non-negotiable in designing these connections. Cutting corners can lead to catastrophic consequences, jeopardizing lives, causing operational downtime, and incurring significant financial losses.

SDC Verifier empowers you to achieve industrial-grade safety by offering a comprehensive solution for navigating the complexities of engineering codes. The software boasts a vast library specifically tailored to the demands of industrial civil engineering projects.

This includes:

Eurocode 3 (EC3): A cornerstone for steel structures in Europe, with a specific focus on bolt design:

- Standard used: EN 1993-1-8:2005
¾ Actions on structures ¾ Part 1-8: Design of joints
- Key features:
 - Bolt checks according to Section 3: Connections made with bolts, rivets or pins.
 - Considers factors like bolt position, thread pitch, shear plane location, countersunk bolts, class of friction surfaces, etc.
 - Analyses both bolt capacity and slip resistance.
 - Users can define material properties, safety factors, and other relevant parameters.

AISC 360-10 Bolts (14th Edition, 2010):

The gold standard for steel construction in North America:

- Standard used: AISC 360-10 Specification for Structural Steel Buildings (Chapter J3: Bolts and Threaded Parts)
- Key features:
 - Bolt checks based on Chapter J3 provisions.
 - Considers factors like nominal bolt diameter, thread influence on shear strength, minimum fastener tension, and nominal tensile/shear strength.
 - Capability for slip-critical connection design (Chapter J3.8).

- Integrates safety factors based on hole type.
- Users can override default values for various properties.

VDI 2230 (Part 1, 2015): A German engineering standard for calculating single-bolt joints:

- Standard used: VDI 2230 Beiblatt 1: Berechnung von Einzelbolzverbindungen (calculation of single-bolt joints)
- Key features:
 - Systematic method for calculating bolted joints using a step-by-step approach.
 - Considers factors like bolt type (through-bolt, socket head), rolled bolts, temperature loading, Young's modulus of materials, forces, number of loading cycles, nut dimensions, etc.
 - Analyses various aspects like sealing area, clamping length, friction radius, edge distances, and more.
 - Users can define material properties, tightening factors, friction coefficients, strength limits, and bolt dimensions.
 - A library of bolts to choose from.

In addition to these core standards, SDC Verifier offers an extensive library catering to specific industrial needs.

By integrating these essential standards, the software streamlines the code compliance process. The software automates code checks, meticulously evaluating your connection design against the selected standard's provisions.

SDC Verifier offers additional functionalities to complement its core code checking capabilities.

For instance, the Beam Member and Joint Checks App enables comprehensive analysis of connections in large, complex structures, especially those found in offshore applications. This app performs critical checks according to various industry standards, including:

- AISC 360-10 (American Institute of Steel Construction standards for member design)
- Eurocode 3 (EN 1993-1-1)

The Beam Member and Joint Checks App also leverages a Beam Member Finder tool. This tool automatically detects the buckling lengths of beam members in three directions (Y, Z, and torsional), ensuring accurate analysis independent of the model mesh.

Optimizing steel connection design

While SDC Verifier excels at ensuring code compliance for connections, the software also empowers you to optimize your steel connection design through a range of additional features:

Member design checks (EC3, EN 1993-1-1): This feature allows you to analyse individual steel members like beams and columns against the provisions of Eurocode 3 (EC3), specifically EN 1993-1-1. This check ensures these members possess the necessary strength and stability to carry their intended loads. By performing member design checks alongside connection analysis, you gain a more holistic understanding of your entire structural system, potentially revealing opportunities to optimize connection design.

Plate buckling checks (EC3, EN 1993-1-5): This functionality assesses the susceptibility of steel plates within your connections to buckling under compressive loads. Understanding buckling behaviour is crucial for optimizing connection design. For instance, identifying a plate prone to buckling might prompt you to modify the connection geometry or to introduce stiffeners for greater resistance.

Furthermore, SDC Verifier offers comprehensive fatigue analysis tools to optimize your steel structure designs for long-term performance. This is especially critical for industrial applications where connections undergo repeated loading and unloading cycles from machinery and equipment.

Built-in fatigue analysis capabilities:

- Standards support: Conduct fatigue checks according to established industry standards, including Eurocode 3 Fatigue (EN 1993-1-9) and DNV-RP-C203 Fatigue.
- Streamlined workflow: The fatigue analysis module employs the Palmgren-Miner rule and S-N curves for efficient fatigue life estimation.
- Automated weld identification: The Weld Finder tool automatically locates welded sections within your connection model. This eliminates the need for manual weld modelling and allows direct assignment of weld properties for a more accurate analysis.

The software also allows you to define Fatigue Groups for advanced users, enabling even more precise fatigue analysis. This feature is particularly useful for complex loading scenarios where you want to group similar load cases for a more granular assessment of fatigue damage.

This allows you to analyse both the connections themselves and the connected members, fostering a more informed and efficient design process.

This can potentially optimize the connection design by using holistic analysis to enable the use of less material while still achieving the required strength and stability.

Moreover, well-optimized connection design can lead to a more efficient structure, potentially reducing the need for overly robust connections or members.

SDC Verifier does not just ensure compliant connections; it also unlocks the potential to create efficient and cost-effective steel structures.

Example: a steel structure using M24 bolts in the connections

Consider a steel structure using M24 bolts in the connections with a FEA model created in a compatible software like Ansys or Femap. The goal is to verify the adequacy of the M24 bolts under AISC 360-10.

SDC Verifier analysis:

- **Bolt force extraction:** SDC Verifier automatically extracts the internal axial and shear forces acting on the M24 bolt elements within the FEA model.
- **Material properties:** The software considers the bolt diameter (24 mm) and retrieves the material properties (likely yield strength) from the FEA model or allows user-defined values if needed.
- **AISC 360-10 checks:** SDC Verifier performs various AISC 360-10 checks based on the extracted forces and material properties:
 - **Tensile and shear strength:** The software compares the extracted bolt forces with the allowable tensile

15. Bolts_M24

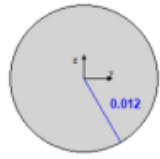
Property	Value	Property Shape
Type / Elements	Beam / 154	
Material	12.Bridge girders_detailed	
Mass [kg]	29.8	
Gravity Center [m]	[15.2; 10.6; 20.0]	
Area, [m ²]	4.524e-04	
I1, [m ⁴]	1.629e-08	
I2, [m ⁴]	1.629e-08	
I12, [m ⁴]	0	
Torsion Contrast, [m ⁴]	3.254e-08	
Y Shear Area, [m ²]	4.009e-04	
Z Shear Area, [m ²]	4.009e-04	
Nonstructural Mass, [kg]	0	
Perimeter, [m]	0.1	
Warping Constant, [m ⁶]	0	
Y Neutral Axis Offset A, [m]	0	
Z Neutral Axis Offset A, [m]	0	
r [m]	0.0120	

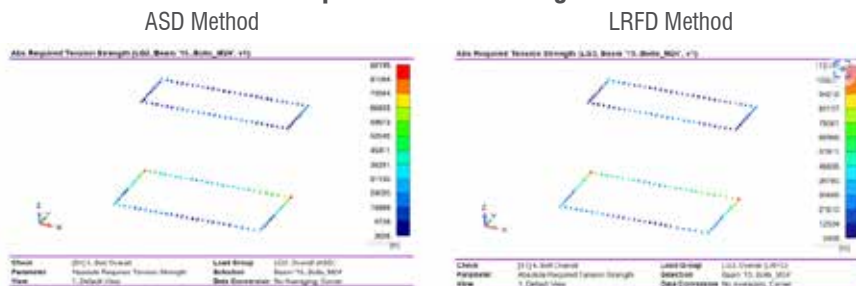
Table J3.2
Nominal Strength of Fasteners and Threaded Parts, ksi (MPa)

Description of Fasteners	Nominal Tensile Strength, F_{ts} , ksi (MPa) ^[a]	Nominal Shear Strength in Bearing-Type Connections, F_{vb} , ksi (MPa) ^[a]
A307 bolts	45 (310)	27 (188) ^{[c] [d]}
Group A (e.g., A325) bolts, when threads are not excluded from shear planes	90 (620)	54 (372)
Group A (e.g., A325) bolts, when threads are not excluded from shear planes	90 (620)	68 (457)
Group B (e.g., A490) bolts, when threads are not excluded from shear planes	113 (780)	68 (457)
Group B (e.g., A490) bolts, when threads are not excluded from shear planes	113 (780)	84 (579)
Threaded parts meeting the requirement of Section A3.4, when threads are not excluded from shear planes	$0.75F_u$	$0.45 F_u$
Threaded parts meeting the requirement of Section A3.4, when threads are not excluded from shear planes	$0.75F_u$	$0.563 F_u$

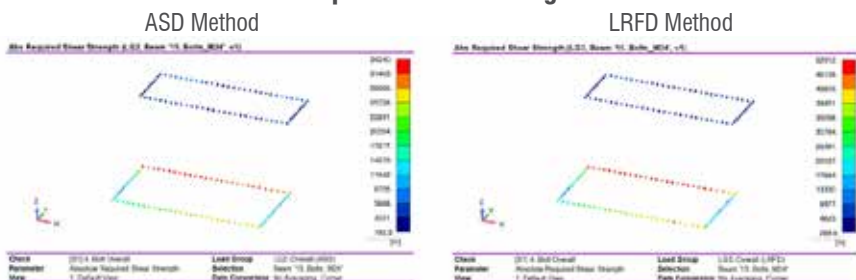
strength ($F_{t,Rd}$) and shear capacity ($F_{v,Rd}$) as specified in AISC 360-10 Table J3.2. These values are based on the bolt material grade.

- **Combined tension and shear:** If the connection experiences both tension and shear, SDC Verifier performs interaction checks considering the combined effect on bolt capacity. This adheres to the provisions of AISC 360-10 Section J3.
- **Bearing strength at bolt holes:** The software assesses the bearing strength of the material surrounding the M24 bolt holes based on AISC 360-10. This ensures the material can manage the applied shear stress without failure.

Required Tension Strength



Required Shear Strength



- **Results and reporting:** SDC Verifier presents the results in a clear and concise format. This might include:

- **Utilization factor (UF):** The ratio between the calculated bolt stress and allowable stress for each bolt. A UF less than 1 indicates a safe design.
- **Required vs. Available bolt strength:** Plots or tables comparing the calculated tensile and shear force demands on the bolts with their allowable capacities according to AISC 360-10.

- **Multiple load cases:** If the FEA model considers multiple load cases, SDC Verifier can analyse the results based on load groups. This identifies the worst-case scenario (absolute maximum utilization) for each bolt across all load combinations.

Conclusion

SDC Verifier offers a comprehensive suite of tools to streamline the process, enhance accuracy, and promote informed decision-making for engineers working on steel connection design projects. In summary, its key benefits include:

- Automated efficiency. Repetitive tasks like bolt checks and weld strength analysis become automated, saving engineers valuable time and minimizing the risk of errors associated with manual calculations.
- Code compliance assurance. With a vast library of pre-built engineering standards, including a strong focus on Eurocode 3 (EC3) for steel connections, SDC Verifier ensures your designs comply with the latest regulations and safety requirements.
- Holistic design analysis. The software goes beyond connection checks, offering functionalities like member design and plate buckling considerations. This fosters a more comprehensive understanding of the entire structural system, facilitating informed design choices.
- Enhanced communication and documentation. Automated reports and clear visualizations within SDC Verifier contribute to improved communication and collaboration within engineering teams, resulting in well-documented design decisions.

For more information:

Alessio Trevisan - EnginSoft
a.trevisan@enginsoft.com

ASD Method

All (9 loads, Beam '15. Bolts_M24')						
Check Selection	[S]14_Bolt Overall	Beam '15. Bolts_M24'	Loads Count	9		
Load	Required Tension Strength [N]	Required Shear Strength [N]	Required Tension Stress [Pa]	Required Shear Stress [Pa]	UF ASD Overall	
Load Set '1..Load Set 1.1 - ASD'	35.1e+3	15.7e+3	77.6e+6	34.7e+6	0.39	
Load Set '2..Load Set 1.2 - ASD'	70.9e+3	20.5e+3	156.7e+6	45.2e+6	0.53	
Load Set '3..Load Set 1.3 - ASD'	36.1e+3	31.8e+3	79.8e+6	70.3e+6	0.69	
Load Set '4..Load Set 1.4 - ASD'	85.2e+3	34.2e+3	194.9e+6	75.6e+6	1.10	
Load Set '5..Load Set 1.5 - ASD'	36.1e+3	34.2e+3	79.8e+6	75.6e+6	0.74	
Load Set '6..Load Set 1.6 - ASD'	82.8e+3	31.8e+3	183.0e+6	70.3e+6	0.97	
Load Set '7..Load Set 1.7 - ASD'	33.5e+3	20.5e+3	73.9e+6	45.2e+6	0.51	
Load Set '8..Load Set 1.8 - ASD'	72.9e+3	15.7e+3	161.0e+6	34.7e+6	0.61	
Load Group '2..Overall (ASD)'	88.2e+3	34.2e+3	194.9e+6	75.6e+6	1.10	

LRFD Method

All (9 loads, Beam '15. Bolts_M24')						
Check Selection	[S]14_Bolt Overall	Beam '15. Bolts_M24'	Loads Count	9		
Load	Required Tension Strength [N]	Required Shear Strength [N]	Required Tension Stress [Pa]	Required Shear Stress [Pa]	UF LRFD Overall	
Load Set '9..Load Set 1.1 - LRFD'	44.2e+3	22.3e+3	97.7e+6	49.2e+6	0.36	
Load Set '10..Load Set 1.2 - LRFD'	84.7e+3	30.5e+3	187.1e+6	67.3e+6	0.44	
Load Set '11..Load Set 1.3 - LRFD'	45.8e+3	49.4e+3	101.2e+6	109.2e+6	0.71	
Load Set '12..Load Set 1.4 - LRFD'	112.4e+3	52.5e+3	248.3e+6	116.1e+6	0.96	
Load Set '13..Load Set 1.5 - LRFD'	46.4e+3	52.5e+3	102.5e+6	116.1e+6	0.76	
Load Set '14..Load Set 1.6 - LRFD'	105.2e+3	49.4e+3	232.5e+6	109.2e+6	0.85	
Load Set '15..Load Set 1.7 - LRFD'	42.2e+3	30.5e+3	93.1e+6	67.3e+6	0.48	
Load Set '16..Load Set 1.8 - LRFD'	87.8e+3	22.3e+3	194.1e+6	49.2e+6	0.47	
Load Group '3..Overall (LRFD)'	112.4e+3	52.5e+3	248.3e+6	116.1e+6	0.96	

About SDC Verifier

SDC Verifier is a mechanical and structural design engineering company providing all-in-one design and code checking software and engineering consultancy services. Since 1998 we have won the trust of leading global companies in the Offshore and Maritime, Heavy Lifting, Oil and Gas, Defence, and other industries. SDC Verifier software is a powerful design and standard inspection tool that works independently of and within several FEA solutions such as Ansys, Femap, and Simcenter 3D. It helps to automatically verify FEA results against numerous industry standards such as DIN, EN, Eurocode, FEM, AISC, NORSOK, ISO, DNV, ABS, FKM Fatigue, and DVS code for weld checks. SDC Verifier is proven to increase the productivity of engineering teams and take them to a new level of comfort. Contact SDC Verifier when in need of consultancy on FEA, modelling, standards-based design review, or for your other specialized software needs related to FEA or to industry standards. **Visit sdcverifier.com or email info@sdcverifier.com**



Rubber fatigue \neq metal fatigue: mean strain effects

by William V. Mars
Endurica LLC

Rubber and metal are very different materials that exhibit vastly different behaviour. Consider the effect of mean strain or stress on the fatigue performance of these materials.

Fig. 1 illustrates a few typical constant amplitude strain cycles, each at a different level of mean strain. If the stress amplitude is equal to the mean stress, we say that we have pulsating tension or fully relaxing tension. If the mean stress is zero, we say that we have fully reversed tension/compression. If the minimum stress is always positive, then we have nonrelaxing tension (i.e. always under load).

Nonrelaxing cycles are quite common in applications. Examples include: pre-loads applied during installation, swaging of a bushing to induce compressive pre-stresses, interference fits, self-stresses occurring due to thermal expansion/contraction, and in tyres, shape-memory effects of textile cords.

In metal fatigue analysis, it is customary to define the effect in terms of stress amplitude σ_a and mean stress σ_m , relative to the yield stress

Type of Constant Amplitude Loading

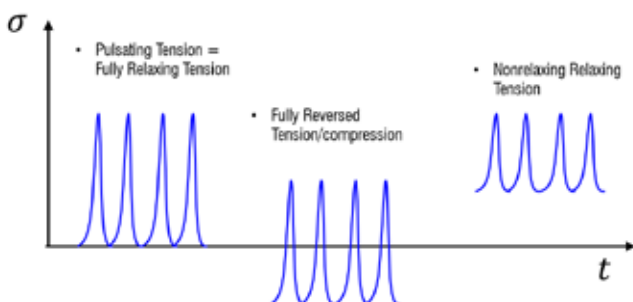


Fig. 1. Constant amplitude cycles at three different mean strains.

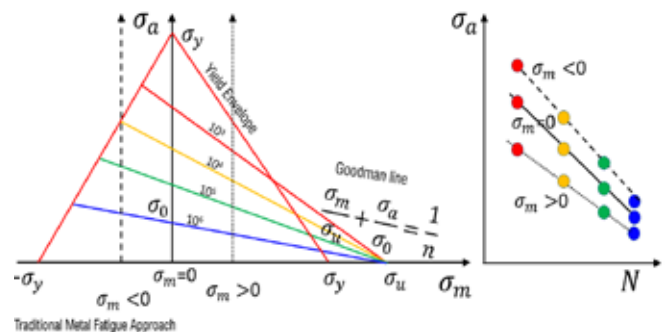


Fig. 2. Haigh diagram (left) and Wohler curves (right) showing mean strain effects on fatigue life for a metal.

σ_y and the ultimate stress σ_u , as shown in Fig. 2. Below the fatigue threshold stress σ_0 , we predict indefinite life. The Haigh (or Goodman) diagram (see the left of Fig. 2) maps fatigue life as a function of these parameters [1]. Wohler curves (see the right of Fig. 2) provide similar information.

For metals, a simple rule may be applied universally: increasing mean strain is detrimental to fatigue life. It is also commonly assumed that the critical plane is perpendicular to maximum principal stress direction.

There are many ways that rubber materials differ from metallic ones:

- At the atomic scale, rubber is composed of long chain molecules experiencing constant thermal motion while interlinked with a permanent network topology. This structure permits large, elastic/reversible straining to occur. Metals could not be more different, existing as individual atoms packed into well-ordered crystals with occasional dislocations or lattice vacancies. This structure permits only vanishingly small strains before inelastic deformation occurs.

Mean Strain Effect in Pulsating Tension: NR vs. SBR

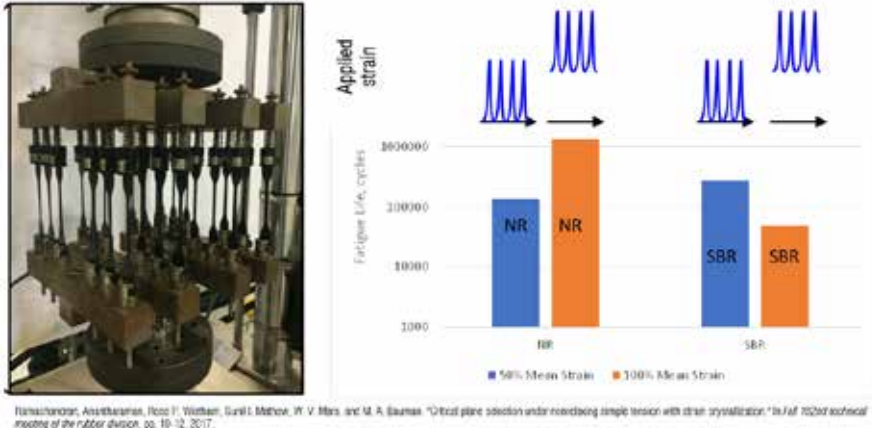


Fig. 3. Fatigue tests run in simple tension under constant amplitude show a significant increase in life for natural rubber (NR), which strain crystallizes, and a decrease of life for styrene butadiene rubber (SBR) which is amorphous [2].

	Amorphous Rubber	Strain Crystallizing Rubber
Crack Growth Rate Law		$r = r_c \left(\frac{T_{eq}}{T_c} \right)^F$
Equivalent Fully Relaxing Tearing Energy	$T_{eq} = \Delta T$ $T_{eq} = T_{max} - T_{min}$ $T_{eq} = T_{max}(1 - R)$	$T_{eq} = T_{max,R}^{F(0)} T_c^{(1 - F(0))}$
Crystallization effect	None	$F(R) = F_0 e^{F_{exp} R}$

Table 1. Models for computing crack growth rate in amorphous and strain-crystallizing rubbers.

- At the meso scale, rubber is typically a composite material containing fillers such as carbon black, silica, or clay, as well as other chemical agents. The mesoscale of a metal is generally described in terms of crystalline grain boundaries and inclusions or voids. Rubber exhibits many “special effects” that are not seen in metals: rate and temperature dependence, ageing, cyclic softening.

It is unsurprising therefore that analysis methods for rubber differ substantially from those applied for metals. Rubber’s fatigue performance has a more complex dependence on mean strain. For amorphous (i.e. non-crystallizing) rubbers, increasing mean strain reduces the fatigue life, as with metals. But for rubbers that exhibit strain-induced crystallization, mean strain can greatly increase fatigue life, as illustrated in Fig. 3. Fatigue simulations therefore must take account of the strain crystallization effect.

Mean strain effects are specified in the Endurica fatigue code in terms of fracture mechanical behaviour, using the concept of an equivalent fully relaxing tearing energy T_{eq} . The tearing energy for fully relaxing conditions is considered equivalent when it produces the

same rate of crack growth as the nonrelaxing condition. For amorphous rubbers, the equivalent $R=0$ tearing energy T_{eq} is simply the range ΔT of the tearing energy cycle, which can be expressed in terms of the min. and max. tearing energies T_{min} and T_{max} , or in terms of $R=T_{min}/T_{max}$.

Plugging this rule into the power law crack growth rate function yields the well-known Paris law, which predicts faster crack growth for increasing mean strain. For a strain crystallizing rubber, the equivalent fully relaxing tearing energy can be specified using the Mars-Fatemi law. In this case, the equivalent fully relaxing

tearing energy depends on a function $F(R)$, which specifies the crystallization effect in terms of its influence on the power law slope of the crack growth rate law. The relationship for amorphous and crystallizing rubbers is summarized in Table 1 [3,4].

The fatigue behaviour of rubber can be charted in a Haigh diagram, but the contours can be quite different from those of metal. In metal fatigue analysis, we assume that cracks always develop perpendicular to the max. principal stress direction. This is not always true for rubber, especially in cases involving strain crystallization and nonrelaxing loads.

For rubber fatigue analysis one must therefore use critical plane analysis [5], in which fatigue life is computed for many potential crack orientations, and in which the crack plane with the shortest life is identified as the most critical plane. Fig. 4 shows the dependence of the fatigue life and the critical plane orientation on strain amplitude and mean strain. A sphere is plotted for each pair of strain amplitude and mean strain coordinates on which the colours represent fatigue life, and unit normal vectors indicate critical plane orientations. Different combinations of mean strain and strain amplitude can produce a range of crack plane orientations.

The Haigh diagrams for NR and for SBR are shown in Fig. 5. In these images, red represents short fatigue life and blue long life. For NR (on the left), the long-life region of the Haigh diagram exhibits a notable dome-like shape, indicative of a beneficial effect of mean strain under the influence of strain-induced

Critical Plane Analysis of Haigh Diagram

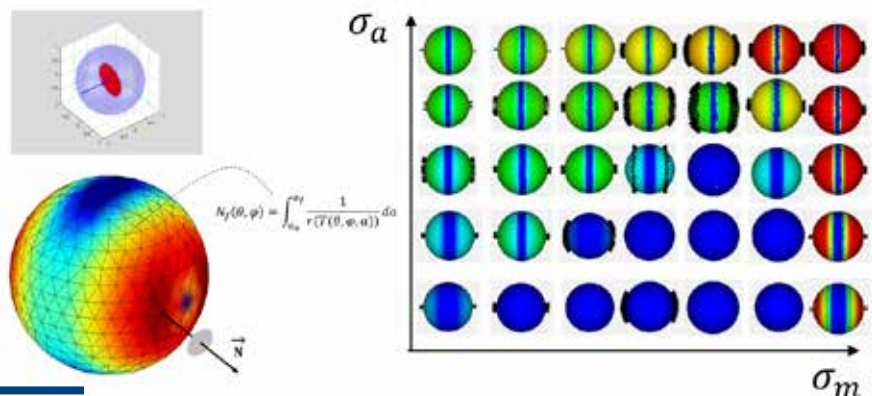


Fig. 4. Critical plane analysis consists of integrating the crack growth rate law for every possible crack orientation, and identifying the orientation that produces the shortest life (left). Each point in the Haigh diagram (right) is associated with its own critical plane orientation.



Haigh diagram: crystallizing vs noncrystallizing

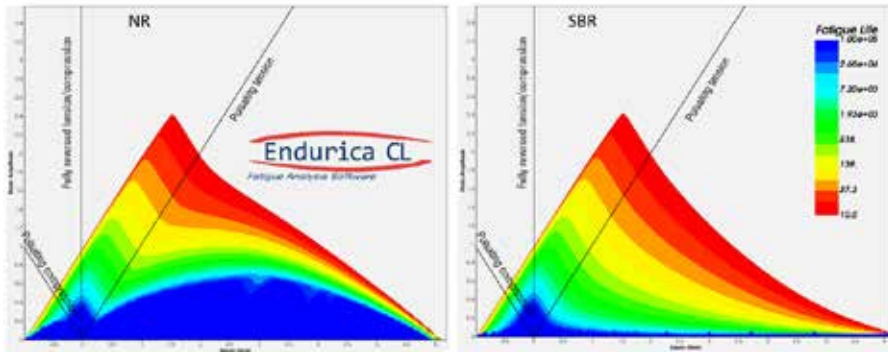


Fig. 5. Haigh diagrams computed for NR (left) and for SBR (right) rubbers.

Effect of Temperature - Experiments by Ruellan et al

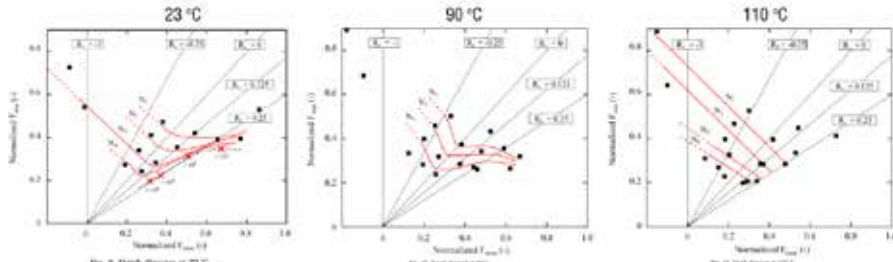


Fig. 6. Experimental Haigh diagram [6] for NR at three temperatures (top), compared to computed Haigh diagram (bottom). Increasing temperature tends to reduce the beneficial effect of strain crystallization.

Effect of Temperature on crystallization

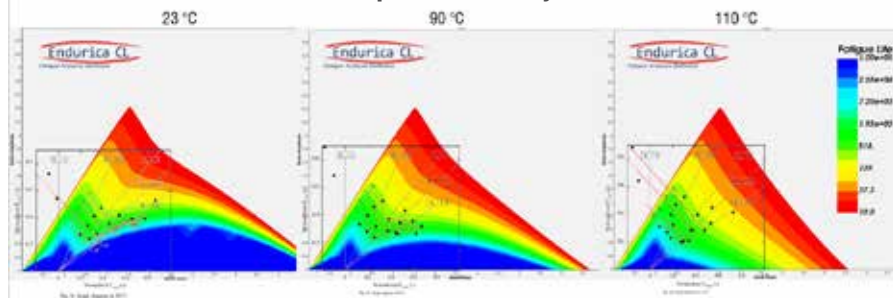


Fig. 6. Experimental Haigh diagram [6] for NR at three temperatures (top), compared to computed Haigh diagram (bottom). Increasing temperature tends to reduce the beneficial effect of strain crystallization.

crystallization. In contrast, SBR always exhibits decreased fatigue life as mean strain increases. Even so, the Haigh diagram for SBR has a nonlinear character associated with the material's hyper elasticity that is also distinct

from a metal. It should be noted that the strain crystallization effect in rubber depends on temperature. At colder temperatures the effect is stronger and at higher temperatures it is weaker.

Fig. 6 compares experimental Haigh diagrams [6] (top) for a crystallizing rubber to computed results (bottom) for three temperatures.

In summary, while tensile mean stresses are always detrimental in metals, in rubber they may be either beneficial or harmful depending on whether the rubber can strain crystallize. The benefits of mean stresses in rubber can be quite strong - sometimes amounting to more than several orders of magnitude. The beneficial effect is stronger at colder temperatures and is reduced at higher temperatures.

Critical plane analysis is essential for accurately predicting the effects of strain crystallization in rubber. Wohler curves, commonly used for metal fatigue analysis, incorrectly assume that the worst-case plane is always normal to the max. principal stress direction. This is not an accurate approach for strain crystallizing rubber under mean strain. Use the Endurica fatigue solvers to accurately capture these effects when it is important to get durability right!

For more information:
Alessio Trevisan - EnginSoft
a.trevisan@enginsoft.com

About Endurica

Endurica provides software, materials characterization services, consulting, testing instruments and training to help companies meet rubber durability targets during product design. The company's solutions put engineers in control of rubber durability issues early in the development cycle, when the greatest opportunities exist to influence performance, and before investing in costly testing of prototypes. Endurica is the world's best-validated fatigue life simulation system for elastomers and its workflow gets rubber products to market faster. Endurica serves leading companies in many sectors including aerospace/defence, agriculture, automotive, chemicals, consumer products, education/research, energy, healthcare/medical devices, high tech, industrial manufacturing, infrastructure, marine, raw materials suppliers, silicone suppliers, rail, and tyres. It provides rubber fatigue analysis tools that are accurate, complete and scalable. **Visit endurica.com**

References

- [1] R. I. Stephens, A. Fatemi, R. R. Stephens et al. Metal Fatigue in Engineering (2nd edn., John Wiley & Sons: New York, 2000).
- [2] Ramachandran, Anantharaman, R. P. Wietharn et al. "Critical plane selection under nonrelaxing simple tension with strain crystallization", pp. 10-12, presented at the 192nd technical meeting of the ACS Rubber Division, Akron, OH, USA, Sept. 2017.
- [3] W. V. Mars, "Computed dependence of rubber's fatigue behaviour on strain crystallization", Rubber Chemistry and Technology, 82/1 (2009): 51-61.
- [4] R. J. Harbour, A. Fatemi, and W. V. Mars, "Fatigue crack growth of filled rubber under constant and variable amplitude loading conditions", Fatigue & Fracture of Engineering Materials & Structures, 30/7 (2007): 640-652.
- [5] W. V. Mars, "Critical plane analysis of rubber", Fatigue Crack Growth in Rubber Materials: Experiments and Modelling, (2021): 85-107.
- [6] B. Ruellan, J. B. Le Cam, I. Jeanneau et al. "Fatigue of natural rubber under different temperatures", International Journal of Fatigue, 124 (2019): 544-557.



Battery modelling and the Goldilocks zone

by Prashant Srivastava, Ankur Patel, Aditya Pandav
oorja

With the global shift towards electrification as a primary energy storage solution, there is an escalating need to better understand the behaviour of batteries. As battery technologies advance, incorporating several rare-earth elements and achieving higher energy densities, safety considerations become paramount.

Therefore, understanding the behaviour and performance of batteries under different operating conditions is critical to the large-scale adoption of batteries. Predictive modelling that can accurately forecast safety, performance, and lifetime is therefore indispensable.

The traditional approach to this type of analysis involves physics-based modelling, which, while powerful, presents considerable challenges. Batteries are complexly designed devices consisting of multiple materials layered together. Their functionality depends on an intricate interplay of various phenomena — electrochemistry, heat transfer, and fluid dynamics, to name a few — that control the transport of ions and electrons and the production of heat within the battery.

To effectively model these phenomena within the overall structure of an electrochemical cell, accurate design, transport, and degradation parameters are required to get physically relevant results from a physics-based model.

A key challenge during digital battery twinning is identifying the “Goldilocks zone” for parameters. For predictions to be dependable, the entire set of parameters must be precisely calibrated over the battery’s lifecycle. However, obtaining and validating the correct set of parameters is not easy. Inaccuracies in parameter estimation can lead to significant errors in model predictions, reducing the reliability of safety assessments and performance predictions.

This complexity underlines the need for sophisticated tools capable of offering robust multi-parameter optimization, like the hybrid software solution, oorja, which extracts essential information from HPPC (hybrid pulse power characterization) data to simulate real-world battery behaviour under various operating conditions.

Approach

At oorja, engineers have pioneered a hybrid approach that combines data and physics-based models to perform multi-parameter optimization with limited data sets to provide detailed information on transport and degradation parameters for Lithium-ion (Li-ion) cells.

Multi-parameter optimization techniques for estimating parameters using HPPC data involve adjusting the model parameters until a satisfactory fit is achieved between the model and the experimental

data. The objective function for optimization is defined by the sum of the squares of the errors between the predicted and experimental values. The error is split into two parts.

- At the beginning of the step change in the pulse (e_{step}).
- During the pulse (e_{pulse}).

During the step change in the pulse, the loss function is computed using the following formula:

$$e_{\text{step}} = \sum [V_{\text{model}}(t_i) - V_{\text{exp}}(t_i)]^2,$$

where t_i corresponds to the first of the pulses at which the step change in the current occurs, and during the pulse, the loss function is given by:

$$e_{\text{pulse}} = \sum [V_{\text{model}}(t_i) - V_{\text{exp}}(t_i)]^2,$$

where t_i is the time duration of the pulse. Thereafter the total loss function is computed as the weighted sum of the e_{step} and e_{pulse} :

$$e_{\text{total}} = (e_{\text{step}} \cdot w_{\text{step}} + e_{\text{pulse}} \cdot w_{\text{pulse}}),$$

where w_{step} and w_{pulse} are the respective weights.

Among all the electrochemical parameters associated with the Single Particle Model (SPM), a set of five parameters (namely the internal resistance of the cell, the Li-ion diffusion coefficients of positive and negative electrodes, and the reaction rate constant of the positive and negative electrodes) are found to be sensitive to operating conditions, especially when considerable temperature fluctuations occur. Optimization algorithms adjust these parameters to minimize the differences between model predictions and experimental data. After optimizing the set parameters and obtaining the prediction fit, users can adjust these parameters to improve the prediction fit further based on their informed judgment.

Results

In HPPC tests, the battery is subjected to a sequence of charge and discharge pulses of different magnitude and duration in different states of charge (SoC). Its voltage response is observed and recorded.

Using the technique described previously, parameter optimization simulations were performed on experimentally obtained HPPC data

About oorja

Headquartered in Bangalore in India, oorja aims to empower automotive companies to design better batteries. Through a first of its kind cutting-edge technology that combines the best of Machine Learning and Physics, oorja enables automotive OEMs to make informed decisions to optimize battery packs by reducing time to market and costs.

sets of cylindrical 21700 commercial cells (LGM50) with a nominal capacity of 3Ah at temperatures 0°C, 25°C, and 40°C. Conditioning was carried out for 40 minutes. The resulting parameter values at various temperatures are shown in Table 1.

The prediction voltage responses obtained from the simulations and the percentage error plots are shown in Fig.1. ((a)-(c)) and ((d)-(f)), respectively, at different temperatures. The prediction responses obtained from the simulations correspond well with the experimental data, as seen in Fig.1. The error is limited to 7% in most of the test except in some cases in the middle and final part of the test where the error spikes above 7%.

Table 1 clearly shows the sensitivity of the model parameters to the varying operating conditions, particularly temperature. As the temperature increases cell resistance decreases, while the reaction rate constants of the positive and negative electrodes increase. Due to strong interactions with other factors, the solid-state diffusion coefficients of the positive and negative electrodes show no correlation with the temperature.

Discussion

The cell's internal resistance and reaction rate constants (of the anode and the cathode) are expected to decrease and increase with temperature, respectively. These relevant trends are captured through our simulations. In general, the diffusion coefficient for both positive and negative electrodes is expected to decrease with temperature, which was not observed in our simulations, thus requiring further investigation. In addition, larger deviations are

Optimization parameters	Initial values	Optimized parameter values obtained at		
		0°C	25°C	40°C
Internal resistance (mΩ)	2	1.91	1.65	1.46
Positive electrode diffusion coefficient (m ² /s)	3 x 10 ⁻¹⁵	3.0251 x 10 ⁻¹⁵	2.9586 x 10 ⁻¹⁵	3.0006 x 10 ⁻¹⁵
Negative electrode diffusion coefficient (m ² /s)	2 x 10 ⁻¹⁴	1.9547 x 10 ⁻¹⁴	2.0781 x 10 ⁻¹⁴	2.0551 x 10 ⁻¹⁴
Positive electrode reaction rate constant (mol ^{1.5} /m ^{5.5})	2 x 10 ⁻⁶	2.3384 x 10 ⁻⁶	2.8279 x 10 ⁻⁶	2.9302 x 10 ⁻⁶
Negative electrode reaction rate constant (mol ^{1.5} /m ^{5.5})	4 x 10 ⁻⁷	6.1249 x 10 ⁻⁷	7.8374 x 10 ⁻⁷	8.1862 x 10 ⁻⁷

Table 1: Optimization parameters obtained at various temperatures.

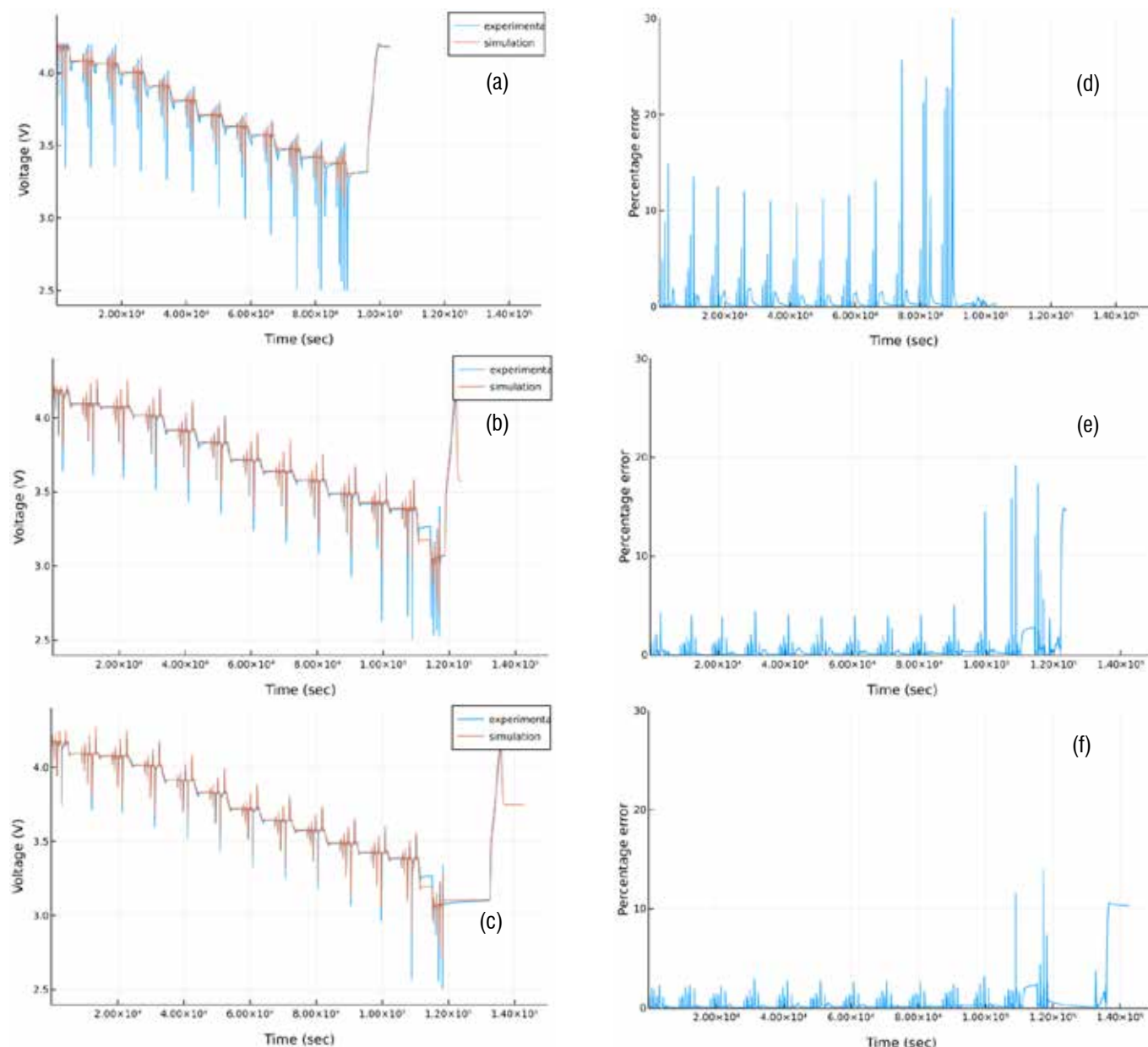


Fig. 1. Comparison of responses obtained from simulation and experiment for the HPPC data set at 0°C, 25°C, and 40°C are shown in (a)-(c). The error plots, showing the error between the experimental data and model prediction, are shown in (d)-(f).

observed in the voltages mounted to the lower SoC. This is due to the low sensitivity of the SoC to open circuit voltage (OCV). During regularization, higher weights can be used at low SoC to improve the quality of the fit.

Conclusion

This work shows the successful identification of the Goldilocks Zone for electrochemical parameters using the HPPC data. The optimization parameters show good physical trends with respect to temperature sensitivity. Furthermore, the comparison of voltage responses between predicted and experiment data shows a good match.

The accuracy of the parameters is also sensitive to the load on the different parts of the HPPC pulses. Further improvements can be made by adjusting of the individual error terms.

In the present method orja regularizes the parameters obtained on different SoCs to obtain a set of parameters representing the cell for the SoC range. The weight of the regularization can be controlled to make the parameters dependent on the SoC. This will improve the adaptation to different states of charge. Moreover, in the current exercise, the cell design parameters are taken from the literature, and the accuracy of fit can be further improved by using design parameters obtained from the cell measurements.

For more information:
 Marcello Bruno - EnginSoft
m.bruno@enginsoft.com



Tethered drones: understanding rotor loads

by **Brian Saiia¹**, **Timothy Hunter²**

1. Menet Aero - 2. Wolf Star Technologies

Menet Aero of Oak Creek in Wisconsin in the USA creates a unique style of drone. It specializes in manufacturing tethered unmanned aircraft systems (TeUAS) or drones which provide secure, on-demand wireless communications. These high-performance platforms, designed in heavy and light configurations, support a variety of payloads for applications such as high-bandwidth digital battlefield communications, signal intelligence, electronic warfare, and force protection and targeting.

Menet Aero systems are used by the Army, Air Force, Navy, and Marines in the USA, and also by joint organizations for a variety of applications, including telecommunications, intelligence, surveillance, and reconnaissance (ISR).

Engineered from the start to be tethered systems, they are more rugged and last longer than battery systems that have been modified to use ground-based power through a tether. Menet Aero's TeUAS are powered

via a tether that connects the aircraft to a power source, and can be integrated into various vehicles, trailers, vessels, and other platforms to provide seamless integration into the mission and battlefield. They accommodate payloads of up to 40lbs (18.143kg) and can be optimized to reach hover heights up to 1,000feet (304.8m) AGL (above ground level).

For these critical missions, Menet Aero wanted a higher fidelity understand of the loading on its drones in order to use these loads to design and optimize better aircraft. The company worked with Wolf

Star Technologies to explore an initial implementation of Wolf Star's True-Load load reconstruction software on its hexacopter. For the initial application, Menet and Wolf Star agreed to concentrate on just two of the six arms on the hexacopter to generate an initial understanding of the applicability of the technology while minimizing instrumentation logistics.

Menet hexacopters have carbon-fibre arms. The True-Load technology requires an FEA (fixed element analysis) model of the structure and will eventually need to place strain gauges on the arms.



As part of the development exploration into the application of the True-Load technology, Menet agreed to swap out the carbon-fibre arms with thin aluminium tubes. This would allow for easier FEA modelling and simpler strain gauge application. The plan is to follow up with a carbon-fibre FEA model and specialized carbon-fibre strain gauges once the demonstration has been successfully completed.

True-Load theory

True-Load load reconstruction works on structures that behave linearly during the event of interest. The structure can undergo non-linear behaviour prior to or after the event of interest. The term “linear” in this context means that the strain response is proportional to the applied loading. Portions of the structure may behave non-linearly. For example, local yielding near welds, bolted joints, or boundary conditions may undergo non-linear strain response. Load reconstruction will continue to be effective if the nominal portions of the structure undergo linear response to the applied loading. Structures with gross yielding will not be appropriate for load reconstruction. Schematically, the concept of linearity is illustrated in Fig. 1.

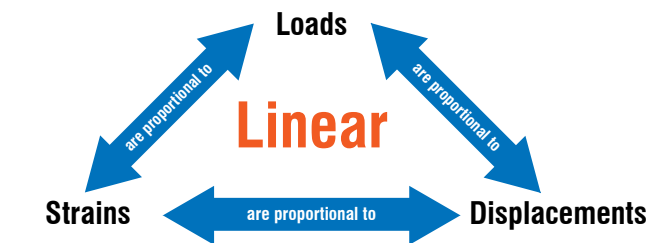


Fig. 1. Linear material behaviour schematic.

This linear relationship can be represented mathematically as follows:

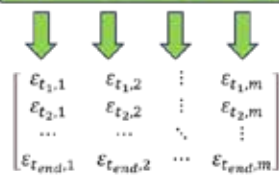
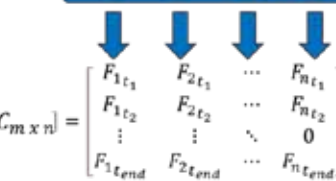
$$F = Kx$$

Equation 1: Hooke's Law.

$$\epsilon C = F$$

Equation 2: Influence coefficient equation.

Applying this strategy to field testing yields the following relationship:

Time Histories of Strain	Time Histories of Load
	
$[C_{m \times n}] =$	

Equation 3: Time series coefficient equation.

The strain matrix on the left-hand side of the time series coefficient equation represents strain gauge values (reported in the columns) at each time point of data collection (reported in the rows). This is the strain data that was collected from a test event. The right-hand side of the equation represents a set of vectors for scaling each load case. When the individual load cases are scaled by each vector and the results are linearly superimposed, the resulting strains at the gauge locations of the corresponding row in the test strain matrix are guaranteed to match. Furthermore, any other response in the structure can be expanded backwards through this superposition.

True-Load application

To develop a True-Load application, one first constructs an FEA model with unit load cases representing the exterior loading. In the case of the Menet Aero hexacopter, we observed that the electric motors on the arm were exciting very high frequency modes. If these modes were not accounted for, the load calculations could be erroneous.

Fig. 2 shows the FEA model of the arm and the reference geometry. Note the FEA model of the arm is just a tube with remote attachments for masses and loads. The geometry for the prop and motor are shown only for graphical representation; they are represented only as point masses in the FEA model. Fig. 3 shows the unit loads on the FEA model. The True-Load software identifies optimal strain gauge placement. In this application, 12 strain gauges were used. Typically,

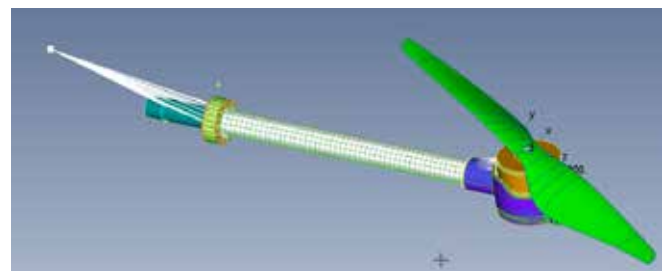


Fig. 2. FEA model of hexacopter arm.

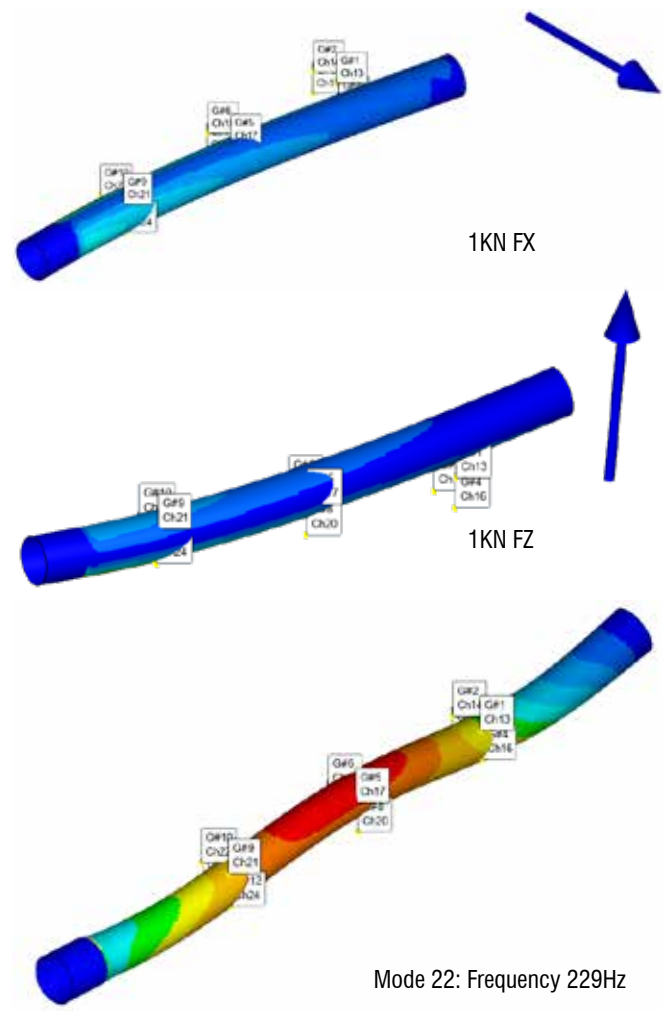


Fig. 3. Unit loads / modes used for True-Load.



Fig. 4. Virtual gauge placement.

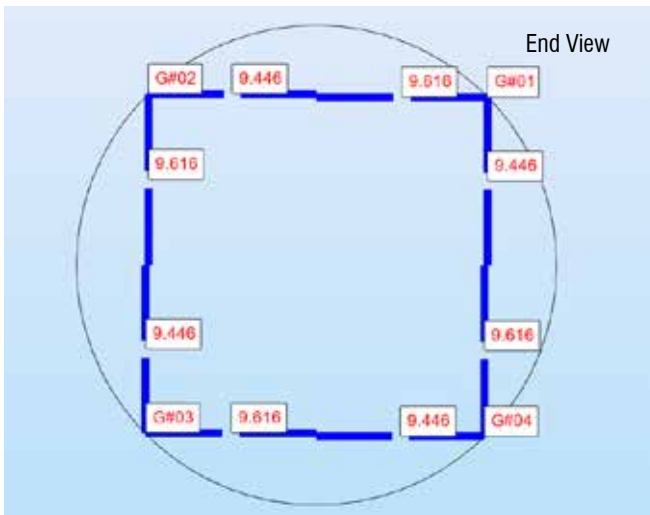
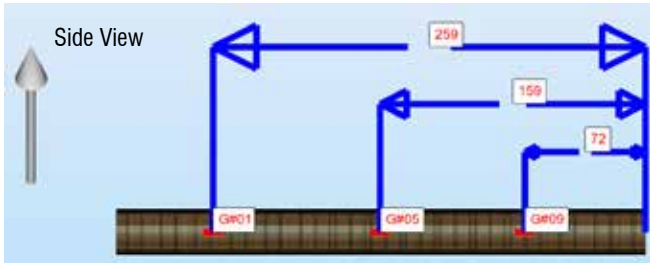


Fig. 5. Gauge dimensions.



Fig. 6. Strain gauged arms and DTS DAQ mounted on the drone.

for an application of three-unit loads / modes, True-Load would require just six strain gauges. However, since this was a learning and discovery project, extra strain gauges were used. Specifically, three sets of four strain gauges were used. Fig. 4 shows the virtual strain gauge placement in True-Load.

Each set of four gauges was equally spaced around the circumference of the arm. Fig. 5 shows the gauge placement. Note that the gauges are not placed on the top and bottom fibres, but rather at 45° from the top and bottom fibres.

This allows all gauges to be active (non-zero) during testing. If gauges were aligned to the top and bottom fibres, then two other gauges would be on the neutral fibre and would thus theoretically read zero strain. The parts were then strain gauged and connected to a data acquisition system (DAQ). The DAQ used was a DTS Slice Micro. The DTS Slice Micro is extremely compact (45mm³) and runs off a small external battery. It was programmed to sample at 2KHz and was then mounted onto the drone connected to the strain gauges (Fig. 6).

Several events were conducted and the DAQ measured the strain data. Over 30 events were measured. Fig. 7 shows the strain response from three of the 30 events. Note that the strain values have been blurred to protect Menet Aero's intellectual property.

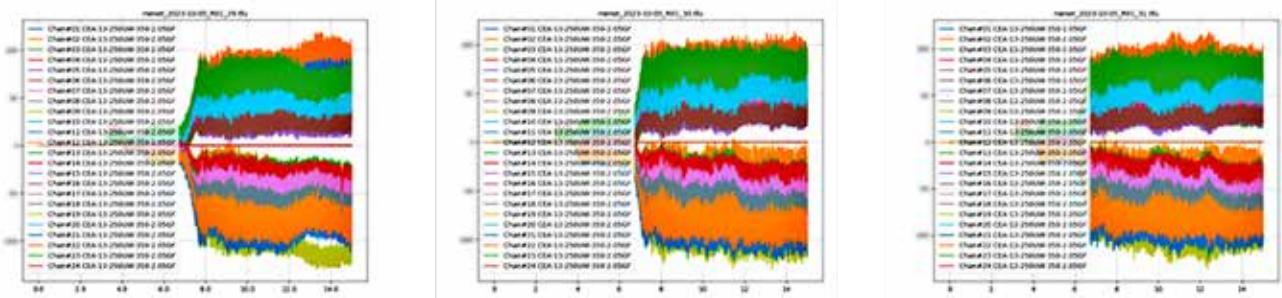


Fig. 7. Measured strain response.

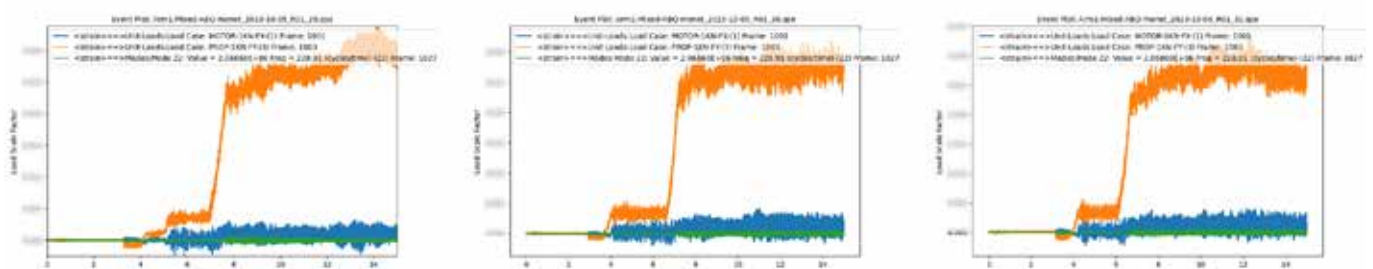


Fig. 8. Loads calculated from strain.

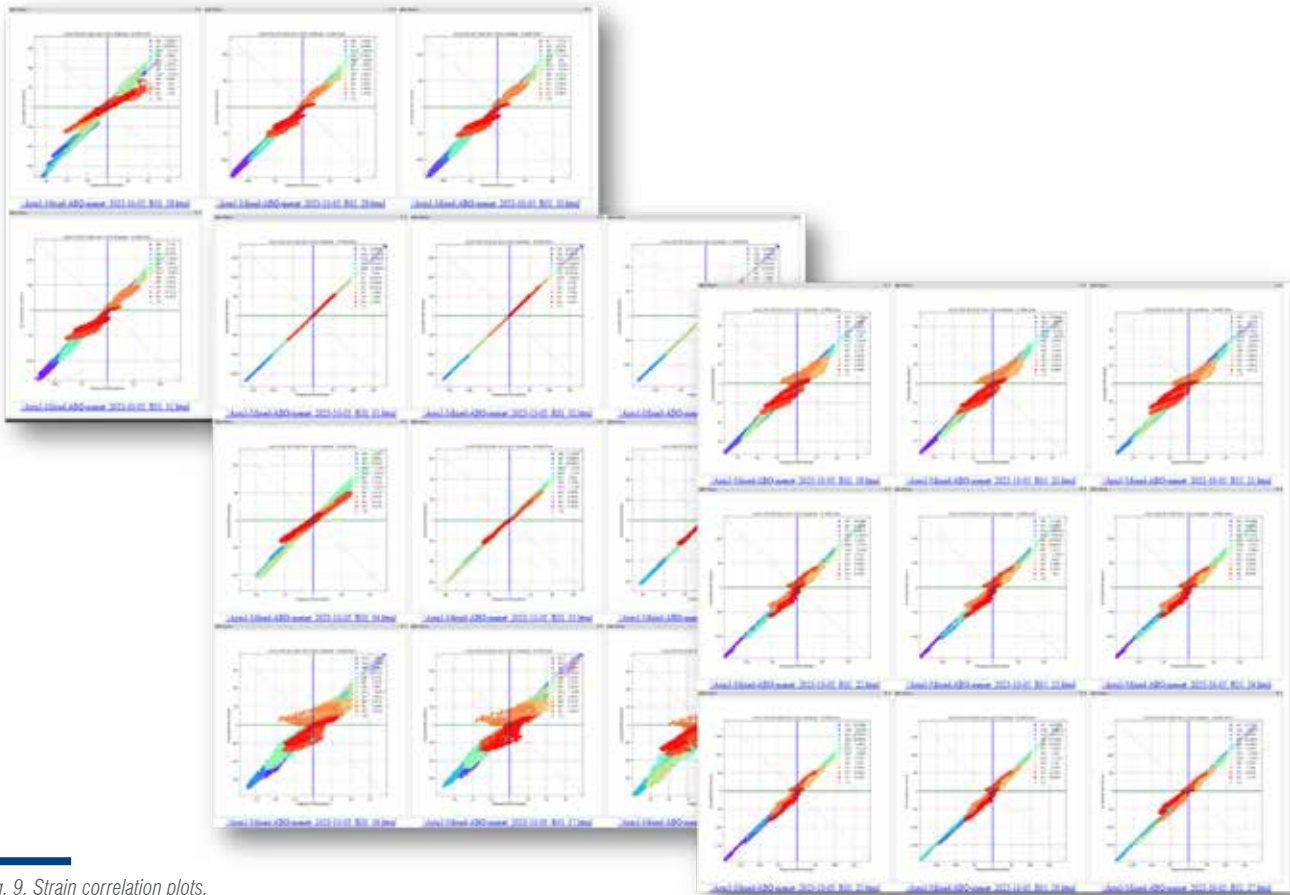


Fig. 9. Strain correlation plots.

The purpose of True-Load load reconstruction is to convert measured strain data into calculated operating loads. Fig. 8 shows the resulting load calculations for the strains measured in Fig. 7. The orange curve shows the lift force; the blue curve shows the tangential loads due to motor shaking; and the green curve shows the MPF of mode 22.

Fig. 9 shows the automatic strain correlation plots created by True-Load for all 30+ test events. The horizontal axis on the plots illustrates measured strain and the vertical axis represents simulated strain from loads calculated by True-Load. As can be seen the strain correlation is excellent. This informs us that the calculated strains are indeed the actual operating loads.

From this exercise Menet Aero now has the operational loads for its drone. The company can use these loads to optimize its drones for weight and cost. The True-Load methodology was an efficient and effective use of FEA models and testing techniques. For a small investment in strain gauges (\$10/gauge), Menet acquired mission critical, valuable data on its designs.

For more information:
 Danilo Col – EnginSoft
d.col@enginsoft.com

About Menet Aero

Menet Aero is an aerospace solutions provider specializing in manufacturing Tethered Unmanned Aircraft Systems (TeUAS) or drones. Our high-performance platforms, designed in heavy and light configurations, support a variety of payloads for applications such as high bandwidth digital battlefield communications, signal intelligence, electronic warfare, and force protection and targeting.

As a U.S. -owned and veteran-operated small business, we take pride in offering top-quality solutions to our customers.

About Wolf Star Technologies

Wolf Star Technologies specializes in globally proven, first-to-market software solutions that solve fundamental Product Development problems.

Their software packages, True-Load, True-QSE, and True-LDE are game-changers for Product Development. They extract decision ready data from FEA models and bring a unique understanding to the dynamic loading of structures. To find out more, visit: www.wolfstartech.com



Dynamic CFD analysis of a vertical-axis washing machine with a hydraulic balancer

by Mario Cagliari, Alberto Del Rizzo
SPM Engineering

A vertical-axis washing machine (Fig. 1) is a household appliance mainly used in the Asian and US markets. It consists of a plastic tub suspended by four spring-dampened rods containing a rotating basket which holds the laundry to be cleaned and that is completely immersed in water and detergent.

The washing process involving alternating relative movements between the tub/basket and an agitator mounted at its base is not the focus of this work, which instead concentrates on the final centrifugal phase of the work cycle where the dehydration of the placed laundry occurs.

When spinning at high speed, the garments are pressed against the walls of the basket, expelling water through holes in the walls. This phase is critical because the load, which is randomly distributed around the basket,

COMPONENTS	
1	TUB
2	BASKET
3	BALANCING RING
4	AGITATOR
5	MOTOR/TRANSMISSION
6	SUSPENSION RODS

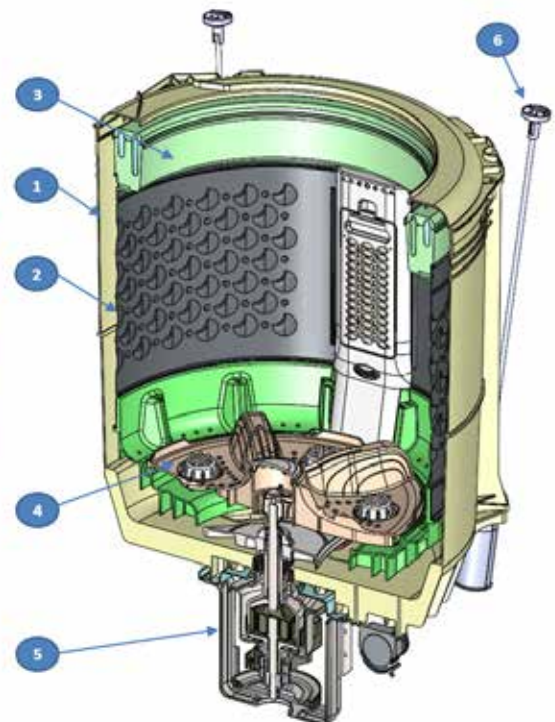


Fig. 1. The components of a vertical-axis washing machine.

always presents a certain level of imbalance and, although there are systems that detect excessively unbalanced loads and prevent them from being spun, the forces and vibrations transmitted to the structure remain a concern for engineers.

A special device in this type of washing machine is the so-called hydraulic balancer: a component consisting of a hollow plastic ring fitted in the top of the tub and partially filled (about 50-60%) with salt water.

A series of blades distributed radially around the circumference of this ring (Fig. 2) force the water to follow the ring's movement while channels allow the water to flow (Fig. 3).

In fact, the hydraulic balancer, rotating with the basket, acts as a counterbalance because it positions the fluid volume to the side opposite the imbalance [1].

This phenomenon is a common response of flexible rotors to unbalanced loads and occurs until the rotational speed reaches the natural frequency of the tub/drum's flexible mode, the value of which must be maintained above the maximum operating speed with a safety margin.

The challenge

SPM received a prototype of a new machine from its customer that showed large displacements and sometimes even contact between basket and tub at a speed of 700rpm when a concentrated offset test mass of 0.5kg was placed on the upper side of the basket, according to the customer's internal procedures for product acceptance.

Typically a concentrated offset test mass is used instead of laundry in laboratory tests to maintain repeatability and consistency with mathematical models because the behaviour of laundry is clearly difficult to simulate.

Since SPM's customer had already identified a problem in the flexibility of the tub and proposed a modification to stiffen the

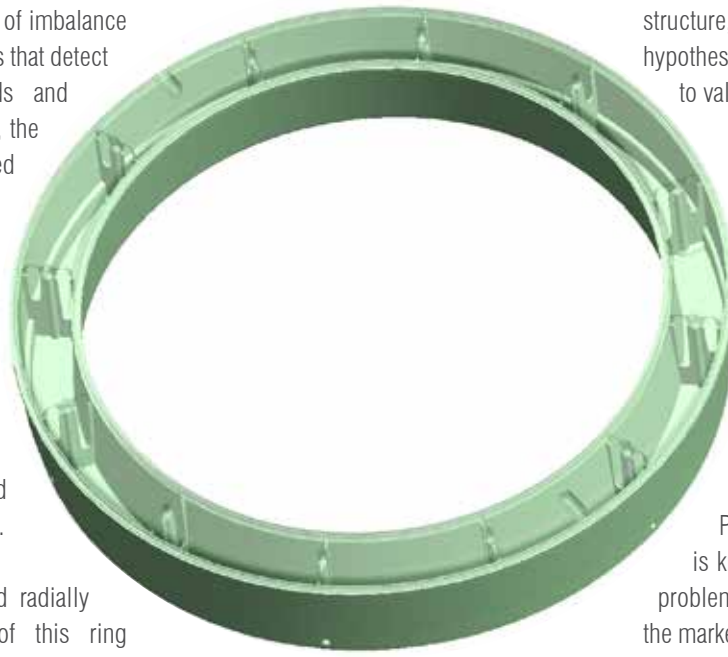


Fig. 2. Hydraulic balancing ring

structure, SPM's task was to confirm the hypothesis by evaluating the two designs and to validate the solution.

Structural flexibility influences the behaviour of the hydraulic balancer and SPM, experienced with flexible multibody dynamics but not yet with this device, had to tackle the problem of fluid-structure coupling for the first time.

Method

Particle-based CFD methodology is known to be suitable for this type of problem and of the software available on the market, SPM identified Promotech's Particleworks 8.0.1 as the best solution for its requirements.

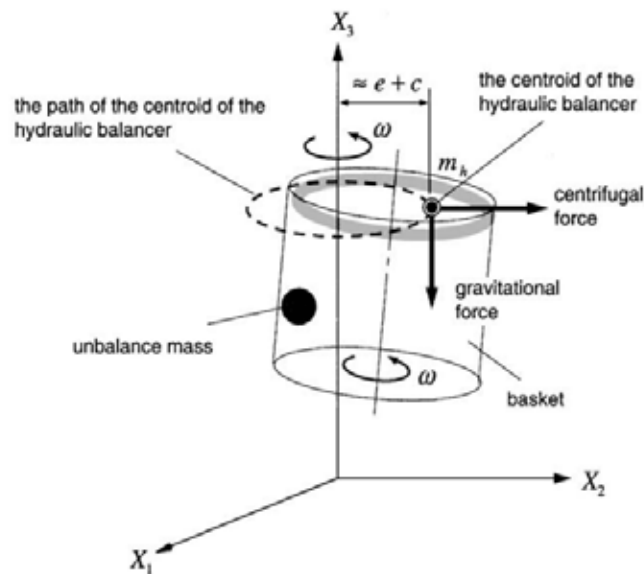


Fig. 3. Forces resulting from the hydraulic balancer [1].

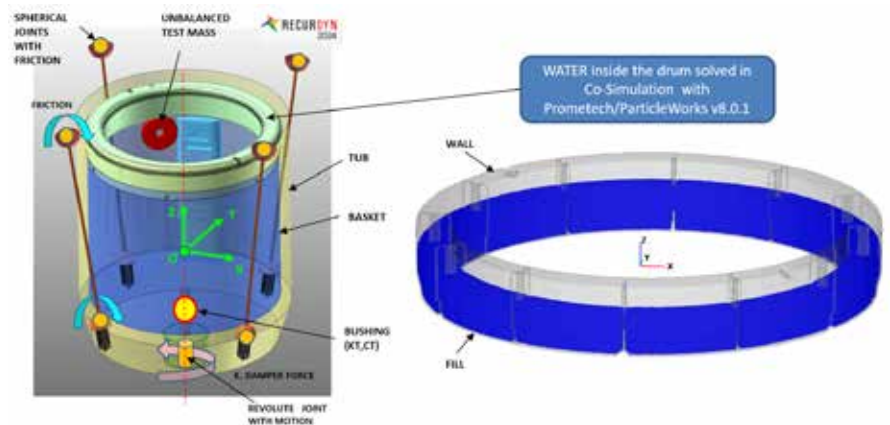


Fig. 4. Multibody model of the oscillating group.

SPM has already collaborated with EnginSoft in the past, and despite having other solutions for dynamic analysis in-house, the company decided to follow EnginSoft's recommendation to combine FunctionBay/ Recurdyn 2024 as a multibody solver for co-simulation with Particleworks due to proprietary connection interface between the two products.

The coupling of two pieces of software is mandatory in this particular case because the motion of the fluid affects the dynamics of the oscillating group and vice versa making it impossible to solve the two problems separately.

The oscillating group was modelled within Recurdyn 2024 (Fig. 4). The tub and basket were treated as rigid bodies with simplified geometries but accurate inertial properties obtained via CAD; the only component that required an actual shape was the ring, imported via Parasolid and included in the basket body.

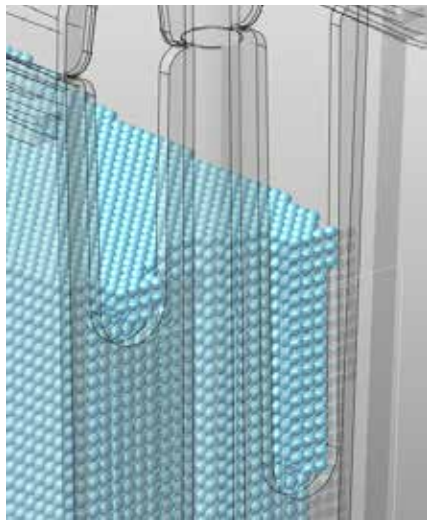


Fig. 5. Filling display in Recurdyn.

SPM decided to avoid flexible bodies to reduce any additional computing effort compared to CFD, and flexibility was introduced into the system by means of a bushing element, whose elastic properties, together with the friction of the joint, were identified by means of laboratory tests.

Modelling the ring in Particleworks is very easy and straightforward: it only requires the definition of the wall, performed within Recurdyn, which is used as a boundary for the fluid; some water properties such as density and surface tension; and some simulation parameters such as Courant Factor, particle size, and time step. The most difficult part is to identify the particle size as a trade-off between realistic filling and calculation time. Using a ring with 1.5L of water and allowing at least five particles in a row to pass through the narrow channels on each blade resulted in a population of 768,000 particles with diameter of 1.25mm (Fig. 5) and a time step of 2.21 e-5s.



Fig. 6. Laboratory test configuration.

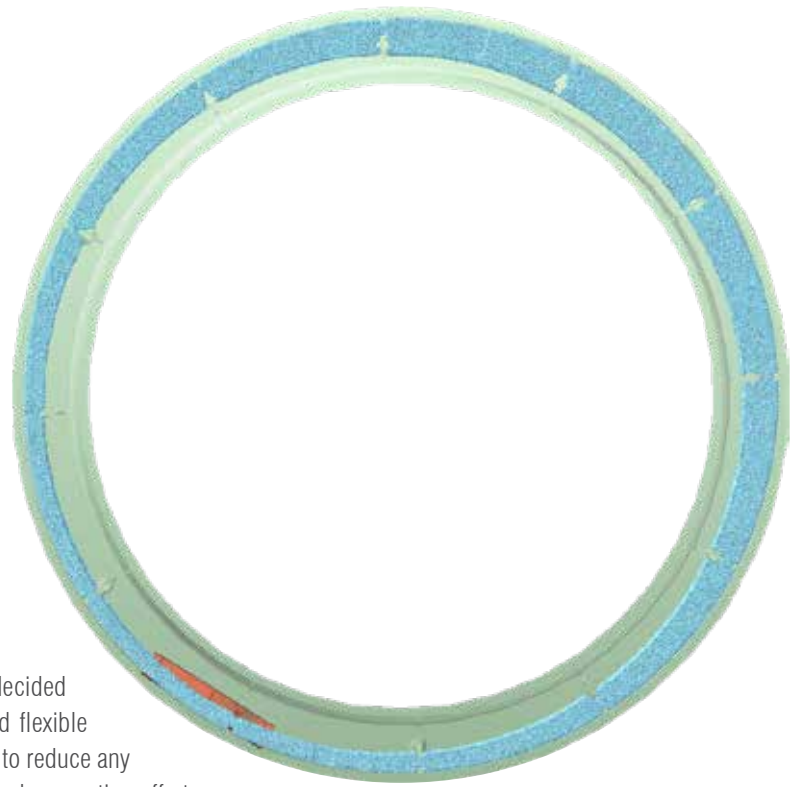


Fig. 7. Water displacement at 700rpm, opposite the imbalance

The maximum speed requirement of 700rpm was achieved with a 50-second linear acceleration based on the actual rotation ramp.

Laboratory tests

SPM supports simulation activities with laboratory tests whenever possible and, for washing machines, has developed a procedure to capture the three-dimensional movement of the oscillating group by means of six uniaxial accelerometers placed around the drum and thus obtain the X,Y,Z displacements and rotations at a central reference point (0) or any other position of interest.

The entire evolution of motion during machine acceleration to max spin speed using the unbalanced test mass was plotted in terms of amplitudes against the number of revolutions and this was used to validate the dynamic model with special attention to damping.

The bushing properties resembling flexibility were configured to obtain the equivalent basket deformation based on laser measurements taken during machine operation with no fluid inside the ring.

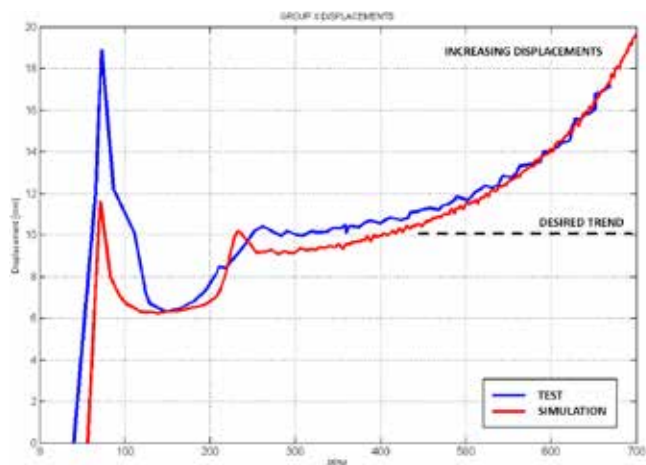


Fig. 8. Post-processing of time dependent results for amplitude v. RPM.

Results

The main output required from this simulation regarded the transfer of water within the ring, which was impossible to visualize in the actual machine, with the aim of investigating whether an instability occurring at high speed could be responsible for the large deflections and internal contacts.

The co-simulation determined that the water displaces correctly (Fig. 7), compensating for about half of the unbalanced mass required, but that the structure actually needs to be stiffened. In fact, both the simulation and laboratory test show increasing displacements with

velocity instead of the constant trend that should appear after crossing the resonance of a low-speed rigid body spring-mass system (around 100rpm, see Fig. 8).

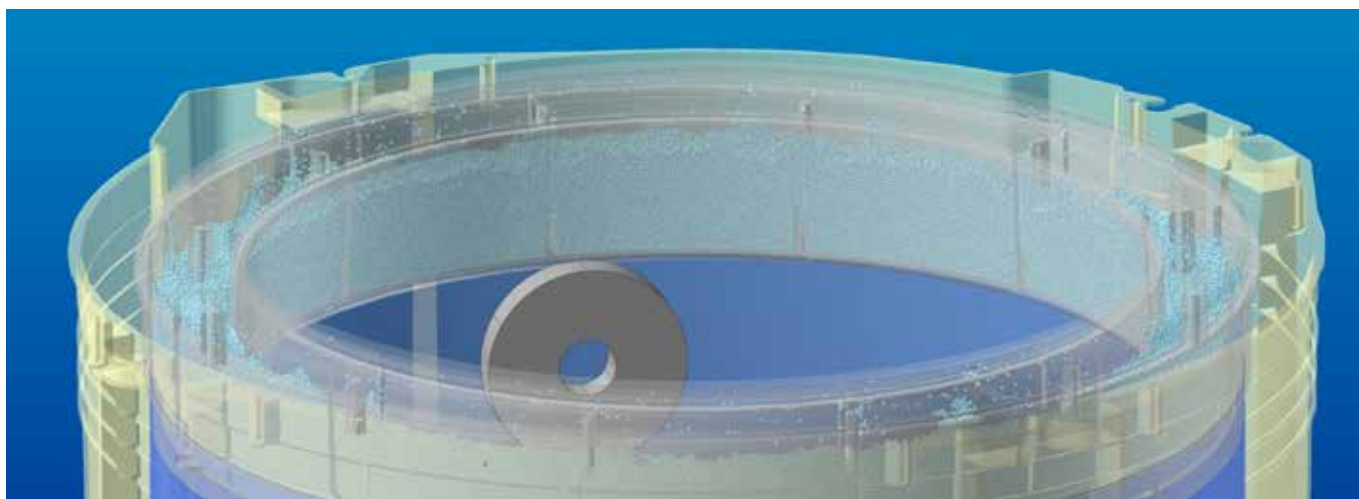
Conclusions

Although this type of dynamic CFD analysis is inherently difficult, all of EnginSoft's assertions about the ease of use of the two solvers combined together in a simple and flawless process turned out to be correct. The help of their experts was obviously fundamental in configuring the simulation for the CFD part developed in Particleworks. For the multi-body side with Recurdyn, SPM proceeded according to its experience after some training on the new interface.

The company is satisfied with the results obtained so far and believe that this approach is perfect for studying a component such as the hydraulic balancing ring where an experimental approach would be more expensive and time consuming and would involve special prototypes with transparent materials and high-speed cameras.

At this stage, flexible bodies were not used, but will certainly be a future improvement.

As far as computing effort is concerned, the 50-second simulation with this small-time step was performed in about 15 hours using the GPU cores of an Nvidia RTX5090 graphics card which is the most critical hardware component, Particleworks being the most demanding task during frame calculation.



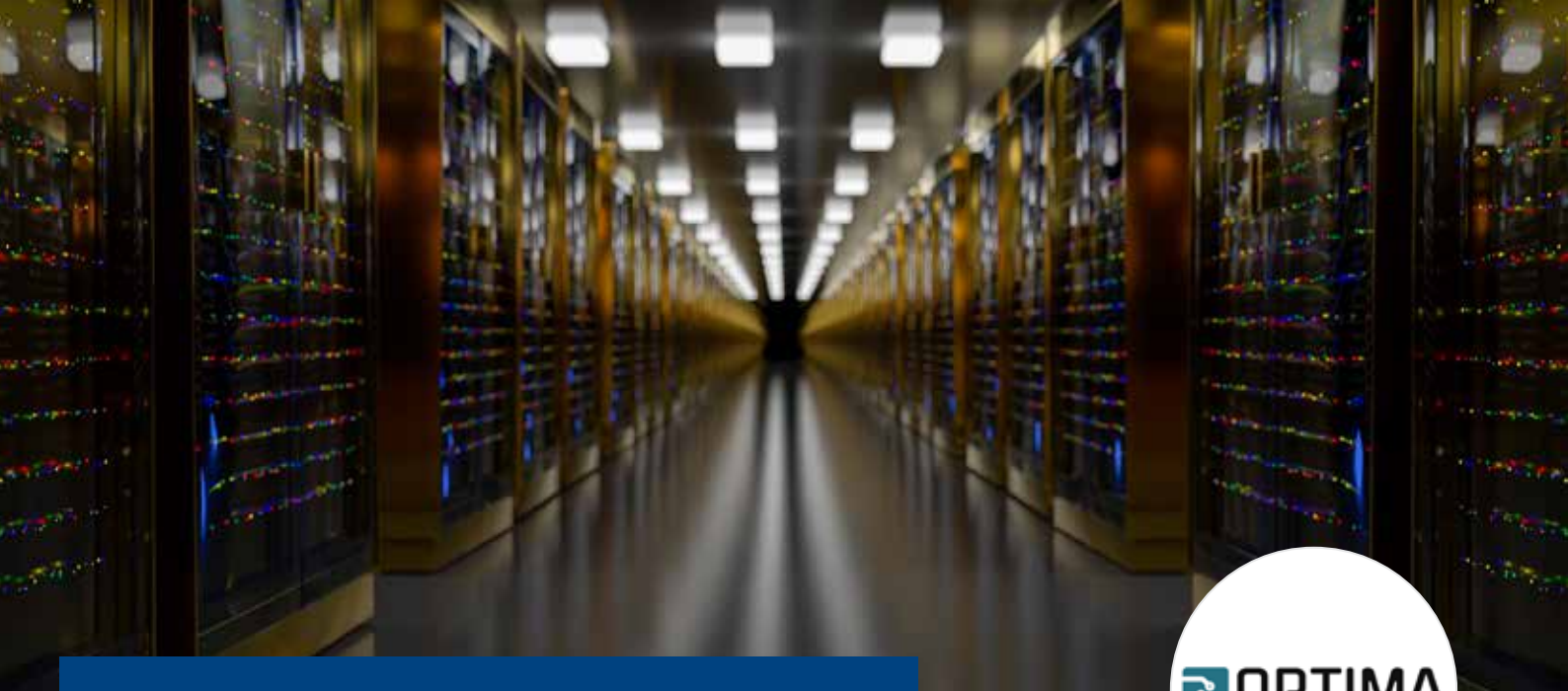
About SPM Engineering

SPM Engineering is a service company founded in 1975 and based in Fiume Veneto in the province of Pordenone in Italy. Its mission is to provide innovative design services for the development of new products for the mechanical, home appliance, motorcycle and scooter, and plastics industries. The skill and expertise of its engineers, technicians and management team and the company's capacity to use technologically advanced tools make SPM a unique and reliable company able to take Italian product engineering know-how all over the world. www.spmengineering.it

References

- [1] S. Bae, J.M. Lee et al. "Dynamic analysis of an automatic washing machine with a hydraulic balancer", Journal of Sound and Vibration, Vol. 257/1 (2002): 3-18.

For more information:
 Alberto Sartor – SPM Engineering
asartor@spmengineering.it



OPTIMA project revolutionizes HPC for industrial applications: interview

The EuroHPC JU-funded project OPTIMA is reshaping HPC in Europe with field-programmable gate array (FPGA) technologies.

OPTIMA, a EuroHPC JU (Joint Undertaking)-funded project launched in 2021, has developed an FPGA-based chip which allows the optimization and transfer of industrial applications on HPC (high performance computing) systems. FPGAs (field programmable gate arrays) are programmable computer chips that boost the performance of industrial applications, minimize energy consumption, and will help propel Europe towards global leadership in supercomputing.

The OPTIMA project is an initiative driven by a consortium of small and medium-sized enterprises (SMEs) and is the result of the teamwork of ten partners, six of which are SMEs from six different countries: Greece, Germany, Spain, Italy, Switzerland and the Netherlands. The project had a budget of €4,100,000 from Horizon Europe, the EU's funding programme for research and innovation, and completed its work in November 2023.

The EuroHPC JU interviewed Iakovos Mavroidis, researcher at the Technical University of Crete (TUC) and OPTIMA's project coordinator. He explains the key features of the project and explains what has been accomplished so far.

Can you please describe the OPTIMA project in your own words?

Sure! The primary objectives of the OPTIMA project were to optimize and test industrial applications and open-source libraries on HPC systems using FPGA chips.

These special chip technologies known as field-programmable gate arrays (FPGAs) function as high-performance engines and accelerators for specific applications needed to run a supercomputer. FPGA chip technologies are known for their lower power consumption compared to other chips like server-class CPUs (computer processing units) and GPUs (graphical processing units). FPGAs reduce power consumption in various applications for supercomputing and could foster new, more economic and environmentally friendly, approaches to HPC.

To accomplish this task, the OPTIMA project used high-performance servers based on JUMAX and Alveo technology equipped with FPGA chips to test different types of simulation in the fields of robotics, geosciences and computational fluid dynamics (CFD).

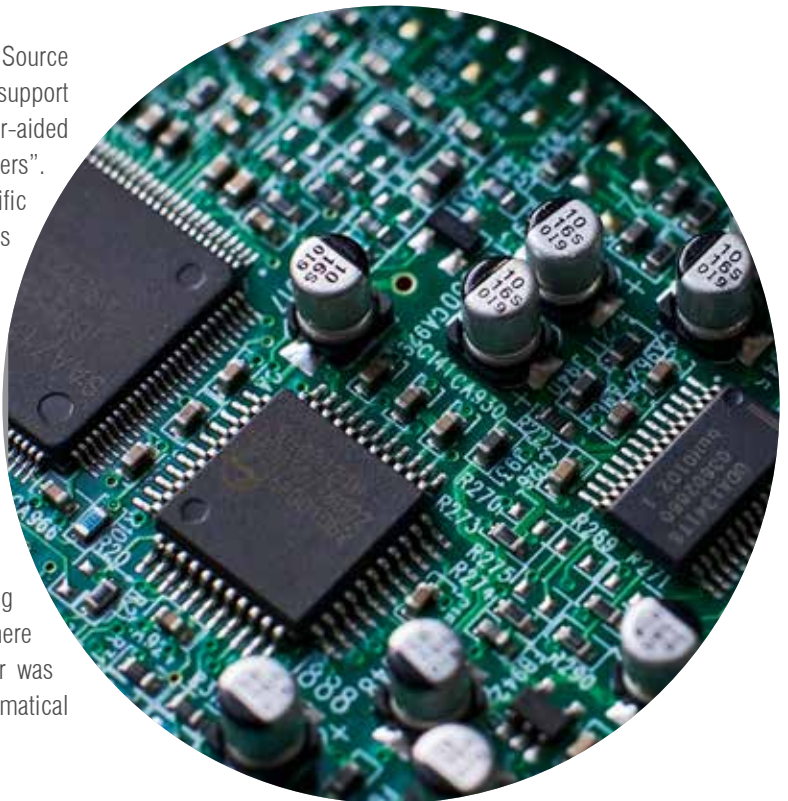




What was achieved?

A major achievement is the development of the OPTIMA Open Source (OOPS) library, which includes 31 hardware components to support fundamental linear algebraic operations and CAE (computer-aided engineering) problem-solving methods, also known as “solvers”. The OOPS library not only enhances raw performance for scientific algorithms, but also promotes high energy efficiency. This is achieved through the optimization of basic mathematical operations, known as BLAS kernels, which are fundamental components in computational mathematics. These result in potential energy savings of up to 50 times per BLAS kernel.

In addition, OPTIMA demonstrated remarkable results in tests on hardware prototypes: it doubled the speed of the preconditioned conjugate gradient (PCG) algorithm, which is a widely used method for solving complex mathematical equations. Tests with Robotic simulation software (involving convolutional Neural Networks) for autonomous driving were 3.4 times faster on average, CFD Lattice Boltzmann solver was 3.4 times faster and seven times faster than a basic mathematical operation on standard HPC software.



Can you give some examples of how OPTIMA supports European HPC users and how it promotes greener and more sustainable supercomputing?

Certainly: to support European HPC users, OPTIMA has made the OOPS library openly available. This allows developers to port legacy applications and code to FPGA-supported HPC systems without restrictions. We encourage users to download the template project of the OOPS library and try any of the available kernels/components. The library is accessible to anyone on GitHub [1, 2, 3].

As far as sustainable supercomputing is concerned, I am proud to say that the OOPS library enables significant performance improvements and reduced power consumption, which aligns perfectly with EuroHPC’s goals for energy-efficient supercomputing!

What were the main challenges you encountered during the project's development, if any?

We encountered several challenges while developing use cases on OPTIMA FPGA-based infrastructures. The most notable of these were the following:

- FPGA-based MPSoCs (multiprocessor systems-on-chip) offer flexibility, but managing resources efficiently poses a significant challenge. There are several hardware constraints related to the number of DDR (double data rate) memory controllers and distribution and FPGA chip technologies. We had to carefully balance functionality between these two technologies to ensure optimal performance without exceeding hardware constraints.
- While there have been significant advancements in FPGA-chip-related tools, there are still difficulties in developing efficient FPGA-based applications. Providing a simple interface for the programmer is still a challenge, and it remains easier to manually implement this design on an FPGA chip.

- In today’s FPGA-based infrastructures, communication between an FPGA-accelerated application and the host processor requires high-latency memory transfer via PCIe (peripheral component interconnect express), a high-speed serial computer expansion bus standard.
- As FPGA chip designs become increasingly complex, it becomes more challenging to ensure that all signals meet timing requirements.

Overall, we were able to overcome most of these challenges through careful planning, rigorous testing, and collaboration among team members with FPGA design, hardware, and software development experience.





How is the development of such a platform supporting the ambition of the EuroHPC JU to make Europe a world-leader in supercomputing?

By advancing HPC capabilities through FPGA optimization tools and chip technologies for industrial applications, OPTIMA contributes to Europe's competitiveness in the global HPC landscape. In this way, the OPTIMA project aligns with the ambition of the EuroHPC JU to position Europe as a global leader in HPC. OPTIMA is also a good example of an innovative SME-driven EuroHPC project.

What's next for OPTIMA?

The participating SMEs are already using the experience they gained from porting applications to OPTIMA's heterogeneous platforms. They are developing new applications for advanced cloud systems, AI accelerators, GPUs, and other chip designs.

In addition, the OOPS library will be continuously updated with additional support for FPGA chips and tools, new kernel implementations, and

further improvements to existing ones. OPTIMA expects the OOPS library to become a valuable tool for software developers who want to map their applications onto FPGA-supported HPC platforms.

Furthermore, the advanced FPGA-based infrastructure developed by OPTIMA is currently being used both to reproduce complex hardware systems under design (SuDs) and to execute high-end AI-powered applications.

For more information,
please visit OPTIMA Project Website

optima-hpc.eu and eurohpc-ju.europa.eu/optima-project-revolutionises-hpc-industrial-applications-interview-2024-04-24_en

References

- [1] github.com/cslab-ntua/OPTIMA-ICCS
- [2] github.com/cyberbotics/optima
- [3] github.com/GabrieleRolleri/optima_lbm

EnginSoft is proud to have been recognized as Key Innovator by the European Commission for its work in the OPTIMA project and for its innovative results achieved in a Custom HPC solution for CFD. We plan to provide custom CFD solvers for embedded controllers for edge computing to enable real-time simulation and analysis of complex fluid dynamics problems. In the energy sector, edge CFD can be used to optimize the performance of wind turbines and solar panels. This innovation is still under development and requires a further feasibility study and an internal prototyping phase before being introduced to the market for commercial exploitation, but improvements are already being transferred to and shared with customers in the automotive and aerospace markets. In addition, the sectors of smart, green and integrated transport, and of safe, clean and efficient energy could benefit from our achievements in the OPTIMA project.

We concentrated on the final CPU+FPGA hybrid version of the Lattice-Boltzmann (LBM) code, working in message passing interface (MPI) on several digital front ends (DFEs). To implement the new version, we started from the PALABOS library and made various modifications to the D2Q9 lattice. Beginning with pure CPU code, our team analysed the instrumented code and developed three different sub-versions:

- a CPU buffered code (exactly resembling the FPGA code);
- an FPGA code with vector buffering (one domain line per call);
and
- a full domain buffer running on FPGA.

For the LBM-CFD method, our implementation of a D2Q9 lattice within multi-FPGA and MPI tasks increased performance 1.5—3 times (depending on the number of MPI tasks) compared to the Juman supercomputing infrastructure, according to the final evaluation. We evaluated the performance of applications developed on a hybrid CPU+FPGA system (Juman), focusing specifically on their optimization from a CPU-only system to the hybrid system.

The results showed that the hybrid CPU+FPGA application for medium-size models performed best, both in terms of speed and energy savings compared to the CPU-only version. Energy KPIs were evaluated based on the mean consumption of the boards/processors due to the lack of other information or monitoring systems.

We have confirmed the various exploitation paths already identified for FPGA-based HPC and are willing to invest time and effort in:

- (i) building on the knowledge and expertise gained from OPTIMA and other successful projects in order to expand our capabilities in extreme scale computing, seamless hardware-software integration, and the ability to tackle complex network challenges and to use these strengths to develop innovative, tailored solutions that meet the specific needs of our clients;
- (ii) evaluating and recommending energy-efficient solutions to the heterogeneous private cloud systems market, especially in simulation engineering, where FPGA accelerators are becoming increasingly integrated, and particularly as the use of FPGAs becomes more prevalent in fluid dynamic applications due to their ability to perform high-speed calculations and data processing;
- (iii) assessing and proposing embedded solutions for customized devices for the automotive and aerospace market, in order to perform reduced order modelling techniques.

By applying the principles and techniques learnt from our past successes, we can confidently take on new and exciting projects that require state-of-the-art problem-solving strategies.

For more information:

Marisa Zanotti - EnginSoft
m.zanotti@enginsoft.com



Introduction to shading analysis for solar complexes

by Sunggil Jo
TAE SUNG S&E

As fossil fuels deplete and environmental concerns rise, interest in new and renewable energy sources is growing. In response, the government of the Republic of Korea is striving to increase the utilization of solar and wind energy through its “Renewable Energy 3020 Implementation” plan. Against this backdrop, we will introduce a method for analysing shadows within solar power plants using the solar load model in Ansys Fluent.

Causes of shading in solar panels

There are several reasons for the occurrence of shadows. Major causes include obstacles such as adjacent buildings and vegetation, as well as significant shading caused, in the northern hemisphere, by the front row in south-facing solar cell arrays. Shadows can also result from other factors like leaves, bird droppings, or water and dust accumulating on the panels.

The following steps can mitigate shading:

- maintaining adequate separation distance between rows to prevent the front row from casting shadows on the back row during the designated hours of power generation (10.00a.m. to 3.00p.m. on the winter solstice);

- elevating the bottom edge in ground-mounted arrays by at least 0.6m above the ground to avoid shading from the accumulation of muddy water;
- implementing measures to address shading caused growing vegetation;
- reviewing the module’s cleaning schedule periodically.

Characteristics of the shading that occurs in solar panels

Solar cell modules within an array are interconnected in series and parallel configurations. This means that a thorough design review is essential to prevent reduced power generation from shading.

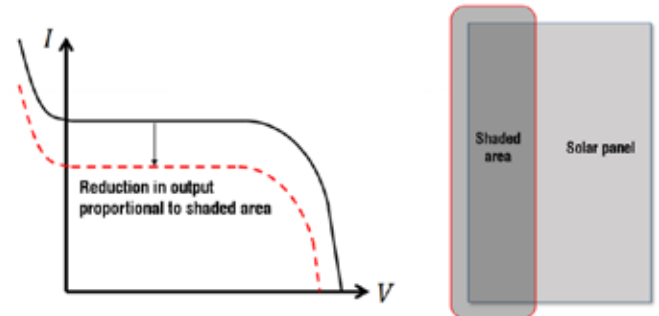


Fig. 1. Power reduction characteristics in relation to shaded area.

As depicted in Fig. 1, when solar cells are shaded, their output decreases in proportion to the size of the shaded area, so it is important to mitigate the effect of shading through careful design considerations.

The solar load model

The solar load model function calculates the incidence of solar energy. It works similarly to Fluent’s radiation models but is classified as a distinct feature rather than as a separate radiation model.

Solar ray tracing option

This method uses a tracking algorithm to automatically calculate solar ray traces for sun-exposed areas and then assigns the calculated solar radiation to these areas as the source values.

The main advantage is that you can use Fluent’s radiation model even while disabled by directly entering the flux into the source term. This method in particular allows shading to be calculated without the need for additional repetitive calculations when analysing the shaded areas between solar panels.

Solar irradiation option

This option represents a more advanced analysis technique and can be used in conjunction with Fluent’s DO or MC radiation models. It enables more precise heat flow analysis by applying the solar radiation condition directly to the boundary conditions, rather than the source term. However, it is important to note that the functionality of the solar load model is limited to the 3D analysis mode.

Shading analysis using the solar load model

We will now explore how to set up a shading analysis for solar panels. The solar load model provides two options; we will focus on conducting shadow analysis using the solar ray tracing option.

As illustrated in Fig. 2, the Solar Load model requires the user to insert the solar position vector, direct solar radiation, and diffuse solar radiation parameters, which can either be done manually or by using the solar calculator tool to obtain the necessary values.

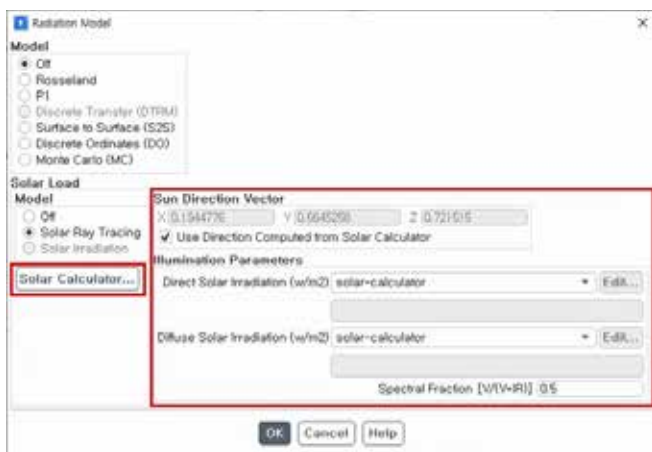


Fig. 2. Selecting the Solar Load model.

The solar calculator computes the amount of solar radiation (see Fig. 3). Users insert location parameters such as latitude, longitude, and time zone after which they can specify the date and time information. They can then enter a vector to indicate the orientation of the grid system being analysed. The fourth setting is the solar irradiation method, which offers the choice between applying the theoretical maximum value or calculating it based on sunlight data from clear skies. The sunshine factor also acts as an adjustable linear coefficient to change the calculated amount of radiation as needed. For example, if the calculated direct solar radiation is 1,000W/m² and the Sunshine Factor is set to 0.5, the direct solar radiation applied would be 500W/m².

Latitude

The area north of the equator is designated as northern latitude, while the area south of the equator is designated as southern latitude. Latitude is measured from the equator, with North ranging from 0° to 90°N and South from 0° to 90°S. However, in Fluent, the input convention for latitude represents all values in the range from -90° to 90°, with northern latitudes being positive and southern latitudes being negative values.



Fig. 3. Solar calculator.

Longitude

Longitude is divided into the eastern and western hemispheres using the prime meridian (0° longitude) as the reference point.

Longitudes east of the prime meridian are expressed as positive values between 0° and 180°E, while longitudes west of the prime meridian are expressed as negative values between 0° and 180°W. The input convention for longitude in Fluent is to represent all values between -180° and 180°.

Time zone (+- GMT)

GMT, short for Greenwich Mean Time, is the global standard time zone, since the prime meridian (0° longitude) passes through the Royal Observatory in Greenwich in England. In Fluent, time zones are expressed as a numerical offset from GMT, between -12 and 12.

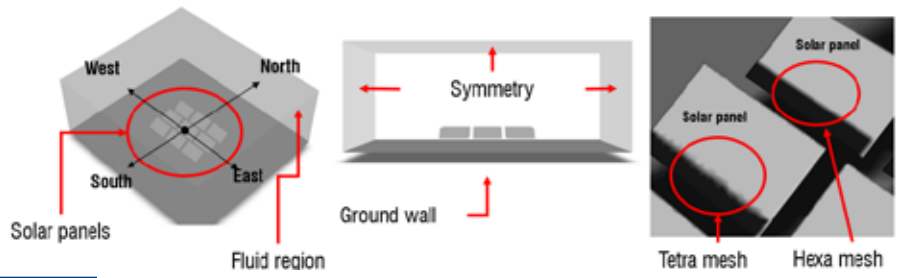


Fig. 4. Solar complex modelling.

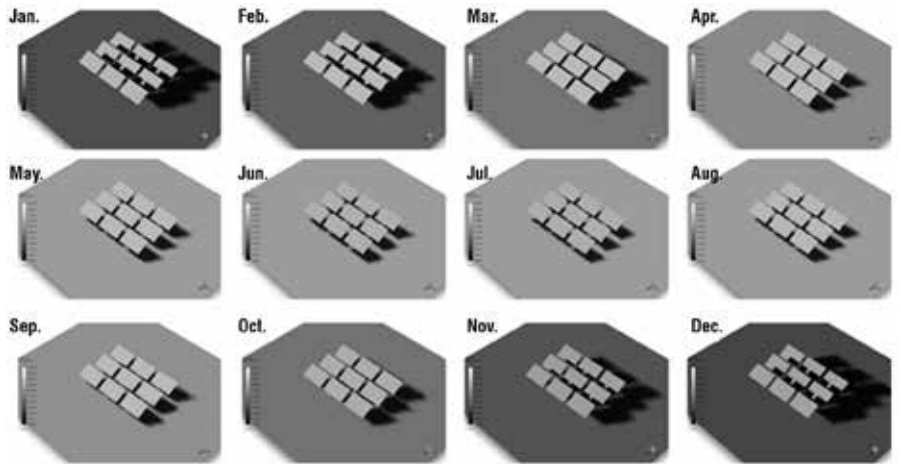


Fig. 5. Shading analysis of a solar complex.

Fig. 4 shows a 3D model of a solar power plant. The ground surface was modelled with a wall boundary condition, while the sides were modelled with a symmetrical boundary condition. Since the main purpose is shading analysis, a simplified solid geometry model can be used to represent the solar panel arrays. Fig. 5 shows the shading calculations performed at 12.30p.m. on the first of each month throughout the year.

As illustrated, shadows are cast on the solar panels during the months of January-February and November-December.

This phenomenon occurs because the angle of the sun is lowest during the winter

season, causing increased shading. Various methods can be used to mitigate this such as optimizing the tilt angle, inter-row spacing, and height of the solar panel arrays.

Conclusion

While Ansys Fluent cannot directly simulate the photoelectric effect of solar panels, its solar load model enables comprehensive analyses beyond shading effects such as thermal analysis of the panels themselves.

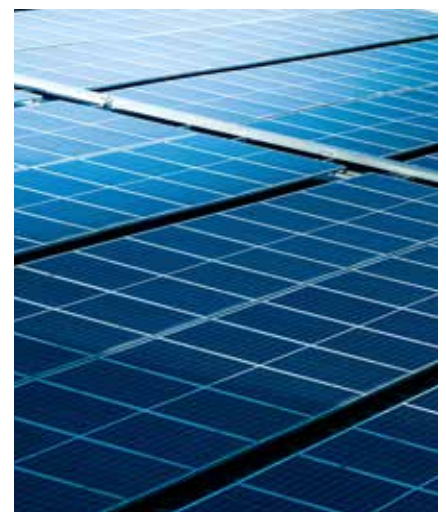
Furthermore, coupled simulations allow stress analyses to be conducted to account

for factors like wind loads and thermal effects. This versatility makes Ansys Fluent a powerful tool for evaluating various environmental factors and identifying optimal configurations to maximize the efficiency of power generation.

For more information:
Sunggil Jo - TAE SUNG S&E
sunggil@tsne.co.kr

About TSNE

Since its establishment in 1988, TSNE has specialized in CAE, providing engineering programs and services to Korean customers. Tae Sung S&E (TSNE) aims to be the “One Stop Total CAE Solution Provider” (OSTS) both in domestic and global markets. The company leverages its large base of business capabilities and its team of CAE experts to provide services to customers in various industries (aerospace, automotive, civil engineering, biomedical, shipbuilding, electrical and electronics, energy, defence, chemical industries, etc.) and is expanding its business scope to research innovative technologies and apply them in the field. It strives to become a global engineering company and increase its potential as a sustainable engineering company. Tae Sung S&E partners all engineers who endeavour to solve challenges. Tae Sung S&E will work with you to achieve “NO PROBLEM, BE HAPPY”.





Leverage SmartUQ to achieve modern artificial intelligence and machine learning for simulation and digital twins

by Gavin Jones
SmartUQ

Simulation is of course widely used to great benefit by engineers in all industries; however, the effective use of simulation does still face challenges which artificial intelligence and machine learning (ML) can help with.

Simulations can for example have long run times that limit the types of analyses that can be performed as well as the number of inputs, scenarios, and design possibilities that can be explored. The accuracy of simulations is also affected by uncertainty regarding, for example, initial conditions, boundary conditions, and model parameters. SmartUQ has best-in-class, unique tools to address all these challenges.

ML models

One approach to address long simulation run times is to train an ML model to predict the results of the simulation. This is sometimes referred to as surrogate modelling. Once trained, such an ML model can predict the outcomes much more rapidly than the required run time for the simulation thus eliminating the limits on the types and depths of analyses that can be performed.

The effectiveness of this approach largely depends on the accuracy of the ML model's predictions compared to the simulation results: SmartUQ's ML models have best-in-class prediction accuracy.

The company has also developed unique ML model variants for situations common to engineering problems. For example, SmartUQ's Spatial/Temporal predictive model can rapidly create accurate ML models for data sets that have a spatial distribution to the outputs - such as for an FEA (finite element analysis) that needs to predict the stress at every node.

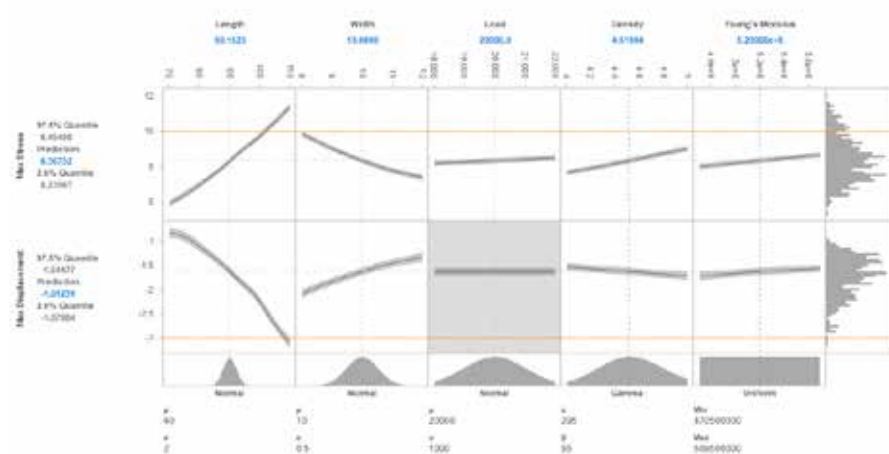


Fig. 1. SmartUQ's MultiView of an ML model showing prediction with a 95% confidence interval and uncertainty propagation.

Design of experiments (DOEs)

Training an ML model of a simulation requires some simulations to be run to collect training data. This is particularly challenging for simulations with longer run times and larger numbers of inputs where it may not be possible to collect sufficient training data.

SmartUQ addresses this challenge in two ways. Firstly, its more accurate ML models require less data to achieve the desired prediction accuracy for a given problem. Secondly, by using modern DOEs such as Latin Hypercube Designs (LHDs), SmartUQ offers more efficient DOEs with unique options to minimize the amount of data

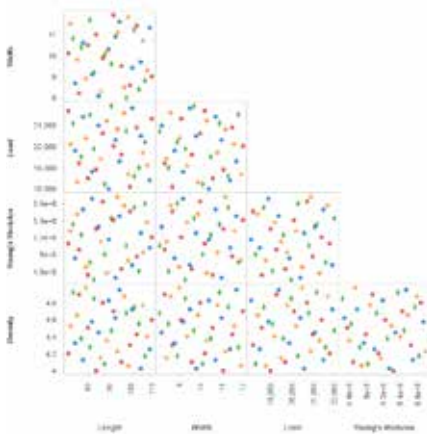


Fig. 2. SmartUQ sliced design of experiments with 5 inputs and 40 total samples.

required to train an accurate ML model, such as by allowing data to be collected in efficient batches (Fig. 2), or by permitting complicated constraints on the problem's input space.

The product also features adaptive sampling techniques that can use an existing ML model to intelligently decide where further data should be collected to have the largest effect on improving the ML model's accuracy.

Statistical calibration

Simulations and ML models that predict simulation results are only useful if their results agree well with physical data such as test or experimental results.

Calibrating simulation to physical data is key to creating and maintaining accurate digital twins. Typical approaches to calibrating simulation models can be time consuming and, worse, often unsuccessful because they only focus on parameter uncertainty either through a manual or an optimization process.

The goal of these approaches is to find the best values for model parameters to obtain the closest agreement with the available physical data. However, this approach ignores the role that model form error plays when there is disagreement between simulation and physical data. For example,

if a linear material model has been selected for a situation that would normally use a non-linear material model, it may be impossible to select parameters to obtain results that agree well with the physical data.

SmartUQ's statistical calibration features account for parameter and model form uncertainty; they can also accommodate the uncertainty in calibration results arising from noise in the physical data being used.

Analytics

Once trained and calibrated (if required), the ML model is ready to be used for analysis. SmartUQ makes performing a large variety of analyses quick and easy. Sensitivity analysis helps identify the inputs with the greatest

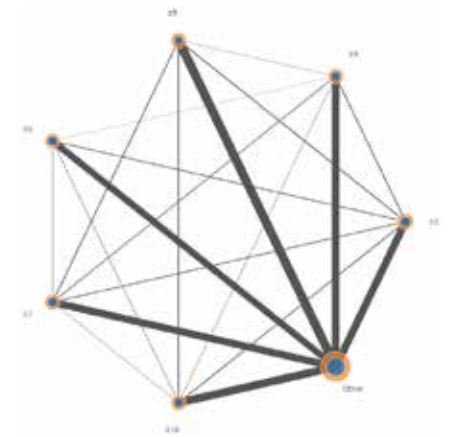


Fig. 3. Results of global sensitivity analysis showing main effects (size of blue circles), total effects (size of orange circles), and strength of two-way interactions between inputs (line thickness).

influence on the outputs (see Fig. 3), while uncertainty propagation can quantify the ambiguity in results due to uncertainty in inputs, for example, the uncertainty in peak stress resulting from uncertainties in geometry and loading. SmartUQ's stochastic and reliability-based optimization can even take such input uncertainties into account as part of the optimization.

SmartUQ is available with both a user-friendly GUI or as a Python API.

For more information:

Robert Goffee - SmartUQ
 robert.goffee@smartuq.com

About SmartUQ

SmartUQ is a Machine Learning (ML) and Artificial Intelligence (AI) tool optimized for engineering applications from ideation and design to manufacturing and sustainment. By providing powerful tools and accurate ML models with user-friendly interfaces, SmartUQ makes it easy to perform predictive modelling, optimized sampling, uncertainty quantification (UQ), and model calibration. From Fortune 500 manufacturers to startups and engineering consulting firms, SmartUQ's best-in-class predictive modelling accuracy helps our customers go beyond analysis to include uncertainty in the decision-making process.

SmartUQ was originally developed to solve UQ challenges for a leading jet engine manufacturer because previous tools could not handle the complexity, scale, and high-dimensionality of their problems. Since then, SmartUQ has become a user-friendly general AI and machine learning tool with users across industry and government in Automotive, Aerospace & Defence, Turbomachinery, Heavy Equipment, Medical Device, Semiconductors, Consumer Electronics, Energy, and Oil & Gas.

The team is headed by world-class experts in statistics and engineering who take pride in creating game-changing solutions where no off-the-shelf solutions exist. Our software has helped our customers solve some of their most difficult analytics problems, saving millions of dollars and thousands of hours of work. **Visit smartuq.com**



2024

COURSE CATALOGUE

Dive into our
full training offer!

www.enginsoft.com/training

Engineering Lifelong Learning



Particleworks experience

2024
September 25-26
Frankfurt, Germany

Conference Schedule

September 25, 2024

Workshop

14.00 – 17.30

During the conference's first day, Particleworks Europe experts will discuss **advanced simulation topics** and provide practical advice on configuring Particleworks models for various complex phenomena, including: 2-phase gaseous-liquid flow, heat transfer in steady-state and unsteady state, Multi-resolution simulations and more.

The workshops are designed to help Particleworks users or potential users build models, define appropriate boundary conditions, and optimize settings to guarantee numerical stability and minimize computational time.

The workshops will highlight **new features and modelling capabilities** of Particleworks.

September 26, 2024

Industrial presentations

9.00 – 17.40

The second day of the conference will begin with a **keynote** address by **Professor Koshizuka** from the University of Tokyo. Professor Koshizuka, renowned as **the creator of the Moving Particle Simulation method (MPS)**, will discuss the **evolution** of MPS in comparison to Smoothed Particle Hydrodynamics (SPH). Additionally, he will share insights on the collaborative relationship among MPS users, vendors, and universities.

The conference will proceed with Prometech's presentation on the **latest versions of Particleworks and Granuleworks** and their roadmap for future development.

The **use cases** will span various topics across different industrial sectors, ranging from **turbomachinery** to **food & beverage**, **electric powertrain** to **hydropower**, and **bearings** to **machining tools**. The speakers will provide insights into cutting-edge applications of meshless CFD and elaborate on how their companies leverage Particleworks digital models for tangible benefits.

particleworks-europe.com/experience

2024

September 25-26
Frankfurt, Germany



Particleworks experience

The benefits, advantages
and how-tos of going meshless

Register now! It's free!

particleworks-europe.com/experience